GENETIC BASIS OF CHRONIC PANCREATITIS: COHORT ANALYSIS AND PRECLINICAL DRUG TESTING

Ph.D. thesis

Zsófia Gabriella Pesei M.D.

Szeged

2023

GENETIC BASIS OF CHRONIC PANCREATITIS: COHORT ANALYSIS AND PRECLINICAL DRUG TESTING

Ph.D. Thesis

Zsófia Gabriella Pesei M.D.

Doctoral School of Theoretical Medicine, Faculty of Medicine, University of Szeged, Szeged

Department of Medical Genetics, Albert Szent-Györgyi Health Centre, Szeged

Supervisors:

Eszter Hegyi M.D.,Ph.D.

Doctoral School of Theoretical Medicine, Faculty of Medicine, University of Szeged, Szeged

Institute for Translational Medicine, Medical School, University of Pécs, Pécs

Prof. Miklós Sahin-Tóth M.D., Ph.D.

Doctoral School of Theoretical Medicine, Faculty of Medicine, University of Szeged, Szeged

Division of General Surgery, Department of Surgery, David Geffen School of Medicine at University of California Los Angeles; Los Angeles

Doctoral School of Theoretical Medicine, Faculty of Medicine, University of Szeged, Szeged

Szeged

2023

List of publications related to the subject of the thesis

I. **Zsófia Gabriella Pesei**, Zsanett Jancsó, Alexandra Demcsák, Balázs Csaba Németh, Sandor Vajda, Miklós Sahin-Tóth: Preclinical testing of dabigatran in trypsin-dependent pancreatitis. *JCI Insight.* 2022; 7(21), e161145. doi:10.1172/jci.insight.161145. **IF_{2021}: 9.484, D1**

II. **Zsófia Gabriella Pesei***, Balázs Csaba Németh*, Eszter Hegyi, Ákos Szücs, Andrea Szentesi, Péter Hegyi, Mark E. Lowe, Miklós Sahin-Tóth: The common truncation variant in pancreatic lipase related protein 2 (*PNLIPRP2*) is expressed poorly and does not alter risk for chronic pancreatitis. *PloS One.* 2018;13(11),e0206869. doi:10.1371/journal.pone.0206869. **IF_{2018}: 2.776, Q1**

*These authors contributed equally.

List of publications not related to the subject of the thesis

I. András Salamon, Rita Török, Evelin Sümegi, Fanni Boros, **Zsófia Gabriella Pesei**, Máté Fort Molnár, Gábor Veres, Dénes Zádori, László Vécsei, Péter Klivényi: The effect of physical stimuli on the expression level of key elements in mitochondrial biogenesis. *Neurosci Lett.* 2019; 698:13-18. doi: 10.1016/j.neulet.2019.01.003. **IF_{2019}: 2.274, Q3**

II. Fanni Annamária Boros, Rita Török, Evelin Vágvölgyi-Sümegi, **Zsófia Gabriella Pesei**, Péter Klivényi, László Vécsei. Assessment of risk factor variants of LRRK2, MAPT, SNCA and TCEANC2 genes in Hungarian sporadic Parkinson's disease patients. *Neurosci Lett.* 2019; 706:140-145. doi: 10.1016/j.neulet.2019.05.014. **IF_{2019}: 2.274, Q3**

Number of full publications:	4
First author publications:	2
Cumulative impact factor:	16.808

Table of contents

List of abbreviations

AP, acute pancreatitis
CEL, carboxyl ester lipase
CEL-HYB1, carboxyl ester lipase hybrid allele 1
CFTR, cystic fibrosis transmembrane conductance regulator
CLDN2, claudin 2
CI, confidence interval
CP, chronic pancreatitis
CPA1, carboxypeptidase A1
CTRB1-CTRB2, chymotrypsin B1-B2
CTRC, chymotrypsin C
dbSNP, single nucleotide polymorphism database (https://www.ncbi.nlm.nih.gov/snp)
ER, endoplasmic reticulum
HEK 293T, human embryonic kidney cell line 293T
k_{cat}, catalytic constant
K_i, inhibitory constant
K_M, Michaelis-Menten constant
nt, nucleotide
PCR, polymerase chain reaction
PDB, protein data bank
PNLIP, pancreatic lipase
PNLIPRP2, pancreatic lipase related protein 2
OR, odds ratio
PRSS1, protease serine 1, human cationic trypsinogen or trypsin
PRSS2, protease serine 2, human anionic trypsinogen or trypsin
PRSS3, serine protease 3, human mesotrypsinogen or mesotrypsin
RAP, recurrent acute pancreatitis
SPINK1, serine protease inhibitor Kazal type 1
T7, mouse cationic trypsinogen or trypsin, isoform T7
T8, mouse anionic trypsinogen or trypsin, isoform T8
T9, mouse anionic trypsinogen or trypsin, isoform T9
T20, mouse cationic trypsinogen or trypsin, isoform T20
T7D23A, mouse model with p.D23A mutation in T7 trypsinogen
T7K24R, mouse model with p.K24R mutation in T7 trypsinogen
T7D22N,K24R, mouse model with p.D22N and p.K24R mutations in T7 trypsinogen
TRPV6, transient receptor potential cation channel subfamily V member 6
VNTR, variable number tandem repeat

I. Introduction

The inflammatory diseases of the pancreas include acute pancreatitis (AP), recurrent acute pancreatitis (RAP), and chronic pancreatitis (CP). These clinical syndromes form a disease continuum, and CP often presents as a progressive, relapsing-recurring disorder, starting with an episode of AP, followed by RAP, and eventually progressing to end-stage CP [1]. Owing to functional impairment and destruction of the endocrine and exocrine pancreas, CP leads to an inevitable decline in the quality of life associated with significant healthcare costs [2,3]. The AP-RAP-CP progression is driven by environmental or genetic risk factors [4]. Modifiable environmental risk factors include chronic alcohol consumption and smoking, while genetic alterations mostly affect genes encoding pancreatic digestive enzymes [5,6].

Genetic variants that modify risk for CP can be classified into mechanistic pathways that explain their pathogenic effect. There are at least 3 major categories recognized to date, the trypsin-dependent, the misfolding-dependent and the ductal pathways (Figure 1) [7]. The trypsin-dependent pathway of genetic risk comprises gene variants that regulate intrapancreatic trypsin activity. These include the serine protease 1 and 2 (*PRSS1, PRSS2*) genes that encode human cationic and anionic trypsinogen, respectively, the serine protease inhibitor Kazal type 1 (*SPINK1*) gene, the chymotrypsin C (*CTRC*) gene, and the chymotrypsin B1-B2 (*CTRB1-CTRB2*) gene locus [6,7]. The misfolding-dependent pathway of genetic risk includes genes and variants that induce misfolding of digestive enzymes, and result in harmful endoplasmic reticulum (ER) stress in the pancreatic acinar cells. Variants in the carboxypeptidase A1 (*CPA1*) gene, a subset of *PRSS1* variants, rare mutations in carboxyl ester lipase (*CEL*), a hybrid allele (*CEL-HYB1*) between *CEL* and its pseudogene *CELP*, a few *CTRC* variants and some rare pancreatic lipase (*PNLIP*) variants belong to this group [8,9]. Finally, the ductal pathway of genetic risk comprises genetic alterations in proteins expressed by the ductal epithelium that typically function as ion-channels and may regulate ductal secretion. Variants in the cystic fibrosis transmembrane conductance regulator (*CFTR*) gene, the claudin 2 (*CLDN2*) gene locus, the *TRPV6* gene and possibly the calcium-sensing receptor (*CASR*) gene fit into this category. [7,10]. The present thesis focuses on the misfolding and trypsin-dependent pathways.

Mutations in digestive enzymes can increase risk for the development of CP through protein misfolding and consequent ER stress, which indicates maladaptive activation of the unfolded protein response pathways [8]. A number of genetic variants that induce enzyme misfolding affect lipase genes, such as the *CEL* and *PNLIP*. Rare single-nucleotide deletions in the variable number tandem repeat (VNTR) region of the *CEL* gene cause maturity-onset diabetes of the

young (CEL-MODY) with fatty pancreas, pancreatic cysts, and pancreatic insufficiency [11]. Functional studies demonstrated that the mutant CEL protein variant was retained inside the cell leading to ER stress and acinar cell damage [12,13]. More frequently, a hybrid allele (*CEL-HYB1*) between *CEL* and its pseudogene *CELP* alters the VNTR region and causes misfolding, thereby increasing the risk of CP [14]. Mouse models with *CEL-HYB1* developed relatively mild, progressive CP, with acinar cell atrophy, fibrosis, macrophage infiltration, acinar-to-ductal metaplasia, and serum amylase elevation [15,16]. This phenotype was highly similar, if not identical, to that of the *CPA1 N256K* mice, the first mouse model of misfolding-dependent CP, carrying the human pancreatitis-associated *CPA1* mutation p.N256K in the mouse *Cpa1* gene [17]. In 2017, two brothers suffering from lipase deficiency were reported to carry the homozygous p.T221M *PNLIP* missense mutation [18]. Although the brothers were not evaluated for CP, their low fecal elastase levels suggested pancreatic insufficiency, in all likelihood secondary to CP. Functional analyses revealed that the mutation induced misfolding of the PNLIP protein, and ER stress in cell culture [19]. Subsequently, a handful of other PNLIP variants were shown to have the same misfolding phenotype in cell culture, although their association with CP was not established [9]. Recently, it has been demonstrated that mice carrying the p.T221M PNLIP variant develop signs of CP including progressive pancreatic atrophy, acinar cell loss, fibrosis, fatty change, immune cell infiltration and reduced exocrine function [20]. Similarly to *PNLIP*, variants in the pancreatic lipase related protein 2 (*PNLIPRP2*) gene, might increase the risk for CP. PNLIPRP2 is homologous to PNLIP, and both belong to the same lipase gene family [21,22]. Unlike PNLIP, PNLIPRP2 is expressed at lower levels, and it has lipase activity against phospholipids and galactolipids beside triglycerides [21]. The relatively common nonsense *PNLIPRP2* variant p.W358X results in a truncated protein. When expressed in transfected HEK 293T cells [23,24], the mutant PNLIPRP2 protein was secreted poorly, and it formed detergent-insoluble aggregates inside the cells. The intracellular aggregates activated the unfolded protein response. These findings suggested that the p.W358X *PNLIPRP2* variant might be a risk factor for CP, however, genetic evidence has been lacking.

In the last decades, genetic studies revealed that mutations of digestive enzymes and their inhibitor contribute to pancreatitis onset and progression through increasing the risk of ectopic, intrapancreatic activation of the digestive protease precursor trypsinogen to its active form trypsin [6,7,25]. Gain-of–function mutations in *PRSS1* block or diminish protective trypsinogen degradation or accelerate trypsinogen autoactivation. Loss-of-function mutations in *SPINK1*

and *CTRC* compromise the antitrypsin defenses, i.e. trypsinogen degradation by CTRC and trypsin inhibition by SPINK1 [6]. Variant p.G191R in the *PRSS2* gene creates a trypsin-sensitive autolytic site and sensitizes anionic trypsinogen for autodegradation [26]. As a result, variant p.G191R protects against CP. Similarly, a common deletion of trypsinogen pseudogenes downregulates *PRSS2* expression and affords some level of protection against CP [27]. Finally, a frequent inversion at the *CTRB1-CTRB2* locus results in elevated *CTRB2* expression, which can degrade anionic trypsinogen and thereby reduce the risk for CP [28].

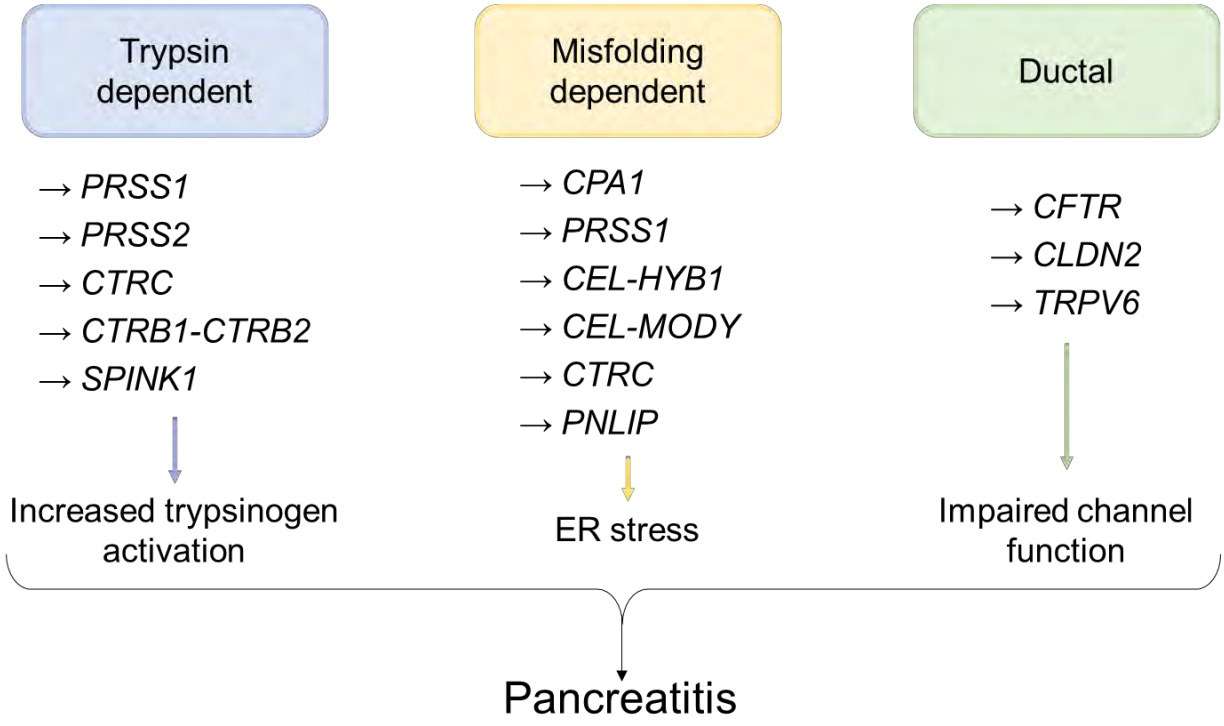

Figure 1. Pathological pathways of genetic risk in CP.

The pathogenic role of trypsinogen in CP has been confirmed by multiple mouse models from the Sahin-Tóth laboratory. These mice carry mutations in mouse cationic trypsinogen (isoform T7) [29,30]. The *T7D23A* and *T7K24R* strains harbor mutations p.D23A and p.K24R in the trypsinogen activation peptide that directly accelerate autoactivation by 50- and 5-fold, respectively. *T7D23A* and *T7K24R* mice exhibit different phenotypes with respect to pancreatic disease. Heterozygous *T7D23A* mice develop spontaneous, early-onset AP with rapid progression to CP. Homozygous *T7K24R* mice do not have spontaneous AP or CP, but exhibit more severe disease than C57BL/6N control mice when AP is induced experimentally by repeated cerulein injections. Furthermore, after the acute episode, *T7K24R* mice continue to progress to CP while control C57BL/6N mice recover rapidly [31]. Thus, the rate of autoactivation of the mutant trypsinogens is the key determinant of the pancreatitis phenotype in mice. This notion was further supported by the *T7D22N,K24R* trypsinogen mutant mouse

model, which exhibits different pancreatic diseases as a function of zygosity [32]. Thus, heterozygous *T7D22N,K24* mice behave like *T7K24R* mice, whereas homozygous *T7D22N,K24R* mice develop spontaneous CP, similarly to *T7D23A* mice. In addition to the knock-in models described above, the laboratory of Dr. Baoan Ji developed several transgenic lines with human *PRSS1* and *PRSS2* genes. These mice exhibit phenotypes similar to those of the *T7K24R* and *T7D23R* mice. Together, the availability of these models sets the stage for preclinical drug testing for the treatment of CP [33].

The genetic, biochemical, and animal modeling evidence identify trypsin as a clear therapeutic target. Although early preclinical testing of trypsin inhibitors like bovine pancreatic trypsin inhibitor (BPTI, aprotinin) [34], and the p-guanidino-benzoate derivatives, camostat (FOY-305), nafamostat (FUT-175) [35], and gabexate (FOY) [36] yielded promising results in rodents [37-44], human clinical trials did not provide convincing evidence for their efficacy [45-50 and references therein]. We note, however, that trypsin-dependent mouse models, such as *T7K24R* and *T7D23A*, were unavailable at the time of these experiments, and clinical trials did not focus on trypsin-dependent disease, which could be verified by appropriate genetic testing. In 2019, the Baoan Ji laboratory reported that the anticoagulant dabigatran etexilate cured/reversed cerulein-induced pancreatitis in transgenic mice carrying human *PRSS1* with the p.R122H mutation (named PRSS1^{R122H} mice in their study). The p.R122H mutation is the most commonly found *PRSS1* variant in hereditary and familial forms of CP [6]. Dabigatran etexilate (brand name PRADAXA) is used worldwide as an orally active, reversible thrombin inhibitor for long-term anticoagulation of patients with atrial fibrillation [51-53]. After absorption from the gastrointestinal tract, the prodrug is converted by nonspecific esterases in the blood to its active form, dabigatran [54]. Dr. Ji and coworkers speculated that the anti-coagulation activity of dabigatran may explain the beneficial effect in pancreatitis. However, dabigatran is a benzamidine derivative and it has been reported to inhibit bovine trypsin with an inhibitory constant (K_i) of 50.3 nM [55]. Therefore, we hypothesized that the observed therapeutic effect of dabigatran in the PRSS1^{R122H} transgenic mice was due to trypsin inhibition in the pancreas rather than inhibition of thrombin in the circulation.

II. Aims

Aim 1. *Genetic analysis of the c.1074G>A (p.W358X) variant in CP*. Our goal was to test the hypothesis that the common *PNLIPRP2* truncation variant p.W358X increases risk for CP.

Aim 2. *Preclinical testing of dabigatran in trypsin-dependent pancreatitis*. Our goal was to test the anticoagulant dabigatran as a trypsin inhibitor against human and mouse trypsin isoforms, and to evaluate the therapeutic efficacy of the prodrug dabigatran etexilate in the *T7K24R* and *T7D23A* mouse models of trypsin-dependent pancreatitis.

III. Materials and Methods

III.1. Genetic analysis of the c.1074G>A (p.W358X) PNLIPRP2 variant in CP

III.1.1. Nomenclature

Nucleotide numbering follows coding DNA numbering with the first nucleotide of the ATG translation initiation codon designated as +1. Amino acids are numbered starting with the initiator methionine of the primary translation product of *PNLIPRP2*. The NCBI genomic reference sequence for *PNLIPRP2* (NC_000010.11, Homo sapiens chromosome 10, GRCh38.p12 primary assembly) and the NCBI coding DNA reference sequence (NM_005396.4) correspond to the minor truncation allele. We used the major full-length *PNLIPRP2* allele as reference for the designation of all *PNLIPRP2* variants. In this manner, the nonsense p.W358X variant becomes the "effect" allele, which is the biologically meaningful representation. Table 1 compares *PNLIPRP2* variant designations using the two different reference sequences and lists the dbSNP numbers for unambiguous identification.

Table 1. Designation of *PNLIPRP2* variants with respect to the NCBI reference sequence corresponding to the minor truncation allele and the full-length major allele used as the reference in this study. The truncation variant is highlighted in bold type. I-10, intron 10; E-11, exon 11; I-11, intron 11; nt, nucleotide; aa, amino acid; dbSNP, single nucleotide polymorphism database (https://www.ncbi.nlm.nih.gov/snp).

		NCBI reference minor truncation allele		**Reference used in this work major full-length allele**	
	dbSNP number	nt change	aa change	nt change	aa change
I-10		c.1070-379delG		c.1070-379delG	
I-10	rs4751994	c.1070-321C>T		c.1070-321T>C	
E-11	rs4751995	c.1074A>G	p.X358W	**c.1074G>A**	**p.W358X**
E-11	rs4751996	c.1084A>G	p.I362V	c.1084G>A	p.V362I
E-11	rs10885997	c.1161A>G	p.S387=	c.1161G>A	p.S387=
I-11	rs7910135	c.1181+55C>A		c.1181+55A>C	

III.1.2. Study subjects

For this study, we used de-identified genomic DNA samples from the registry of the Hungarian Pancreatic Study Group (ethical approval number TUKEB 22254-1/2012/EKU; biobanking approval number IF702-19/2012). Subjects were recruited from 11 Hungarian centers between

2012 and 2018, and all gave informed consent according to the ethical guidelines of the Declaration of Helsinki. This study was also approved by the Institutional Review Board at Boston University ("Analysis of susceptibility genes in patients with chronic pancreatitis"; IRB number H-35382). A total of 256 unrelated patients with CP, including 104 with non-alcoholic CP and 152 with alcoholic CP and 200 control subjects with no pancreatic disease were analyzed. The CP study cohort included patients with a history of recurrent acute pancreatitis and/or pathological imaging findings consistent with CP, such as pancreatic calcifications, duct dilatation or irregularities, with or without exocrine pancreatic insufficiency or diabetes. Patient characteristics are described in Table 2. Alcoholic CP was diagnosed in CP cases with alcohol consumption of more than 80 g/day (men) or 60 g/day (women) for at least two years. De-identified pancreatic cDNA and matching genomic DNA samples (n = 9) from cadaveric donors were obtained from the University of Szeged, Hungary.

III.1.3. DNA sequencing

Primer sequences and amplicon sizes are listed in Table 3. PCR reactions were performed using 1.0 U HotStar Taq DNA polymerase (Qiagen, Valencia, CA), 0.2 mM dNTP, 2.0 µL 10x PCR buffer (Qiagen), 0.5 µM primers, and 10–50 ng genomic DNA or cDNA template in a total volume of 20 µL. Cycling conditions were as follows: 15-min initial heat activation at 95 ^{o}C; 40 cycles of 30 s denaturation at 94 ^{o}C, 30 s annealing at 60 ^{o}C, and 60 s extension at 72 ^{o}C; and final extension for 5 min at 72 ^{o}C. Products were verified by 1.5% agarose gel electrophoresis. PCR amplicons (5 µL) were treated with 1 µL FastAP Thermosensitive Alkaline Phosphatase and 0.5 µL Exonuclease I (Thermo Fisher Scientific, Waltham, MA) for 15 min at 37 ^{o}C and the reaction was stopped by heating the samples to 85 ^{o}C for 15 min. Sanger sequencing was performed using the forward PCR primers as sequencing primer. Amplicons containing the heterozygous c.1070-379delG variant were also sequenced with the reverse primer.

Table 2. Study population. Mean age ± standard deviation (years) are shown. CP, chronic pancreatitis; NACP, non-alcoholic chronic pancreatitis; ACP, alcoholic chronic pancreatitis. M, male; F, female.

	All CP *n=256*		**NACP *n=104***		**ACP *n=152***		**Controls *n=200***	
Gender	M 194	F 62	M 60	F 44	M 134	F 18	M 113	F 87
Age, recruitment	56±10	56±14	57±12	57±16	55±10	53±9	52±12	52±13
Age, disease onset	48±12	48±16	47±12	48±18	48±12	48±9	-	-

Table 3. Oligonucleotide primers used for PCR amplification of exon 11 of *PNLIPRP2* from genomic DNA (e11 primers, amplicon size 836 bp), and a portion of the *PNLIPRP2* coding sequence from pancreatic cDNA (RT primers, amplicon size 732 bp). The annealing temperature was 60 ºC for both primer sets.

Primer name	Sequence (5'>3')
PNLIPRP2 e11 forward	GTT CTG GAG GAT GGA AAT CTG
PNLIPRP2 e11 reverse	CAA AAG GAG TTA GCA CAT GAC T
PNLIPRP2 RT forward	CAT CTG GAT TTC TTT CCA AAT GG
PNLIPRP2 RT reverse	CGA GTG CAT TAA AGA TTT TAT TAC CG

III.2. Preclinical testing of dabigatran in trypsin-dependent pancreatitis

III.2.1. Materials

Bovine trypsin (catalog number LS003707) was purchased from Worthington Biochemical Corporation and was active-site titrated with p-nitrophenyl p'-guanidino-benzoate (catalog number N-8010, MilliporeSigma) [56]. Ecotin was produced and purified as reported previously [57]. The concentration of ecotin was determined by titration against active-site titrated bovine trypsin. Recombinant human pro-enterokinase (catalog number 1585-SE-010) was purchased from R&D Systems and was activated with human cationic trypsin. The trypsin substrate GPR-pNA (catalog number 4000768.0100) was purchased from Bachem Americas. Benzamidine hydrochloride (code number 401790050) was obtained from Acros Organics (through Thermo Fisher Scientific) and dissolved in distilled water to prepare a 100 mM stock solution, which was further diluted with distilled water to a 10 mM working solution. Dabigatran etexilate mesylate (catalog number D100150) and dabigatran (catalog number D100090) were purchased from Toronto Research Chemicals. Dabigatran used for biochemical studies was dissolved in 0.1N HCl first to prepare an 800 μM stock solution, which was further diluted with distilled water to a 10 μM working solution.

III.2.2. Modeling dabigatran binding to trypsin

The dabigatran chemical structure was downloaded from the PubChem database (https://pubchem.ncbi.nlm.nih.gov/). The human mesotrypsin structure 1H4W was downloaded from the Protein Data Bank (PDB) [58]. The docking was carried out by the docking server ClusPro LigTBM (https://ligtbm.cluspro.org/) [59]. The program performed a similarity search in the PDB database to find all trypsin structures or homologs cocrystallized with ligands similar to dabigatran as templates. An ensemble of 1,000 initial conformations was generated

for the ligand. For each template, all conformers were aligned to the template, and only 1 conformer with the lowest root mean square deviation was retained. The resulting protein-ligand structures were subjected to energy minimization to remove possible clashes and "relax" the ligand [60].

III.2.3. Expression, purification, and activation of trypsinogens

Recombinant human and mouse trypsinogens were expressed in *Escherichia coli* BL21(DE3) (Invitrogen), refolded in vitro, and purified by ecotin affinity chromatography (Pharmacia FPLC), according to published protocols [57,61,62]. Sulfated human trypsinogens were purified from archived samples of human pancreatic juice, as described previously, with minor modifications [63,64]. Briefly, 50 mg freeze-dried pancreatic juice was dissolved in 2 mL 10 mM HCl, clarified by centrifugation (21,000g, 5 minutes, 4°C), and loaded onto a MonoQ 5/50 GL column equilibrated with 20 mM Tris-HCl (pH 8.0). Proteins were eluted with a 0–0.5 M NaCl gradient at 1 mL/min flow rate for 30 minutes. The fractions containing the cationic and anionic trypsinogens were further purified with ecotin affinity chromatography. The concentration of trypsinogen preparations was estimated from their UV absorbance at 280 nM using the extinction coefficients reported previously for mouse trypsinogens [62] and 37,525, 38,890, and 41,535/M/cm for human cationic trypsinogen (PRSS1), anionic trypsinogen (PRSS2), and mesotrypsinogen (PRSS3), respectively. To activate trypsinogen to trypsin, approximately 1 μM solution was incubated at 37 °C with 28.2 ng/mL human enterokinase (final concentration) in 0.1 M Tris-HCl (pH 8.0), 10 mM $CaCl_2$, and 0.05% Tween 20 for 1 hour. The activation reaction was followed by measuring trypsin activity: 2 μL trypsin was diluted in 48 μL assay buffer [0.1 M Tris-HCl (pH 8.0), 1 mM $CaCl_2$, and 0.05% Tween 20], and 150 μL of 200 μM GPR-pNA trypsin substrate (in assay buffer) was added. Substrate cleavage resulting in the release of the yellow p-nitroaniline was monitored for 1 minute in a Spectramax Plus 384 microplate reader at 405 nm.

III.2.4. Active-site titration of trypsin

The concentration of trypsin solutions was determined by titration with the trypsin inhibitor ecotin. Briefly, a 2-fold serial dilution of ecotin was prepared in 100 μL assay buffer in a microplate, 100 μL of trypsin solution was added, and the mixture was incubated at 24°C for 30 minutes. The final ecotin concentrations in the 200 μL volume were 0, 0.78, 1.56, 3.1, 6.25, 12.5, 25, and 50 nM, and the final nominal trypsin concentration was 10 nM. Trypsin activity was measured after adding 5 μL of 6 mM GPR-pNA substrate to each well, as described above. The trypsin activity was plotted as a function of the ecotin concentration, and the true trypsin

concentration was determined from the extrapolated x intercept of the linear portion of the inhibition curve.

III.2.5. Enzyme kinetic measurements

Michaelis-Menten kinetic parameters of trypsin isoforms were determined with the chromogenic substrate GPR-pNA at 24 °C. The trypsin concentration was 1 nM and the substrate concentration was varied typically between 1.56 and 200 μM in a final volume of 200 μL assay buffer. The substrate concentration range was 3.1–400 μM for mouse trypsin isoform T7 and 0.4–50 μM for mouse trypsin isoform T20. K_m and k_{cat} values were calculated from hyperbolic fits to plots of reaction velocity versus substrate concentration.

III.2.6. Measuring competitive inhibition by benzamidine and dabigatran

Trypsin isoforms were preincubated with increasing concentrations of benzamidine or dabigatran for 15 minutes at 24 °C, in 100 μL assay buffer. Michaelis-Menten kinetic parameters were then measured after adding 100 μL trypsin substrate, as described above. The final trypsin concentration in the assay was 1 nM, the final benzamidine concentrations were from 12.5 to 100 μM, and the final dabigatran concentrations were from 25 to 200 nM, as indicated in Tables 13 and 14. To determine the K_i, the K_m values were plotted as a function of the inhibitor concentration, and the K_i was calculated by dividing the y axis intercept with the slope of the linear fit. This value corresponds to the negative of the x axis intercept. Alternatively, the substrate saturation curves obtained in the absence and presence of the increasing inhibitor concentrations were globally fitted to the competitive inhibition equation $y = v_{max} \times (x/[K_{mObs} + x])$, where y is the reaction velocity, v_{max} is the maximal velocity, x is the substrate concentration, and $K_{mObs} = K_m \times (1 + [I]/K_i)$, where [I] is the inhibitor concentration. Experiments were performed 3 times and each experiment was analyzed separately. The reported K_i values thus represent the mean (± standard deviation) of 3 determinations. Kinetic analysis was performed with the Prism 8 program (GraphPad).

III.2.7. Experimental animals

The generation and properties of the *T7D23A* and *T7K24R* mice carrying trypsinogen mutations were described recently [29,30]. Heterozygous *T7D23A* and homozygous *T7K24R* mice were used. Protocols for genotyping have been reported earlier [29,30]. C57BL/6N mice were purchased from Charles River Laboratories or produced in our breeding facility from the same stock. Both male and female mice were studied. The number of mice used in the experiments is shown in the figures.

III.2.8. Cerulein-induced pancreatitis in *T7K24R* mice

Pancreatitis was induced in *T7K24R* mice with 8 hourly intraperitoneal injections of the secretagogue peptide cerulein used in a dose of 50 μg/kg. Cerulein (catalog number C9026, MilliporeSigma) was dissolved in sterile normal saline at 10 μg/mL concentration. Mice were sacrificed 96 hours from the first cerulein injection, as indicated, and the pancreas and blood were harvested. Details of histological analysis and measurement of plasma amylase (4 μL assayed) were reported previously [29–31].

III.2.9. Intrapancreatic protease activity in *T7K24R* mice

Trypsin and chymotrypsin activities were measured from freshly prepared pancreas extracts of C57BL/6N and *T7K24R* mice using our recently published protocol [65]. Activity was expressed as the rate of substrate cleavage in relative fluorescent units per second, normalized to the total protein concentration in milligrams.

III.2.10. Dabigatran etexilate treatment of *T7D23A* and *T7K24R* mice

Mice were administered dabigatran etexilate orally either by intragastric gavage of a 20 mg/mL solution to a final dose of 100 or 200 mg/kg using a 24 gauge, 1 inch long feeding needle (catalog number FN7900, Roboz Surgical) or by feeding with solid chow containing the prodrug in 10 mg/g concentration, as indicated in the experimental design. With these treatment protocols, no bleeding, morbidity, or mortality were observed. We note, however, that after administration of dabigatran etexilate, further injections or biopsies were not possible without the risk of significant bleeding. We also inspected hematoxylin-eosin–stained sections of liver, intestine, and kidney from mice treated with dabigatran etexilate or vehicle but found no signs of organ damage. Control mice were given gavage of the vehicle solution or regular chow.

III.2.11. Preparation of gavage solution and solid chow containing dabigatran etexilate

Dabigatran etexilate solution was always freshly prepared before use by dispersing 20 mg prodrug in 1 mL of 35% Captisol solution in a bath-type sonicator (5510 DTH Ultrasonic Cleaner, Branson) for 5–10 minutes at 24°C. Captisol (β-cyclodextrin sulfobutyl ethers, sodium salts, lot number NC-04A-180185) was obtained from Cydex Pharmaceuticals (through Thermo Fisher Scientific) and was dissolved in sterile normal saline (3.5 g in 10 mL). Dabigatran etexilate–containing chow was prepared using regular chow (5053 PicoLab Rodent Diet 20, LabDiet), which was pulverized with a pestle in a ceramic mortar. Solid dabigatran etexilate mesylate (1 g) was mixed with 100 g of powdered chow (10 mg/g final prodrug concentration), and sterile distilled water was added until the chow became malleable. The mixture was then compressed into pellets using the barrel of a 10 mL plastic syringe and a

plunger (Figure 2). The prodrug-containing pellets were allowed to dry at 24 °C for 2 days and stored at 4 °C until use.

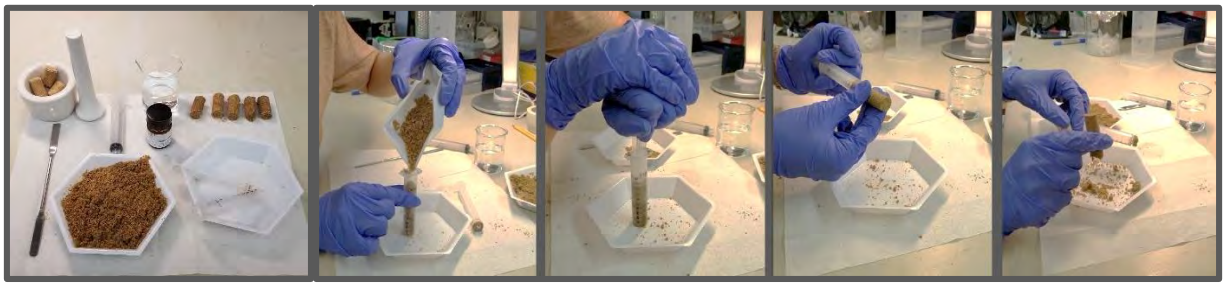

Figure 2. Preparation of solid chow with dabigatran etexilate.

III.2.12. Estimation of absorbed dabigatran etexilate

The oral bioavailability of dabigatran etexilate in humans is around 6.5%, and it is independent of dose and not influenced by food [54]. Accordingly, a 100 mg/kg dose of intragastric gavage can provide a 0.13 mg single dose of systemically absorbed dabigatran etexilate in a 20 g mouse. When dabigatran etexilate is given mixed with solid chow (10 mg prodrug/g chow), mice can consume approximately 4 g chow over a 24-hour period. This would yield a 2.6 mg daily dose of absorbed dabigatran etexilate.

III.2.13. Determination of dabigatran plasma concentration

Dabigatran in the blood plasma was quantified using the HEMOCLOT Thrombin Inhibitors (3 × 2.5 mL) kit (catalog number CK002L-RUO, Hyphen BioMed, purchased from Aniara Diagnostica) [66, 67]. Reagents were diluted according to the manufacturer's instructions. The BIOPHEN Dabigatran Plasma Calibrator set (catalog number 2222801- RUO, Hyphen BioMed, purchased from Aniara Diagnostica) was used to establish a calibration curve for the clotting time as a function of plasma dabigatran concentration. Mouse blood was collected immediately after CO_2 euthanasia. To achieve rapid anticoagulation, 20 µL of a 3.2% solution of sodium citrate was pipetted into the conus of a needle before attaching it to a 1 mL syringe and collecting approximately 180 µL blood by cardiac puncture. Cellular blood elements were sedimented by centrifugation (2,000g, 15 minutes, 4 °C); the plasma was saved and further diluted with normal saline before use (20 µL plasma was mixed with 160 µL saline). A clean microscope slide was placed on the surface of a block heater set at 37 °C. Aliquots of reagents R1 and R2 (110 µL), and the calibrators or plasma specimen (60 µL), were pipetted onto the glass surface and preheated for 2 minutes. Reagent R1 (100 µL) was then mixed with 50 µL of the calibrator or plasma on the slide and incubated for 1 minute before addition of reagent R2 (100 µL). Time to the appearance of the first fibrin clot was measured. Clotting was detected by manual probing of the incubation mixture for fibrin threads with a small pipette tip.

III.2.14. Statistics

Results are given as mean values ± standard deviation or shown as individual data points with the mean ± standard deviation indicated. Differences between means were analyzed by unpaired 2-tailed t test for 2 groups and by 1-way ANOVA for multiple groups, with Tukey-Kramer post hoc analysis for pairwise comparison using Prism 8 (GraphPad). Statistical significance was defined as $P < 0.05$.

III.2.15. Study approval

Animal experiments were performed at the University of California Los Angeles (UCLA) with the approval and oversight of the Animal Research Committee, including protocol review and post-approval monitoring.

IV. Results

IV.1. Genetic analysis of the c.1074G>A (p.W358X) PNLIPRP2 variant in CP

IV.1.1. A common truncation variant in *PNLIPRP2*

The common truncation variant c.1074G>A (p.W358X) in *PNLIPRP2* was first described in 2003 as W357X in European, African and Chinese populations with allele frequencies of 0.53, 0.55 and 0.33, respectively [68]. A 2010 study on the association of common gene variants and human dietary habits described the variant as W358X (rs4751995) with similar allele frequencies [69]. The discrepancy in numbering is because the original cloning study of *PNLIPRP2* missed one of the two consecutive methionine codons at the start of the coding sequence [70]. Interestingly, the first methionine is encoded by a separate upstream exon, which should be counted as exon 1 of the *PNLIPRP2* gene; placing the truncation variant in exon 11. The NCBI reference sequence for *PNLIPRP2* corresponds to the minor truncation allele. To describe the truncation variant in a biologically meaningful manner, in this study we used the major full-length *PNLIPRP2* allele as reference (see Table 1).

IV.1.2. DNA sequence analysis of exon 11 of human *PNLIPRP2*

We genotyped 104 subjects with non-alcoholic CP, 152 subjects with alcoholic CP, and 200 control subjects, recruited from the registry of the Hungarian Pancreatic Study Group. We used direct DNA sequencing after PCR amplification of exon 11 and flanking intronic regions of *PNLIPRP2*. Within the amplified 793 nt sequence, we found 6 nucleotide variants, which included three intronic variants (c.1070-379delG, c.1070-321T>C, and c.1181+55A>C), one synonymous variant (c.1161G>A, p.S387=), one missense variant (c.1084G>A, p.V362I), and the truncation variant c.1074G>A (p.W358X) (Figure 3). The commonly occurring variants c.1070-321T>C, p.W358X, p.V362I, p.S387=, and c.1181+55A>C were found in linkage disequilibrium as a conserved haplotype (CAAAC in Figure 3). Another common haplotype (CGGAA in Figure 3) was formed by variants c.1070-321T>C and p.S387=. When allele frequency was considered, distribution of the variants between patients and controls showed no significant difference (Table 4). Subgroup analysis for non-alcoholic and alcoholic CP patients versus controls revealed no association either (Tables 5 and 6). We also analyzed genotypes using dominant and recessive models but found no significant differences in genotype frequencies between all CP patients or the non-alcoholic and alcoholic cohorts versus controls (Tables 7, 8 and 9). Finally, comparison of the three haplotypes between patients and controls yielded no significant differences with the exception of the CGGAA haplotype (see Figure 3), which was overrepresented in the non-alcoholic CP cohort relative to controls (OR 1.6, P 0.04)

(Tables 10, 11 and 12). We consider this a spurious association due to limited sample size and chance.

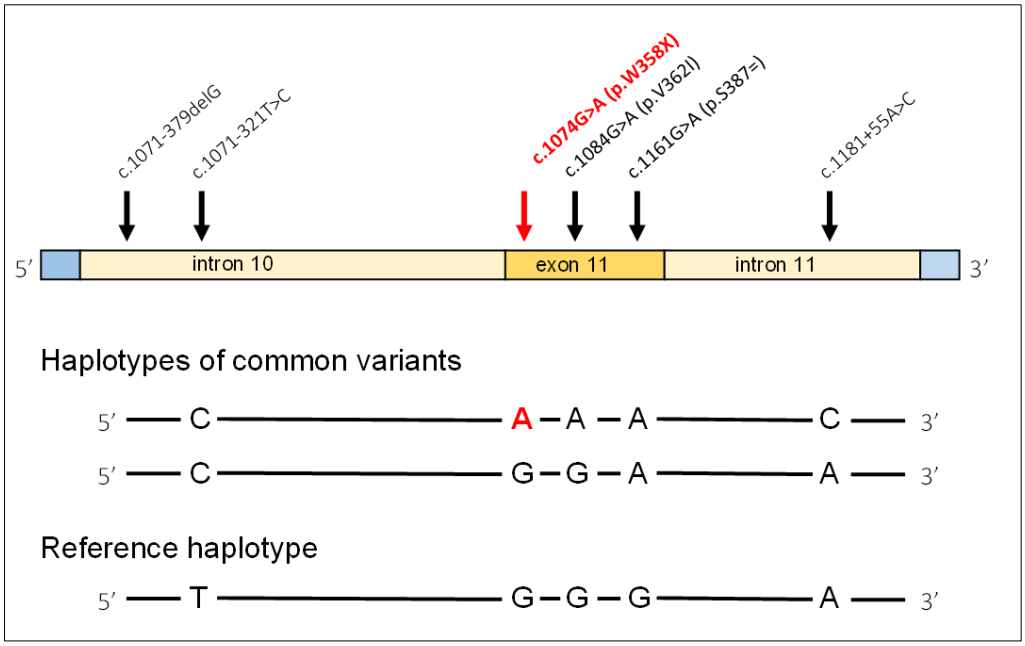

Figure 3. *PNLIPRP2* variants in exon 11 and the flanking intronic regions identified in the present study. The truncation variant is in bold type. The three haplotypes formed by the five commonly occurring variants are also shown.

Table 4. Allele frequency of *PNLIPRP2* variants in patients with chronic pancreatitis (CP) and controls without pancreatic disease. The truncation variant is highlighted in bold type. I-10, intron 10; E-11, exon 11; I-11, intron 11; nt, nucleotide; aa, amino acid; OR, odds ratio; CI, confidence interval.

	nt change	**aa change**	**CP**	**Control**	**OR**	***P***	**95% CI**
I-10	c.1070-379delG		2/512 (0.4%)	1/400 (0.3%)	1.57	0.72	0.14-17.3
I-10	c.1070-321T>C		319/512 (62.3%)	240/400 (60%)	1.1	0.48	0.84-1.4
E-11	**c.1074G>A**	**p.W358X**	**245/512 (47.9%)**	**192/400 (48%)**	**0.99**	**0.97**	**0.77-1.3**
E-11	c.1084G>A	p.V362I	245/512 (47.9%)	192/400 (48%)	0.99	0.97	0.77-1.3
E-11	c.1161G>A	p.S387=	321/512 (62.7%)	240/400 (60%)	1.12	0.4	0.86-1.5
I-11	c.1181+55A>C		246/512 (48%)	192/400 (48%)	1.0	0.99	0.77-1.3

Table 5. Allele frequency of *PNLIPRP2* variants in patients with non-alcoholic chronic pancreatitis (NACP) and controls without pancreatic disease. The truncation variant is highlighted in bold type. nt, nucleotide; aa, amino acid; OR, odds ratio; CI, confidence interval.

	nt change	**aa change**	**NACP**	**Control**	**OR**	***P***	**95% CI**
I-10	c.1070-379delG		1/208 (0.5%)	1/400 (0.3%)	1.93	0.64	0.12-31.0
I-10	c.1070-321T>C		131/208 (63%)	240/400 (60%)	1.13	0.48	0.8-1.6
E-11	**c.1074G>A**	**p.W358X**	**93/208 (44.7%)**	**192/400 (48%)**	**0.88**	**0.44**	**0.63-1.2**
E-11	c.1084G>A	p.V362I	93/208 (44.7%)	192/400 (48%)	0.88	0.44	0.63-1.2
E-11	c.1161G>A	p.S387=	131/208 (63%)	240/400 (60%)	1.13	0.48	0.8-1.6
I-11	c.1181+55A>C		94/208 (45.2%)	192/400 (48%)	0.89	0.51	0.64-1.25

Table 6. Allele frequency of *PNLIPRP2* variants in patients with alcoholic chronic pancreatitis (ACP) and controls without pancreatic disease. The truncation variant is highlighted in bold type. nt, nucleotide; aa, amino acid; OR, odds ratio; CI, confidence interval.

	nt change	**aa change**	**NACP**	**Control**	**OR**	***P***	**95% CI**
I-10	c.1070-379delG		1/304 (0.3%)	1/400 (0.3%)	1.32	0.85	0.08-21.1
I-10	c.1070-321T>C		188/304 (61.8%)	240/400 (60%)	1.08	0.62	0.8-1.5
E-11	**c.1074G>A**	**p.W358X**	**152/304 (50%)**	**192/400 (48%)**	**1.08**	**0.6**	**0.8-1.5**
E-11	c.1084G>A	p.V362I	152/304 (50%)	192/400 (48%)	1.08	0.6	0.8-1.5
E-11	c.1161G>A	p.S387=	190/304 (62.5%)	240/400 (60%)	1.1	0.5	0.82-1.5
I-11	c.1181+55A>C		152/304 (50%)	192/400 (48%)	1.08	0.6	0.8-1.5

Table 7. Genotype distribution of *PNLIPRP2* variants in patients with chronic pancreatitis (CP, entire cohort) and in controls. Data were analyzed assuming dominant (shown in italics) or recessive models of inheritance. The truncation variant is highlighted in bold type. I-10, intron 10; E-11, exon 11; I-11, intron 11; nt, nucleotide; aa, amino acid; OR, odds ratio; CI, confidence interval.

	nt change	**genotype**	**CP**	**Control**	**OR**	***P***	**95% CI**
I-10	c.1070-379delG	GG delG deldel	254/256 (99.2%) 2/256 (0.8%) 0/256 (0%)	199/200 (99.5%) 1/200 (0.5%) 0/200 (0%)	*1.57* 0.78	*0.72* 0.9	*0.14-17.4* 0.02-39.6
I-10	c.1070-321T>C	TT TC CC	37/256 (42.7%) 119/256 (43.6%) 100/256 (13.7%)	27/200 (13.5%) 106/200 (53%) 67/200 (33.5%)	*0.92* 1.27	*0.77* 0.22	*0.54-1.57* 0.87-1.9
E-11	**c.1074G>A**	GG GA AA	68/256 (26.6%) 131/256 (51.2%) 57/256 (22.2%)	50/200 (25%) 108/200 (54%) 42/200 (21%)	*0.92* 1.1	*0.7* 0.75	*0.6-1.4* 0.69-1.69
E-11	c.1084G>A	GG GA AA	68/256 (26.6%) 131/256 (51.2%) 57/256 (22.2%)	50/200 (25%) 108/200 (54%) 42/200 (21%)	*0.92* 1.1	*0.7* 0.75	*0.6-1.4* 0.69-1.69
E-11	c.1161G>A	GG GA AA	37/256 (14.5%) 117/256 (45.7%) 102/256 (39.8%)	27/200 (13.5%) 106/200 (52.5%) 67/200 (33.5%)	*0.92* 1.32	*0.77* 0.16	*0.54-1.57* 0.89-1.9
I-11	c.1181+55A>C	AA AC CC	68/256 (26.6%) 130/256 (50.8%) 58/256 (22.6%)	50/200 (25%) 108/200 (54%) 42/200 (21%)	*0.92* 1.1	*0.7* 0.67	*0.6-1.4* 0.7-1.7

Table 8. Genotype distribution of *PNLIPRP2* variants in patients with non-alcoholic chronic pancreatitis (NACP) and in controls. See Table 7 for details.

	nt change	**genotype**	**NACP**	**Control**	**OR**	***P***	**95% CI**
I-10	c.1070-379delG	GG delG deldel	103/104 (99%) 1/104 (1%) 0/104 (0%)	199/200 (99.5%) 1/200 (0.5%) 0/200 (0%)	*1.93* 1.92	*0.64* 0.75	*0.12-31.2* 0.04-97.4
I-10	c.1070-321T>C	TT TC CC	12/104 (11.5%) 53/104 (51%) 39/104 (37.5%)	27/200 (13.5%) 106/200 (53%) 67/200 (33.5%)	*1.2* 1.19	*0.63* 0.49	*0.58-2.5* 0.73-1.95
E-11	**c.1074G>A**	GG GA AA	26/104 (25%) 63/104 (60.6%) 15/104 (14.4%)	50/200 (25%) 108/200 (54%) 42/200 (21%)	*1.0* 0.63	*1.0* 0.17	*0.58-1.73* 0.33-1.2
E-11	c.1084G>A	GG GA AA	26/104 (25%) 63/104 (60.6%) 15/104 (14.4%)	50/200 (25%) 108/200 (54%) 42/200 (21%)	*1.0* 0.63	*1.0* 0.17	*0.58-1.73* 0.33-1.2
E-11	c.1161G>A	GG GA AA	12/104 (11.5%) 53/104 (51%) 39/104 (37.5%)	27/200 (13.5%) 106/200 (52.5%) 67/200 (33.5%)	*1.2* 1.19	*0.63* 0.49	*0.58-2.5* 0.73-1.95
I-11	c.1181+55A>C	GG delG deldel	103/104 (99%) 1/104 (1%) 0/104 (0%)	199/200 (99.5%) 1/200 (0.5%) 0/200 (0%)	*1.93* 1.92	*0.64* 0.75	*0.12-31.2* 0.04-97.4

Table 9. Genotype distribution of *PNLIPRP2* variants in patients with alcoholic chronic pancreatitis (ACP) and in controls. Data were analyzed assuming dominant (shown in italics) or recessive models of inheritance. The truncation variant is highlighted in bold type. I-10, intron 10; E-11, exon 11; I-11, intron 11; nt, nucleotide; OR, odds ratio; CI, confidence interval.

	nt change	**genotype**	**ACP**	**Control**	**OR**	***P***	**95% CI**
I-10	c.1070-379delG	GG delG deldel	151/152 (99.3%) 1/152 (0.7%) 0/152 (0%)	199/200 (99.5%) 1/200 (0.5%) 0/200 (0%)	*1.32* 1.32	*0.85* 0.89	*0.08-21.2* 0.03-66.6
I-10	c.1070-321T>C	TT TC CC	25/152 (16.5%) 66/152 (43.4%) 61/152 (40.1%)	27/200 (13.5%) 106/200 (53%) 67/200 (33.5%)	*0.79* 1.33	*0.44* 0.2	*0.44-1.43* 0.86-2.1
E-11	**c.1074G>A**	GG GA AA	42/152 (27.6%) 68/152 (44.8%) 42/152 (27.6%)	50/200 (25%) 108/200 (54%) 42/200 (21%)	*0.87* 1.44	*0.58* 0.15	*0.54-1.4* 0.88-2.4
E-11	c.1084G>A	GG GA AA	42/152 (27.6%) 68/152 (44.8%) 42/152 (27.6%)	50/200 (25%) 108/200 (54%) 42/200 (21%)	*0.87* 1.44	*0.58* 0.15	*0.54-1.4* 0.88-2.4
E-11	c.1161G>A	GG GA AA	25/152 (16.4%) 64/116 (42.1%) 63/116 (41.5%)	27/200 (13.5%) 106/200 (52.5%) 67/200 (33.5%)	*0.79* 1.4	*0.44* 0.13	*0.44-1.43* 0.9-2.2
I-11	c.1181+55A>C	GG delG deldel	103/104 (99%) 1/104 (1%) 0/104 (0%)	199/200 (99.5%) 1/200 (0.5%) 0/200 (0%)	*1.93* 1.92	*0.64* 0.75	*0.12-31.2* 0.04-97.4

Table 10. Distribution of common *PNLIPRP2* haplotype alleles in patients with chronic pancreatitis (CP) and in controls. The truncation haplotype is highlighted in bold type. OR, odds ratio; CI, confidence interval. See Figure 3 for more details.

Haplotype	**All CP patients**	**Controls**	**OR**	***P***	**95% CI**
CAAAC	**244/512 (47.7%)**	**191/400 (47.8%)**	**1.00**	**0.98**	**0.77-1.3**
CGGAA	73/512 (14.2%)	48/400 (12.0%)	1.22	0.32	0.83-1.8
TGGGA	191/512 (37.3%)	160/400 (40.0%)	0.89	0.41	0.68-1.2

Table 11. Distribution of common *PNLIPRP2* haplotype alleles in patients with non-alcoholic chronic pancreatitis (NACP) and in controls. The truncation haplotype is highlighted in bold type. OR, odds ratio; CI, confidence interval. See Figure 3 for more details. The asterisk indicates significant association.

Haplotype	**NACP patients**	**Controls**	**OR**	***P***	**95% CI**
CAAAC	**92/208 (44.2%)**	**191/400 (47.8%)**	**0.87**	**0.41**	**0.62-1.2**
CGGAA	38/208 (18.3%)	48/400 (12.0%)	1.64	0.040*	1.0-2.6
TGGGA	77/208 (37.0%)	160/400 (40.0%)	0.88	0.48	0.62-1.3

Table 12. Distribution of common *PNLIPRP2* haplotype alleles in patients with alcoholic chronic pancreatitis (ACP) and in controls. The truncation haplotype is highlighted in bold type. OR, odds ratio; CI, confidence interval. See Figure 3 for more details.

Haplotype	ACP patients	Controls	OR	*P*	95% CI
CAAAC	**152/304 (50.0%)**	**191/400 (47.8%)**	**1.10**	**0.55**	**0.81-1.5**
CGGAA	35/304 (11.5%)	48/400 (12.0%)	0.95	0.84	0.60-1.5
TGGGA	114/304 (37.5%)	160/400 (40.0%)	0.90	0.5	0.66-1.2

IV.1.3. Expression of the *PNLIPRP2* truncation allele

To estimate the relative mRNA expression of the full-length and truncation alleles of *PNLIPRP2*, we used direct sequencing of pancreatic cDNA after PCR amplification of a 732 nt fragment of the coding DNA. We obtained nine de-identified cDNA samples with matching genomic DNA from cadaveric donors. Sequencing of the genomic DNA identified five heterozygous samples and one sample homozygous for the truncation allele. The electropherograms of the heterozygous genomic sequences showed two signals at the position of variants p.W358X and p.V362I, with comparable peak heights (Figure 4A). Surprisingly, when heterozygous cDNA samples were sequenced, only one peak was visible at these positions, which corresponded to the major full-length allele, whereas no signal was apparent for the minor truncation allele (Figure 4B). PCR amplification of the pancreatic cDNA sample with the homozygous truncation allele confirmed the absence of detectable mRNA expression (Figure 4C). We also consulted the Genotype-Tissue Expression (GTEx) Portal (www.gtexportal.org/ home), which database is open-access public resource to study tissue-specific gene expression and its relationship to genetic variation. The project analyzes global RNA expression within individual human tissues from deeply genotyped donors and correlates variations in gene expression with genetic alterations. We found that all five common variants within the truncation haplotype were associated with diminished *PNLIPRP2* mRNA expression (Figure 5).

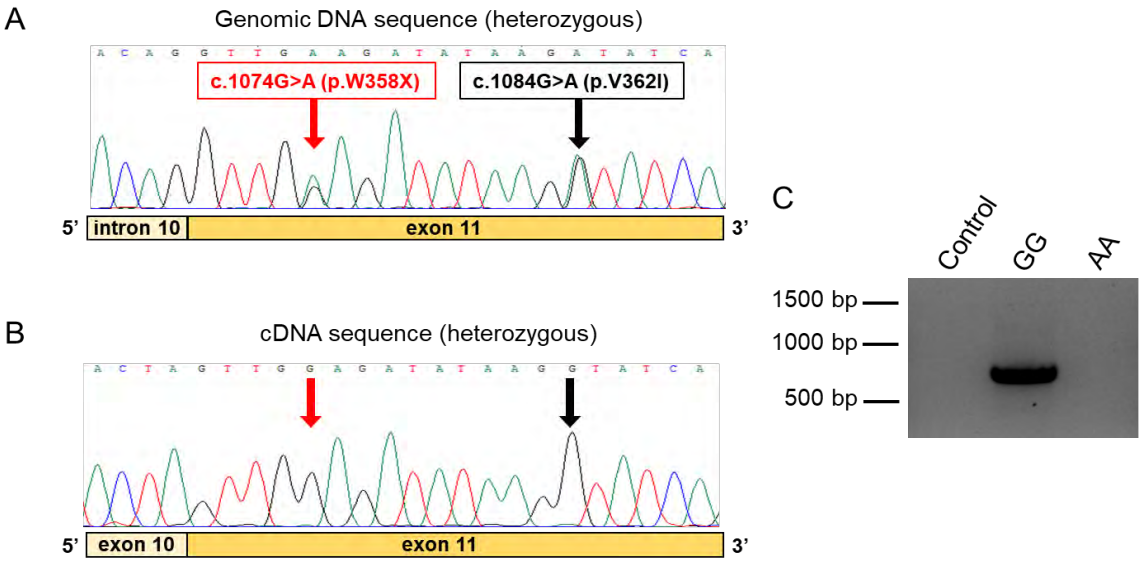

Figure 4. Expression of the *PNLIPRP2* p.W358X truncation variant. **A**, Electropherogram of genomic DNA sequence of a heterozygous carrier showing the double signal at the position of variants p.W358X and p.V362I. **B**, Electropherogram of pancreatic cDNA sequence of the same heterozygous subject. Note the absence of the signal corresponding to the minor truncation allele at the position of the variants. **C**, Agarose gel electrophoresis of PCR amplicons from pancreatic cDNA samples of subjects with homozygous AA (minor truncation alleles) and GG (full-length alleles) genotypes. Control reaction was performed with no added template.

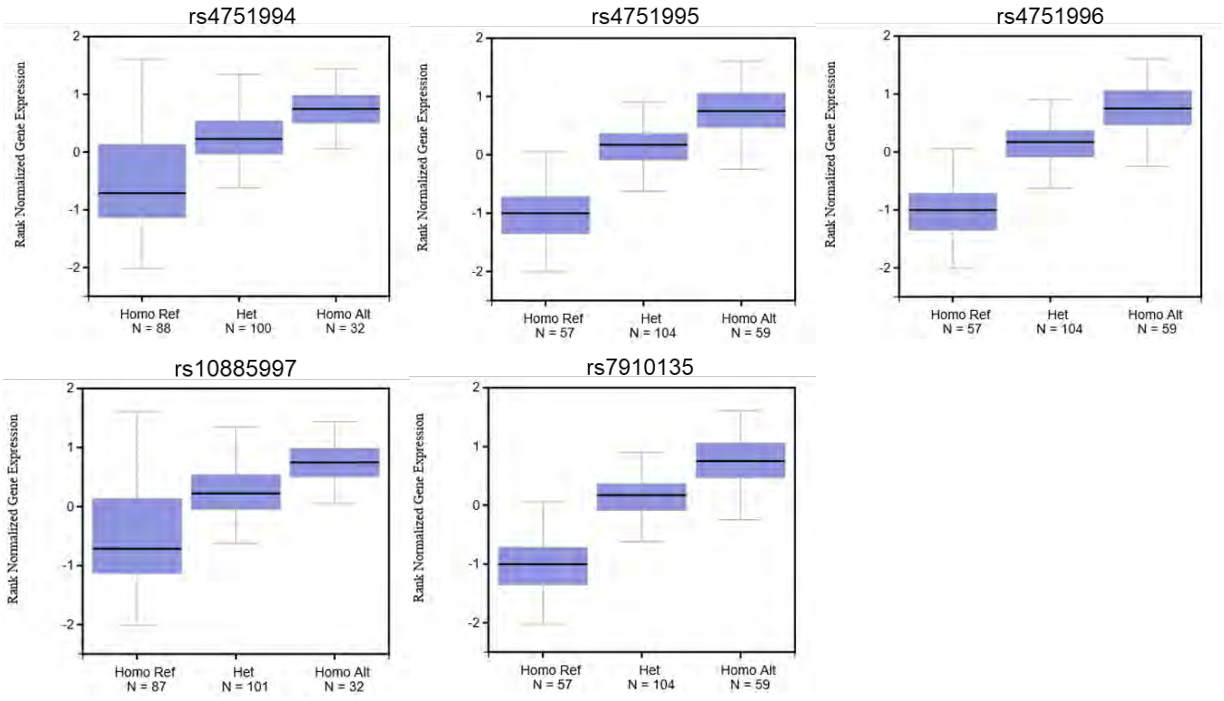

Figure 5. The effect of common *PNLIPRP2* variants on mRNA expression in the pancreas. Box plots were taken from the GTEx Portal (GTEx Analysis Release V7 - www.gtexportal.org). Note the diminished expression of the reference alleles (Ref), which correspond to the truncation haplotype in this database. See Table 1 for variant designation.

IV.2. Preclinical testing of dabigatran in trypsin-dependent pancreatitis

IV.2.1. Inhibition of trypsin by dabigatran

We hypothesized that the reported efficacy of dabigatran etexilate in pancreatitis [70] is related to the trypsin-inhibitory activity of dabigatran. As a benzamidine derivative, dabigatran is expected to inhibit trypsin-like enzymes competitively; however, this inhibitory activity against human and mouse trypsin isoforms has not been demonstrated before to our knowledge. First, we used homology-based docking to demonstrate that dabigatran can bind to the specificity pocket of trypsin. In our model, showing dabigatran docked to human mesotrypsin (PDB structure 1H4W) [58], the amidine moiety of dabigatran interacts with the side chain of Asp194 at the bottom of the specificity pocket, and the N-methyl-benzimidazole scaffold that bridges the benzamidine and the distal pyridine ring and propanoic acid end is positioned above the catalytic triad (Figure 6A). The benzamidine moiety of dabigatran overlaps with the bound benzamidine of the 1H4W mesotrypsin structure (Figure 6B). The docked conformation of dabigatran is also similar to that of the benzamidine-derivative dual-specificity thrombin and factor Xa inhibitor R11 (PubChem SID 820345) co-crystallized with bovine trypsin (PDB structure 1G36) [71]. The latter compound and dabigatran both have the benzamidine group deep in the specificity pocket, connected to an N-methyl-benzimidazole moiety. Dabigatran and R11 differ in the groups at the distal end. R11 has a second methyl-benzimidazole group that lies flat on the protein surface. In contrast, in the docked structure of dabigatran, the carboxyl group of the distal propanoic acid is partially solvent exposed, and the pyridine ring is perpendicular to the plain of the methyl-benzimidazole in R11. Most atoms of dabigatran, including the benzamidine group, are shifted by 0.6–0.8 Å toward the catalytic triad relative to the same atoms in R11 (Figure 6B). Next, we performed enzymatic measurements to compare the effect of benzamidine and dabigatran against human trypsin isoforms PRSS1, PRSS2, and PRSS3, and mouse trypsin isoforms T7 (cationic trypsin), T8, T9, and T20 (anionic trypsins). The trypsin isoforms were produced recombinantly, but human PRSS1 and PRSS2 were also purified from pancreatic juice in their native form, which contains a sulfate group on Tyr154. As a universal reference molecule, commercial bovine cationic trypsin was also assayed. Figure 7A demonstrates a representative experiment for the determination of the competitive inhibitory constant (K_i). As described in *Materials and Methods*, we calculated the K_i values by either individually (Figure 7B) or globally (Figure 7C) fitting the substrate saturation curves and obtained comparable results. Table 13 and Table 14 indicate the K_m and k_{cat} values determined in the absence and presence of increasing benzamidine and dabigatran concentrations. We show

these data to demonstrate that the k_{cat} values remained constant within experimental error across all inhibitor concentrations tested, supporting the competitive nature of the inhibition. Table 15 lists the K_i values for benzamidine and dabigatran. Benzamidine inhibited trypsin with micromolar K_i values (range 3.3–20.6 μM and 4.2–22.6 μM by individual and global fit analysis, respectively), while dabigatran was an about 200- to 400-fold stronger inhibitor, exhibiting nanomolar K_i values (range 10–65 nM and 10.3–78.9 nM by individual and global fit analysis, respectively). Anionic trypsin isoforms were inhibited slightly stronger by benzamidine than cationic trypsins; however, this trend was less conspicuous with dabigatran. Reassuringly, the K_i values reported for dabigatran against bovine trypsin [55] and measured in our experiments were essentially identical. Dabigatran inhibited human trypsins as well as or slightly better than mouse trypsins, suggesting that results from preclinical mouse experiments should be relevant to human clinical trials. The experiments demonstrate that derivatives of benzamidine, such as dabigatran, can have highly improved inhibitory activity against trypsin and are universally effective against various trypsin paralogs.

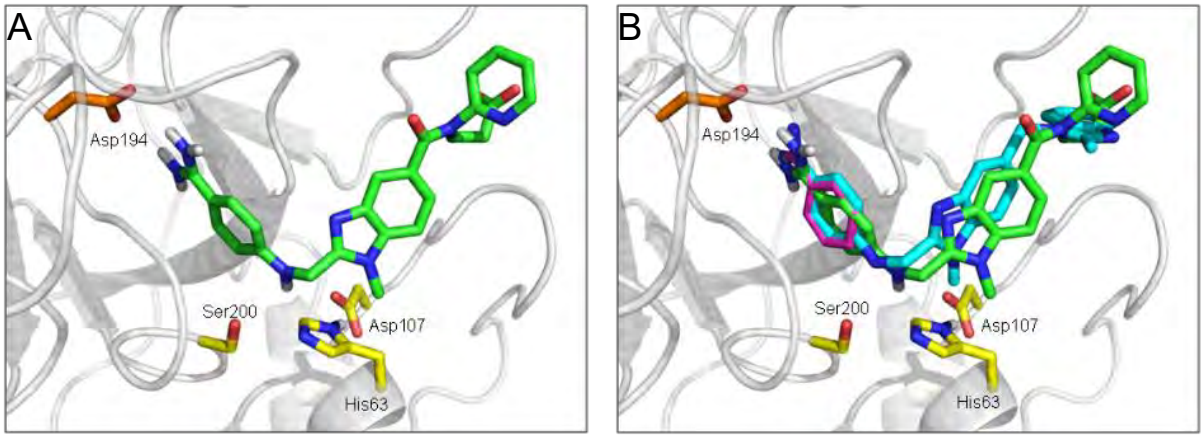

Figure 6. Modeling dabigatran binding to trypsin. **A,** Dabigatran (shown as green sticks) docked to human mesotrypsin (PDB structure 1H4W, shown as grey cartoon). Also indicated are the side chains of the catalytic triad His63, Asp107, and Ser200 (corresponding to His57, Asp102, and Ser195 in conventional crystallographic numbering) and Asp194 (Asp189) at the bottom of the specificity pocket (yellow and orange sticks, respectively). **B**, Superimposition of trypsin-bound dabigatran, with benzamidine (from PDB structure 1H4W, magenta) and the benzamidine-derivative, dual-specificity thrombin and factor Xa inhibitor R11 co-crystallized with bovine trypsin (from PDB structure 1G36, cyan). The figures were created with the PyMOL Molecular Graphics System (https://pymol.org/2/).

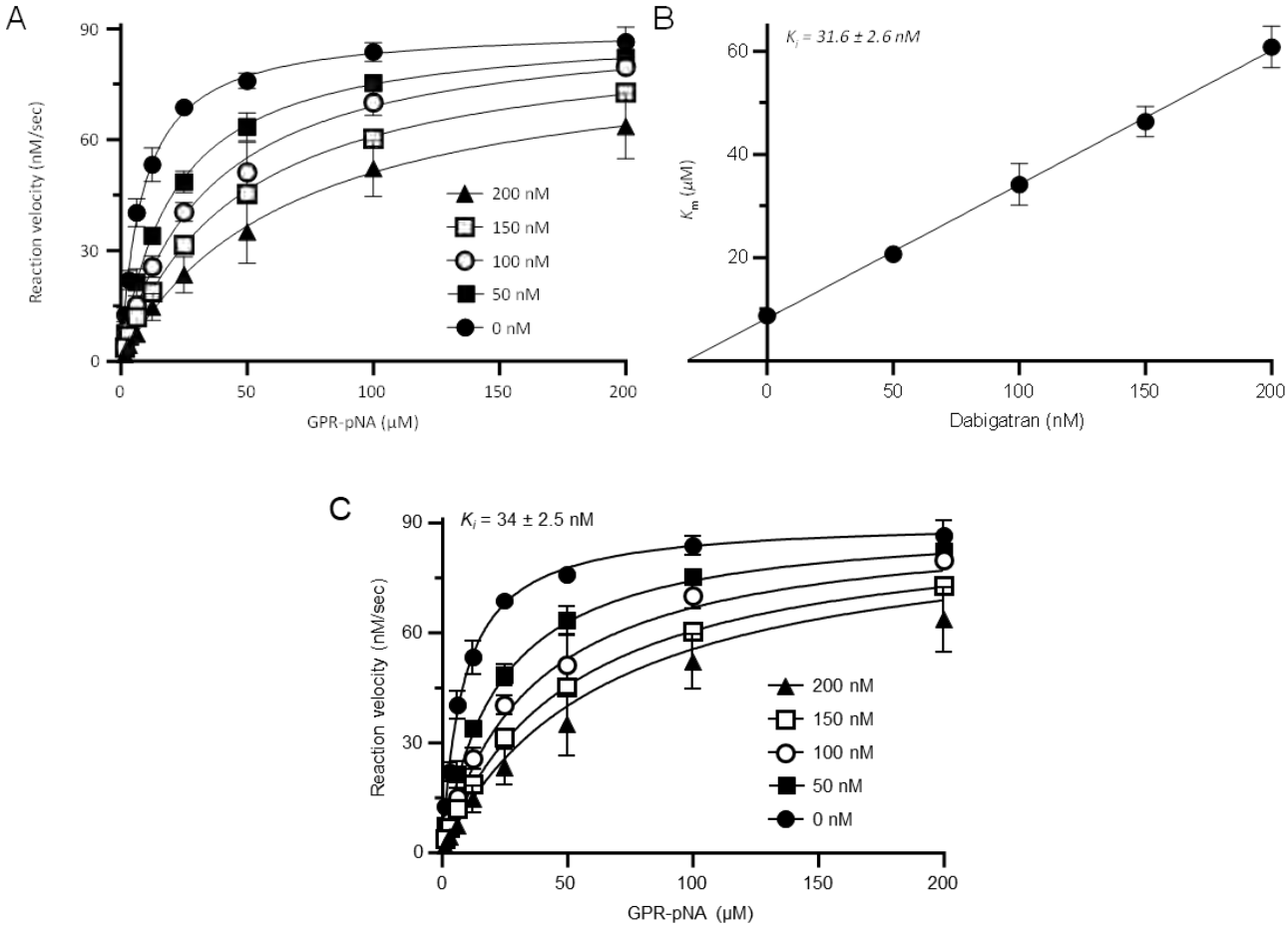

Figure 7. Inhibition of trypsin by dabigatran. Representative graphs of the kinetic assays using mouse anionic trypsin (isoform T8) are shown. Three experiments were performed. For clarity and convenience, the mean of the data points was plotted with standard deviation error bars, even though each experiment was analyzed separately. **A**, Initial rate of trypsin activity as a function of substrate concentration in the absence and presence of increasing dabigatran concentrations. Rates were measured with 1 nM trypsin and the indicated concentrations of the *N*-CBZ-Gly-Pro-Arg-*p*-nitroanilide (GPR-pNA) trypsin substrate. Data sets for given dabigatran concentrations were *individually fitted* to the Michaelis-Menten equation. **B**, Calculation of the competitive inhibitory constant (K_i) of dabigatran (mean ± standard deviation, n=3). The K_m values derived from the saturation curves in panel A were plotted as a function of the dabigatran concentration. The K_i was then determined by dividing the y axis intercept with the slope of the linear fit. This value corresponds to the negative of the x axis intercept. **C**, Calculation of the K_i of dabigatran by global fitting (mean ± standard deviation, n=3). The data points from panel A were *globally fitted* to the competitive inhibition equation, as described in *Materials and Methods.*

Table 13. Effect of benzamidine on the enzyme kinetics of human trypsin isoforms PRSS1, PRSS2, PRSS3, mouse trypsin isoforms T7, T8, T9, T20, and bovine trypsin. Michaelis-Menten parameters (mean ± standard deviation, n=3) were determined in the presence of the indicated inhibitor concentrations with the *N*-CBZ-Gly-Pro-Arg-*p*-nitroanilide trypsin substrate at 24 ºC. See *Materials and Methods* for details. Sulfated human trypsins (PRSS1-SO_4 and PRSS2-SO_4) were purified from pancreatic juice.

PRSS1	**0 µM**	**25 µM**	**50 µM**	**75 µM**	**100 µM**
k_{cat} (s^{-1})	128.3 ± 10.4	134.8 ± 1.7	121 ± 3.3	136.3 ± 9.2	143.2 ± 8.1
K_m (μM)	18.3 ± 1.6	39.1 ± 0.9	59.6 ± 2.5	92 ± 4.4	115.3 ± 9.3
PRSS1-SO_4	**0 µM**	**12.5 µM**	**25 µM**	**37.5 µM**	**50 µM**
k_{cat} (s^{-1})	106.4 ± 2.1	104.1 ± 2.8	112.1 ± 4.9	108.4 ± 5.3	113.6 ± 7.2
K_m (μM)	10.52 ± 0.5	22.3 ± 1.2	41.8 ± 2.8	49.5 ± 1.7	69.7 ± 7.2
PRSS2	**0 µM**	**25 µM**	**50 µM**	**75 µM**	**100 µM**
k_{cat} (s^{-1})	82.5 ± 2.3	78.7 ± 1.7	78.4 ± 1.8	82.1 ± 2.4	78.3 ± 4.5
K_m (μM)	7.5 ± 0.1	15.5 ± 1.5	23.8 ± 0.9	37.5 ± 2	44.5 ± 2.9
PRSS2-SO_4	**0 µM**	**12.5 µM**	**25 µM**	**37.5 µM**	**50 µM**
k_{cat} (s^{-1})	67.5 ± 0.7	64.8 ± 1.6	64.3 ± 1.4	64.5 ± 1.5	69.3 ± 0.3
K_m (μM)	4.5 ± 0.3	15.2 ± 0.5	26.4 ± 0.8	38.2 ± 1.4	54.1 ± 2.8
PRSS3	**0 µM**	**25 µM**	**50 µM**	**75 µM**	**100 µM**
k_{cat} (s^{-1})	206.1 ± 5	211.9 ± 8.6	214.2 ± 4.7	201.3 ± 8	205.7 ± 6.3
K_m (μM)	22.2 ± 2.4	64.4 ± 4.8	114.2 ± 2.6	151.4 ± 6.7	182.9 ± 7.8
T7	**0 µM**	**12.5 µM**	**25 µM**	**37.5 µM**	**50 µM**
k_{cat} (s^{-1})	118.6 ± 2.1	125.4 ± 2.7	125.5 ± 3.5	135 ± 3.9	127.9 ± 7.5
K_m (μM)	37 ± 3.2	74.9 ± 2	110.6 ± 7.6	165.5 ± 6	200.5 ± 6.3
T8	**0 µM**	**12.5 µM**	**25 µM**	**37.5 µM**	**50 µM**
k_{cat} (s^{-1})	106.5 ± 0.5	103.9 ± 7.9	105.6 ± 4.9	100.2 ± 0.8	105.5 ± 7.
K_m (μM)	8.1 ± 0.4	20.9 ± 3.5	37.7 ± 2.4	45 ± 0.6	66.7 ± 3.2
T9	**0 µM**	**12.5 µM**	**25 µM**	**37.5 µM**	**50 µM**
k_{cat} (s^{-1})	112.6 ± 0.4	110 ± 3.4	111.4 ± 2.8	114.8 ± 2.8	112.3 ± 4.5
K_m (μM)	8.8 ± 0.4	23.7 ± 1.5	40 ± 1.4	59.9 ± 2.7	73.6 ± 2.2
T20	**0 µM**	**12.5 µM**	**25 µM**	**37.5 µM**	**50 µM**
k_{cat} (s^{-1})	61.3 ± 3.8	65 ± 1	62.1 ± 1.8	64.7 ± 2.1	65.6 ± 2.1
K_m (μM)	1.4 ± 0.2	4.2 ± 0.7	7 ± 0.7	8.7 ± 0.4	12.4 ± 0.1
Bovine trypsin	**0 µM**	**25 µM**	**50 µM**	**75 µM**	**100 µM**
k_{cat} (s^{-1})	114 ± 16.2	109 ± 9.5	115.8 ± .9	108.4 ± 5.3	113.6 ± 7.2
K_m (μM)	22.23 ± 1.2	48.9 ± 2.5	87.9 ± 14.5	121.8 ± 13.9	151.7 ± 6.3

Table 14. Effect of dabigatran on the enzyme kinetics of human trypsin isoforms PRSS1, PRSS2, PRSS3, mouse trypsin isoforms T7, T8, T9, T20, and bovine trypsin. Michaelis-Menten parameters (mean ± standard deviation, n=3) were determined in the presence of the indicated inhibitor concentrations with the *N*-CBZ-Gly-Pro-Arg-*p*-nitroanilide trypsin substrate at 24 ºC. See *Materials and Methods* for details. Sulfated human trypsins (PRSS1-SO_4 and PRSS2-SO_4) were purified from pancreatic juice.

PRSS1	**0 nM**	**25 nM**	**50 nM**	**75 nM**	**100 nM**
k_{cat} (s^{-1})	92.1 ± 3.4	90.8 ± 2.8	91.6 ± 4.8	95 ± 2.3	99.8 ± 3.3
K_m (μM)	17.4 ± 1.3	31.3 ± 3.6	50.2 ± 2.5	71.1 ± 4.2	88.7 ± 3.1
PRSS1-SO_4	**0 nM**	**25 nM**	**50 nM**	**75 nM**	**100 nM**
k_{cat} (s^{-1})	103.2 ± 0.4	101 ± 2.3	105.5 ± 5.1	103.2 ± 4.2	104.7 ± 2.1
K_m (μM)	10.1 ± 0.6	21.4 ± 1.5	32.7 ± 3	42.8 ± 7.8	57 ± 2.1
PRSS2	**0 nM**	**25 nM**	**50 nM**	**75 nM**	**100 nM**
k_{cat} (s^{-1})	91.7 ± 0.9	90.6 ± 2.6	89.1 ± 1.7	90.2 ± 2.3	87.5 ± 4.4
K_m (μM)	8 ± 0.5	23 ± 1.3	37.6 ± 0.6	46.8 ± 1.5	61.1 ± 6.1
PRSS2-SO_4	**0 nM**	**25 nM**	**50 nM**	**75 nM**	**100 nM**
k_{cat} (s^{-1})	65.8 ± 0.7	63.4 ± 0.4	66.8 ± 1.6	63.8 ± 0.9	67.2 ± 1.9
K_m (μM)	3.9 ± 0.2	13 ± 0.5	23.5 ± 1.3	31.5 ± 0.4	42.4 ± 3.5
PRSS3	**0 nM**	**50 nM**	**100 nM**	**150 nM**	**200 nM**
k_{cat} (s^{-1})	202.8 ± 4.2	214.6 ± 4.9	215.5 ± 4.6	217.5 ± 10.8	220.5 ± 4.1
K_m (μM)	7.5 ± 0.1	15.5 ± 1.5	23.8 ± 0.9	37.5 ± 2	44.5 ± 2.9
T7	**0 nM**	**50 nM**	**100 nM**	**150 nM**	**200 nM**
k_{cat} (s^{-1})	118.6 ± 2.1	48.1 ± 0.9	47.5 ± 2	50.1 ± 1.5	49.3 ± 1.7
K_m (μM)	37 ± 3.2	63.5 ± 1.7	87.2 ± 1.1	130.7 ± 8,9	144.3 ±10.2
T8	**0 nM**	**50 nM**	**100 nM**	**150 nM**	**200 nM**
k_{cat} (s^{-1})	90.9 ± 3.5	90.4 ± 1	92.3 ± 1.6	88.9 ± 1.3	85.1 ± 7.2
K_m (μM)	8.8 ± 1.6	20.6 ± 1.5	34.2 ± 4.1	46.3 ± 3	60.8 ± 4
T9	**0 nM**	**50 nM**	**100 nM**	**150 nM**	**200 nM**
k_{cat} (s^{-1})	74 ± 0.7	75.8 ± 2	72.5 ± 2.6	78.4 ± 0.1	77.6 ± 2.5
K_m (μM)	7.9 ± 0.4	19.8 ± 2.7	28.3 ± 2.8	46.1 ± 2.4	56.7 ± 7.3
T20	**0 nM**	**50 nM**	**100 nM**	**150 nM**	**200 nM**
k_{cat} (s^{-1})	52.1 ± 2.1	52 ± 4	51.1 ± 1.7	48.7 ± 3.3	50 ± 6.3
K_m (μM)	3.7 ± 0.3	9.5 ± 1.3	19.5 ± 0.5	22.5 ± 2.5	28.5 ± 2.2
Bovine trypsin	**0 nM**	**50 nM**	**100 nM**	**150 nM**	**200 nM**
k_{cat} (s^{-1})	122.8 ± 2.1	127.7 ± 0.8	126.6 ± 3.5	123.8 ± 2.9	130.1 ± 1.4
K_m (μM)	24.8 ± 2.3	49.5 ± 3.3	71.6 ± 3.5	91.9 ± 4.9	125.8 ± 7

Table 15. Competitive inhibitory constant (K_i) values (mean ± standard deviation, n=3) of benzamidine and dabigatran against human trypsin isoforms PRSS1, PRSS2, PRSS3, mouse trypsin isoforms T7, T8, T9, T20, and bovine trypsin. Kinetic measurements with the *N*-CBZ-Gly-Pro-Arg-*p*-nitroanilide trypsin substrate in the presence of increasing inhibitor concentrations were analyzed either by individually or globally fitting the substrate saturation curves, as indicated. See *Materials and Methods* for details. Sulfated human trypsins (PRSS1-SO_4 and PRSS2-SO_4) were purified from pancreatic juice.

Enzyme	K_i benzamidine (μM)		K_i dabigatran (nM)		K_i ratio	
	individual fit	global fit	individual fit	global fit	individual fit	global fit
PRSS1	15.7 ± 4.7	22.5 ± 4	21 ± 2.3	28.2 ± 4.5	748	798
PRSS1-SO_4	8.3 ± 2.2	10.5 ± 0.9	21.2 ± 0.9	23.3 ± 2	392	451
PRSS2	8.6 ± 2.2	8.9 ± 0.7	17.9 ± 3.3	14.1 ± 1.1	480	631
PRSS2-SO_4	3.3 ± 0.5	4.2 ± 0.7	10 ± 3.2	10.3 ± 0.5	330	408
PRSS3	15.5 ± 2.3	13.3 ± 0.8	35.1 ± 2.4	51.6 ± 2.1	442	258
T7	20.6 ± 3	14.9 ± 0.3	65 ± 0.6	78.9 ± 9.5	317	189
T8	6.7 ± 1.3	6.7 ± 0.5	31.6 ± 2.6	30.4 ± 2.5	212	220
T9	6.8 ± 1	6.8 ± 0.1	28.4 ± 7.1	35.8 ± 3.5	239	190
T20	6.9 ± 1.1	7.6 ± 0.5	33.6 ± 4.8	22.6 ± 0.7	205	336
Bovine trypsin	15.2 ± 3.6	17.8 ± 0.6	48.7± 1.7	56.7 ± 3.6	312	314

IV.2.2. Plasma levels of dabigatran after oral administration of dabigatran etexilate

Before embarking on experiments with trypsin-dependent pancreatitis models, we measured plasma concentrations of dabigatran in C57BL/6N mice after oral administration of the prodrug dabigatran etexilate. First, we performed intragastric gavage of a single dose (100 mg/kg) and followed plasma levels up to 8 hours. As shown in Figure 8A, dabigatran levels sharply rose to micromolar values within 30 minutes of oral gavage and peaked around 1 hour, after which time levels steadily decreased, with very little dabigatran measurable at the 4- and 8-hour time points. Importantly, peak concentrations of dabigatran were more than 2 orders of magnitude above the K_i values measured for trypsin inhibition. Second, we fed mice with solid chow containing dabigatran etexilate (10 mg/g) for 1 week and measured their plasma dabigatran concentration. Compared with acute administration of the prodrug by gavage, chronic feeding resulted in lower but steadier plasma concentrations (Figure 8B), with most values falling in the 600–800 nM range. This drug level is still more than 10-fold higher than K_i values of dabigatran against mouse trypsins. Third, we measured the dabigatran plasma concentration in 3-week-old *T7D23A* and C57BL/6N mice after consuming dabigatran etexilate laced chow (10 mg/g) for one week (Table 16). We detected no significant difference between the plasma

dabigatran levels from C57BL/6N and *T7D23A* mice, indicating that the two strains consumed the prodrug-containing chow similarly, and the spontaneous CP of *T7D23A* mice had no impact on the bioavailability of dabigatran. We were unable to measure dabigatran levels in the pancreas tissue due to interference of pancreatic proteases with the Hemoclot assay.

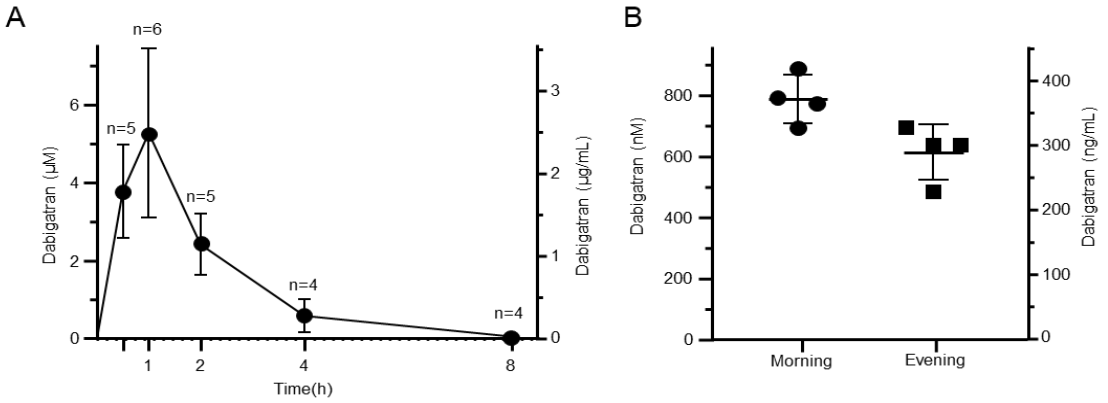

Figure 8. Dabigatran plasma concentrations in C57BL/6N mice following oral administration of dabigatran etexilate. Dabigatran levels were measured as described in *Materials and Methods*. **A**, Mice (6-8 weeks of age) were given a single dose of 100 mg/kg dabigatran etexilate by oral gavage. Mice were euthanized at the indicated times. **B**, Mice (12 weeks of age) were fed regular chow containing dabigatran etexilate at 10 mg/g concentration for 7 days. Mice were euthanized on day 8 either in the morning (9 a.m.) or in the evening (5 p.m.). Mean dabigatran concentrations (± standard deviation, n=4) measured at these time points were 787 ± 79 and 614 ± 91 nM, respectively.

Table 16. Dabigatran plasma concentration in 3-week-old *T7D23A* (n=5) and C57BL/6N (n=4) mice after consuming dabigatran etexilate laced chow (10 mg/g) for 1 week. Plasma concentration was analyzed at 5 p.m. SD, standard deviation.

Genotype	dabigatran (nM)	Mean ± SD
T7D23A	619.1 568.5 771.2 1058.3 2206.3	**1044.7 ± 676.8**
C57BL/6N	1109 1985.7 970.2 777.7	**1210.7 ± 336.1**

IV.2.3. Effect of dabigatran etexilate on cerulein-induced pancreatitis in *T7K24R* mice

The *T7K24R* mouse strain carries the p.K24R mutation in mouse cationic trypsinogen (isoform T7), which is analogous to the p.K23R pancreatitis-associated human *PRSS1* mutation [30]. The mutation increases autoactivation of trypsinogen about 5-fold and thereby sensitizes the pancreas to experimental pancreatitis. Jancsó and Sahin-Tóth (2022) recently demonstrated that cerulein-induced pancreatitis in *T7K24R* mice is progressive; and after the acute episode,

marked acinar atrophy develops with fibrosis and macrophage infiltration [31]. The acinar cell dropout is most prominent on days 4–6 and involves essentially the entire pancreas. This trypsin-dependent outcome is convenient to monitor and quantify. Before testing the effect of dabigatran etexilate, we characterized intrapancreatic trypsin and chymotrypsin activity in *T7K24R* mice after 8 hourly injections of saline or cerulein (Figure 9A). Protease activities were measured at 1 hour, 1 day, 2 days, and 3 days after the cerulein injections.

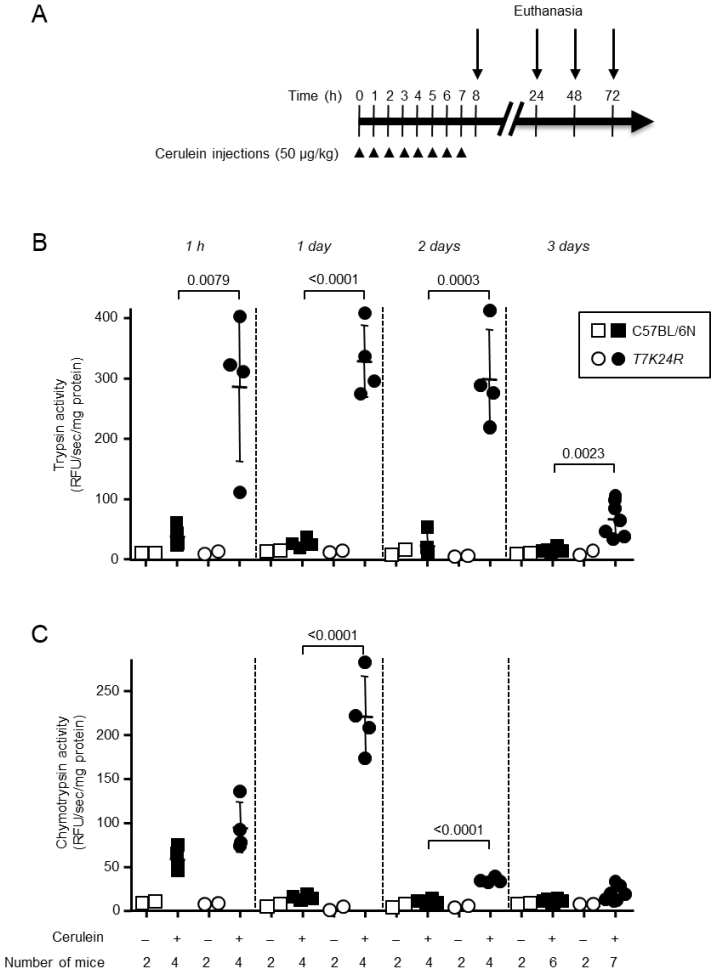

Figure 9. Intra-pancreatic trypsin and chymotrypsin activity in *T7K24R* mice given saline or cerulein. **A**, Experimental design. C57BL/6N and *T7K24R* mice (8-9 weeks of age) were treated with 8 hourly injections of saline or cerulein (arrow-heads). Animals were euthanized at the indicated times (arrows), and the pancreas was freshly homogenized and assayed, as described in *Materials and Methods*. **B**, Trypsin activity. **C**, Chymotrypsin activity. Individual data points with mean and standard deviation are shown. The difference of means between the groups was analyzed by one-way ANOVA with Tukey-Kramer post-hoc test.

Relative to cerulein-treated C57BL/6N mice, pancreatic trypsin activity in *T7K24R* mice was at least 10-fold elevated (Figure 9B), and this high value persisted on days 1 and 2, finally diminishing on day 3, as acinar atrophy develops [31]. Pancreatic chymotrypsin activity was also significantly higher in *T7K24R* mice, with peak activity (20-fold higher than in C57BL/6N mice) seen on day 1, which sharply declined by days 2 and 3 (Figure 9C). The different temporal

kinetics of intrapancreatic trypsin and chymotrypsin activities are intriguing, although an explanation is not readily apparent. As expected, no intrapancreatic protease activation was observed in saline-treated control mice. The high trypsin activity in the pancreas of cerulein-treated *T7K24R* mice suggests that trypsin-inhibitory therapy should be efficacious against pancreatitis in this model.

Therefore, in our experiments, we induced pancreatitis in *T7K24R* mice by 8 hourly injections of cerulein and euthanized the mice 96 hours (i.e., 4 days) later. To test the effect of dabigatran etexilate, a single dose of the prodrug was administered 30 minutes after the last injection (Figure 10A). Negative control mice without pancreatitis and vehicle-treated positive control mice with pancreatitis served for comparison. When the body weight of mice at the beginning and at the end of the experiment was compared, vehicle-treated mice with pancreatitis showed a slight decrease (Figure 10B). This phenomenon is due to a transient digestive dysfunction associated with the rapid development of acinar atrophy [31]. In contrast, dabigatran etexilate–treated *T7K24R* mice with pancreatitis showed no change in body weight by the end of the experiment, suggesting a protective effect of the drug. The pancreas weight of vehicle-treated *T7K24R* mice with pancreatitis was significantly reduced, to almost half the normal pancreas size (Figure 10C). The atrophic weight loss of the pancreas remained prominent even after the pancreas weight was normalized to body weight (Figure 10D). Remarkably, however, the pancreas weight of the dabigatran etexilate–treated mice with pancreatitis was significantly higher, in some cases approaching the values of control mice with no pancreatitis, suggesting that the drug prevented and/or reversed acinar atrophy to a large extent. *T7K24R* mice exhibited low plasma amylase activity 4 days after the induction of cerulein-induced pancreatitis, close to the levels seen in control mice without pancreatitis (Figure 10E). Interestingly, in a subset of dabigatran etexilate–treated mice with pancreatitis (4 of 15), we observed more than 3-fold higher plasma amylase activity values, suggesting ongoing acinar cell injury. Histological analysis of pancreata from 10 vehicle-treated and 15 dabigatran etexilate–treated mice with hematoxylin-eosin staining demonstrated widespread loss of intact acini in vehicle-treated mice (for higher magnification of pathological details, see ref. 20). A dramatic, complete protective effect of dabigatran etexilate was observed in almost 50% of the drug-treated mice (Figure 11A). A significant yet incomplete (30%–50% normal histology) effect was seen in about 20% of the mice, whereas in the remaining 30% of mice dabigatran showed limited efficacy, with less than 25% of normal acini preserved (Figure 11B). This group included 2 cases with no detectable effect. Notably, the 4 drug-treated mice with the elevated plasma amylase activity

all had partial histological responses, with 13%, 15%, 35%, and 45% intact acini visible on pancreas sections. Overall, the proportion of intact acini in the dabigatran etexilate–treated group was significantly higher than in the vehicle-treated group, indicating that dabigatran is effective in this model of trypsin-dependent pancreatitis.

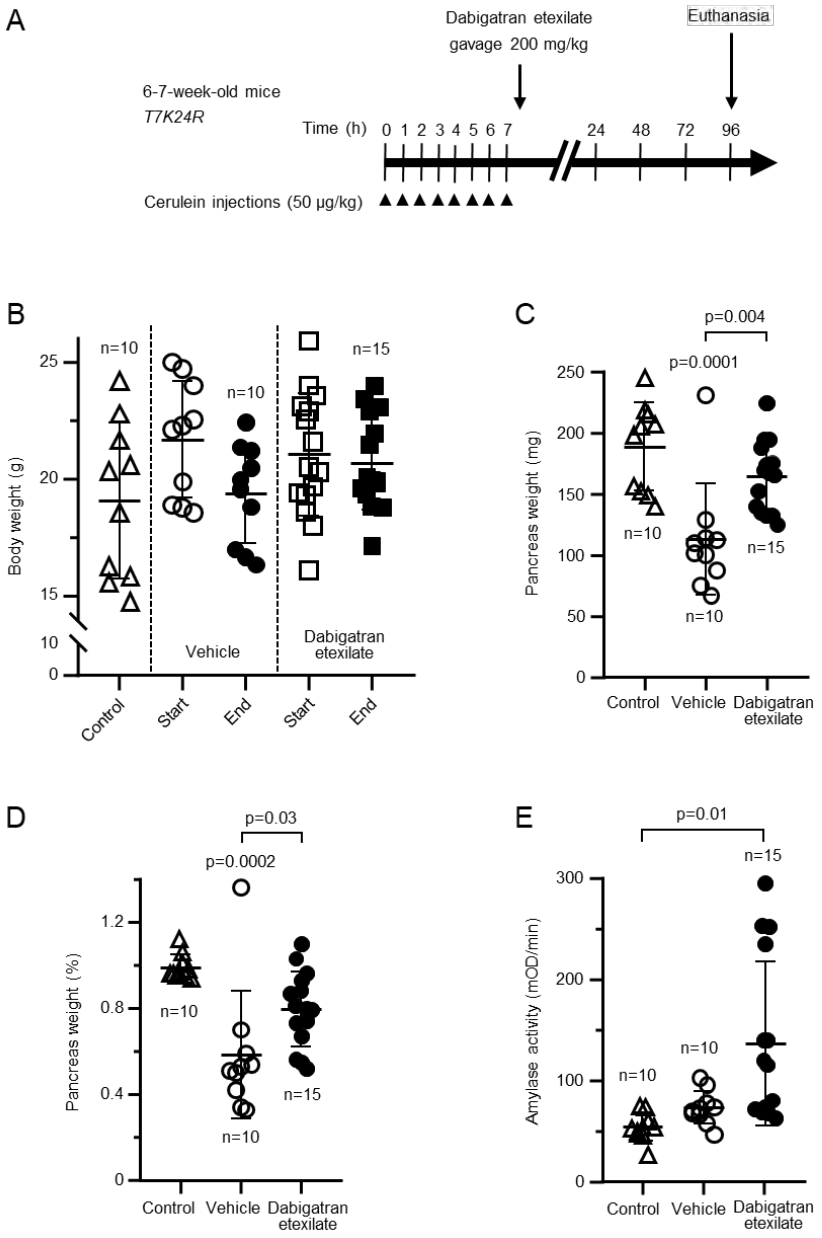

Figure 10. Effect of dabigatran etexilate on cerulein-induced pancreatitis in *T7K24R* mice. **A**, Experimental design. Mice were given 8 hourly injections of cerulein, followed by a single oral gavage of 200 mg/kg dabigatran etexilate or vehicle ad-ministered 30 min after the last cerulein injection. Mice were euthanized 96 hours from the first cerulein injection. **B**, Body weight at the start and end of the experiment. **C**, Pancreas weight in mg units. **D**, Pancreas weight as percent of body weight. **E**, Plasma amylase activity (4 µL assayed). Control mice represent aged-matched *T7K24R* mice without pancreatitis. Individual data points with mean and standard deviation are shown. The difference of means between the groups was analyzed by one-way ANOVA with Tukey-Kramer post-hoc test.

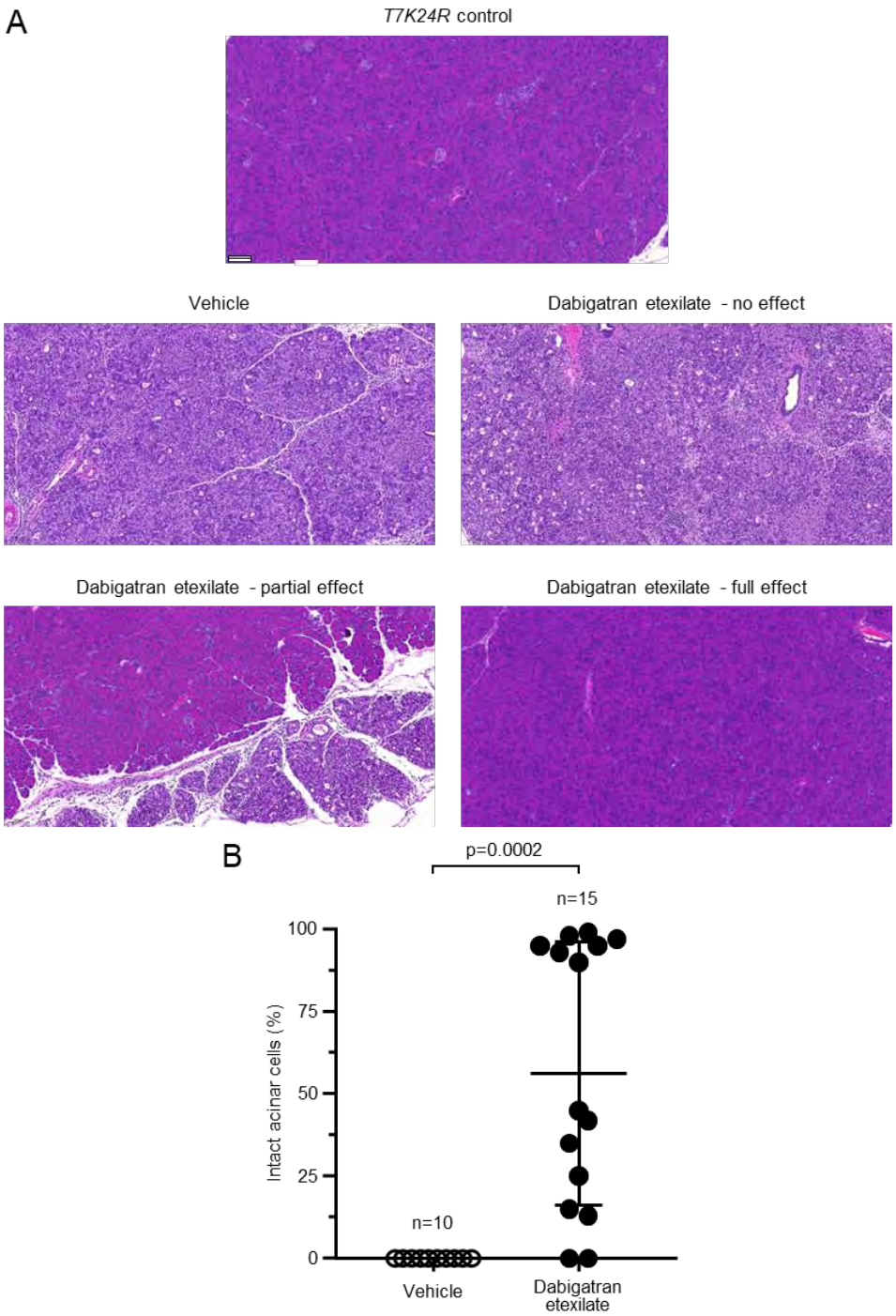

Figure 11. Effect of dabigatran etexilate on pancreas histology in cerulein-induced pancreatitis of *T7K24R* mice. Mice were given 8 hourly injections of cerulein, followed by a single oral gavage of 200 mg/kg dabigatran etexilate or vehicle administered 30 min after the last cerulein injection. Mice were euthanized 96 hours from the first cerulein injection. **A**, Representative pancreas sections stained with hematoxylin-eosin from *T7K24R* mice given vehicle or dabigatran etexilate after the cerulein injections. For comparison, the normal pancreas histology of a control *T7K24R* mouse is shown. Scale bar corresponds to 100 µm. Higher-magnification pictures of cerulein-induced pancreas pathology in *T7K24R* mice are shown in reference [30,31]. **B**, Histological evaluation of acinar cell loss. Pancreas sections from mice given vehicle (n=10) or dabigatran (n=15) were visually scored for the presence of intact acinar cells. The difference of means between two groups was analyzed by two-tailed unpaired t-test.

IV.2.4. Effect of orally gavaged dabigatran etexilate on spontaneous pancreatitis in *T7D23A* mice

Next, we tested the effect of dabigatran etexilate in a more aggressive, spontaneous pancreatitis model. The *T7D23A* mouse strain carries the p.D23A mutation in mouse cationic trypsinogen (isoform T7), which is analogous to the p.D22G pancreatitis-associated human *PRSS1* mutation [29]. The mutation increases autoactivation of trypsinogen about 50-fold and elicits spontaneous, early-onset (3–5 weeks of age), and progressive pancreatitis. In the first experiment, we treated 3-week-old *T7D23A* mice with various doses of dabigatran etexilate via intragastric gavage for 2 weeks (Figure 12A). The dosages used were once daily 100 mg/kg, twice daily 100 mg/ kg, and once daily 200 mg/kg. As controls, untreated *T7D23A* and C57BL/6N mice were used. Mice were euthanized at 5 weeks of age. Based on prior experience, at the beginning of the experiment, the pancreas of 3-week-old *T7D23A* mice was either normal or may have had incipient AP [29]. Conversely, by 5 weeks of age, all *T7D23A* mice were expected to have developed early CP. The body weight of mice was measured at the beginning (3 weeks) and at the end (5 weeks) of the experiment (Figure 12B). As expected, during this period, the mice gained weight, and this was unaffected by gavage treatment. The weight gain of *T7D23A* mice was slightly lower relative to the C57BL/6N parent strain. Compared with untreated C57BL/6N mice, the pancreas weight of untreated *T7D23A* mice was markedly lower, due to the massive pancreas atrophy associated with their early CP (Figure 12C) [29]. This large difference persisted even after normalization of the pancreas weight to the body weight of the mice (Figure 12D). In stark contrast to the effect seen with *T7K24R* mice, dabigatran etexilate treatment did not improve the pancreas weight of *T7D23A* mice. Curiously, a clear trend of worsening atrophy emerged with increasing dabigatran dosages, even though the differences did not reach statistical significance. As expected, plasma amylase activity was reduced in untreated *T7D23A* mice relative to C57BL/6N mice, though the difference did not reach statistical significance (Figure 12E). In agreement with their smaller pancreas weights, drug-treated *T7D23A* mice had significantly lower amylase levels relative to the untreated *T7D23A* controls. Histological analysis of pancreata revealed comparable CP-like disease in all groups of *T7D23A* mice whereas C57BL/6N controls showed normal pancreas morphology.

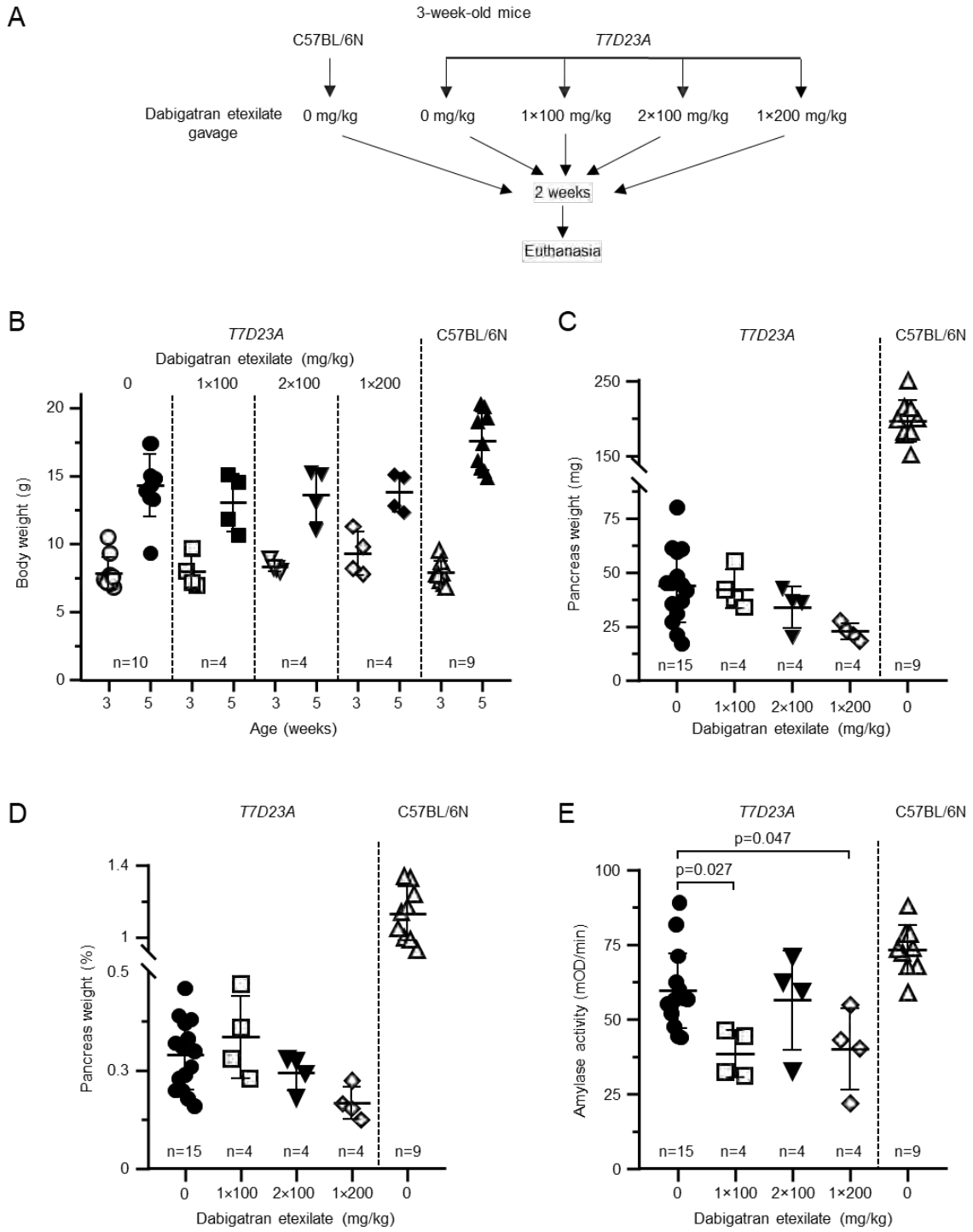

Figure 12. Effect of orally gavaged dabigatran etexilate on spontaneous pancreatitis in *T7D23A* mice. **A**, Experimental design. Mice (3 weeks of age) were given 1×100 mg/kg, 2×100 mg/kg or 1×200 mg/kg daily dose of dabigatran etexilate by intragastric gavage for 2 weeks. Untreated *T7D23A* and C57BL/6N mice served as controls. Mice were euthanized at 5 weeks of age. **B**, Body weight of mice at the beginning (3 weeks) and end (5 weeks) of the experiment. **C**, Pancreas weight in mg units. **D**, Pancreas weight as percent of body weight. **E**, Plasma amylase activity at 5 weeks of age (4 µL assayed). Individual data points with mean and standard deviation are shown. The difference of means between the groups was analyzed by one-way ANOVA with Tukey-Kramer post-hoc test.

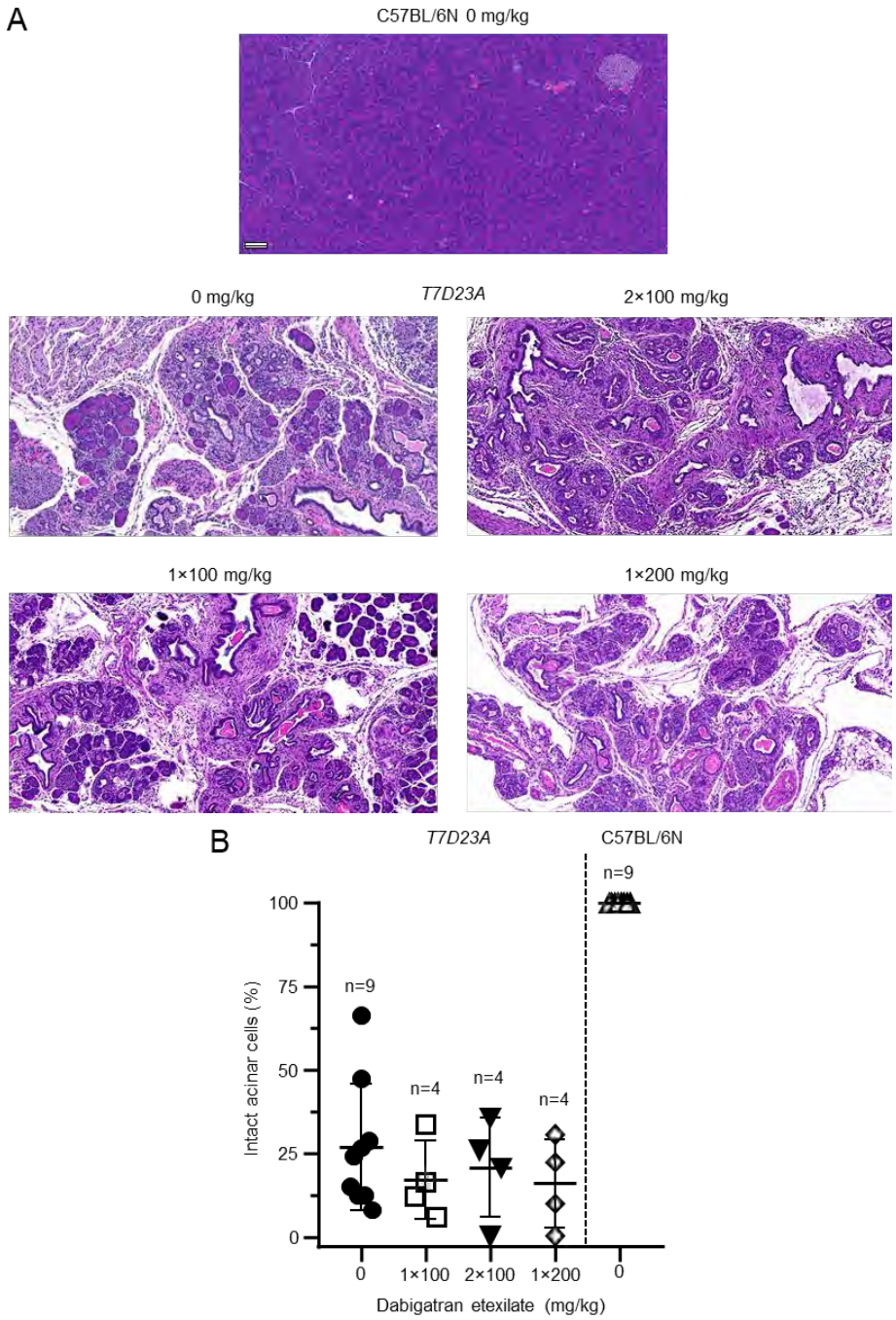

Figure 13. Effect of orally gavaged dabigatran etexilate on spontaneous pancreatitis in *T7D23A* mice. Mice (3 weeks of age) were given 1×100mg/kg, 2×100 mg/kg or 1×200 mg/kg daily dose of dabigatran etexilate by intra-gastric gavage for 2 weeks. Un-treated *T7D23A* and C57BL/6N mice served as controls. Mice were euthanized at 5 weeks of age. **A**, Representative pancreas sections stained with hematoxylin-eosin from untreated C57BL/6N and *T7D23A* control mice, and *T7D23A* mice given dabigatran etexilate. Scale bar corresponds to 100 µm. Histological details of the spontaneous pancreatitis in *T7D23A* mice are also shown in reference [29]. **B**, Histological evaluation of acinar cell loss. Pancreas sections were visually scored for the presence of intact acinar cells. The difference of means between the groups was analyzed by one-way ANOVA with Tukey-Kramer post-hoc test (Figure 12A). For details of the histological phenotype of pancreatitis in *T7D23A* mice, the reader is referred to the original publication [29].

Quantitative analysis of intact acini per visual field showed the expected dramatic cell loss in the pancreata of *T7D23A* mice, but no appreciable difference was seen between the untreated and treated groups (Figure 13B). Taken together, the results from this experiment indicated that dabigatran etexilate introduced by intragastric gavage did not ameliorate the spontaneous pancreatitis of *T7D23A* mice. Furthermore, under certain dosing protocols, the drug seemed to worsen the disease slightly.

IV.2.5. Effect of feeding with dabigatran etexilate–containing chow on spontaneous pancreatitis in *T7D23A* mice

Based on the results of the gavage experiments described above, we speculated that the *T7D23A* mouse model may require sustained drug levels in the blood to achieve full inhibition of pancreatic trypsins and prevention/reversal of disease. Therefore, we tested whether feeding the mice with solid chow containing dabigatran etexilate would be efficacious. We fed 3-week-old-mice for 1 week and euthanized the mice at the age of 4 weeks (Figure 14A). There were 4 experimental groups, treated and untreated C57BL/6N controls, and treated and untreated *T7D23A* mice. Each group gained weight similarly during the 1-week treatment, indicating that mice readily consumed the dabigatran etexilate–containing chow (Figure 14B). When comparing the pancreas weight of treated and untreated mice, we observed a small increase in the drug-treated groups of both strains, indicating that this change is likely unrelated to a drug effect on pancreatitis (Figure 14C). The difference in pancreas weights reached statistical significance when normalized to body weight (Figure 14D). Long-term feeding of mice with trypsin inhibitors causes the pancreas weight to increase, due to luminal trypsin inhibition and a feedback mechanism that increases plasma cholecystokinin levels [72–76]. Presumably, in our experiments, some of the unabsorbed dabigatran etexilate was converted to active dabigatran in the gut lumen and inhibited intestinal trypsins. Plasma amylase activities were comparable in all 4 groups of mice (Figure 14E). Finally, histological analysis showed normal pancreata in C57BL/6N mice and early CP in *T7D23A* mice (Figure 15A). Quantitative assessment of intact acini demonstrated no effect of dabigatran etexilate treatment on pancreatitis severity (Figure 15B). Taken together, the results indicate that feeding *T7D23A* mice with solid chow containing dabigatran etexilate did not prevent or improve their spontaneous pancreatitis.

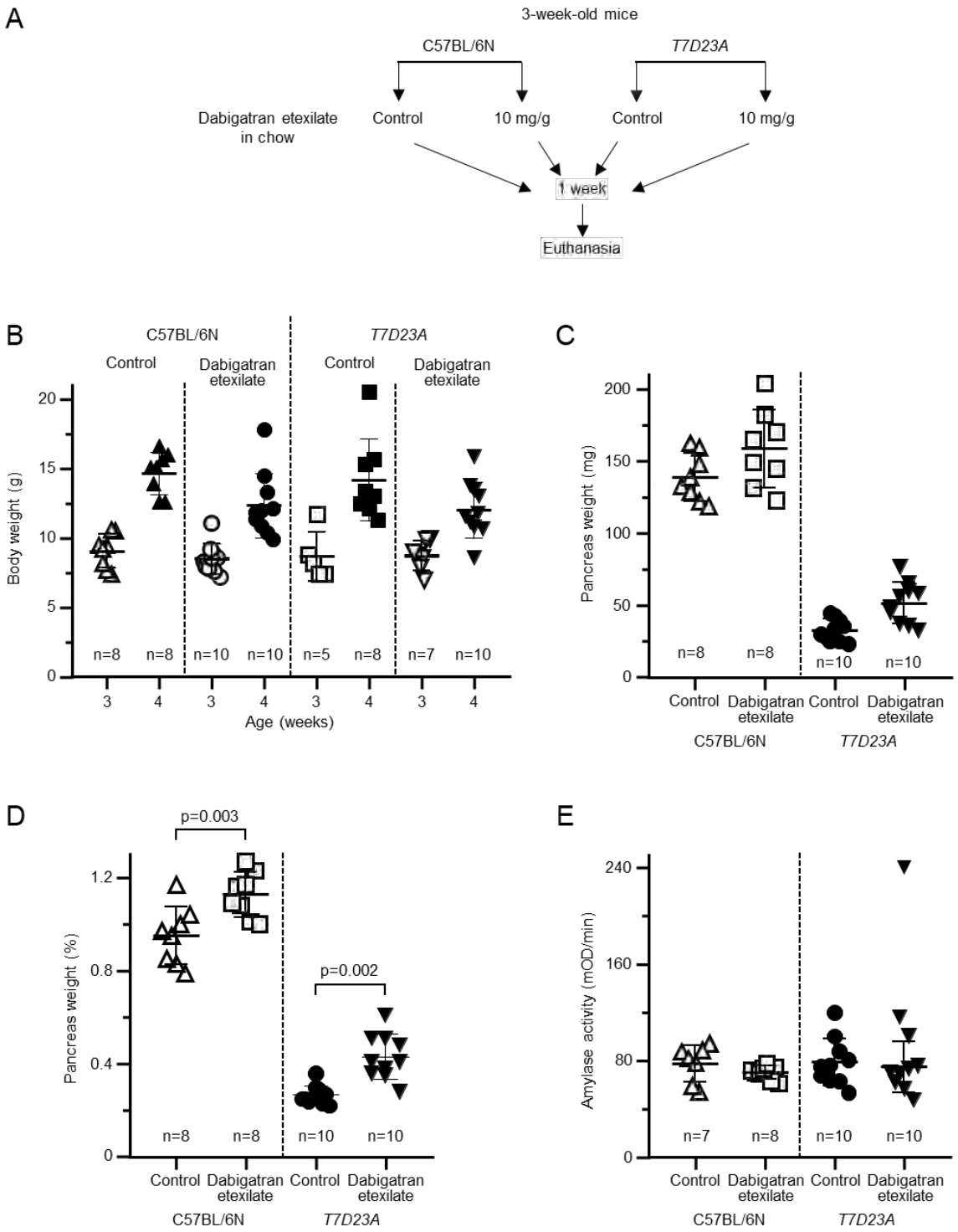

Figure 14. Effect of dabigatran etexilate feeding on spontaneous pancreatitis in *T7D23A* mice. **A**, Experimental design. C57BL/6N and *T7D23A* mice were given solid chow with or without 10 mg/g dabigatran etexilate from 21 to 28 days of age. Mice were euthanized at 28 days of age. **B**, Body weight at the beginning (3 weeks) and end (4 weeks) of the experiment. **C**, Pancreas weight in mg units. **D**, Pancreas weight as percent of body weight. **E**, Plasma amylase activity (4 μL assayed). Individual data points with mean and standard deviation are shown. The difference of means between two groups was analyzed by one-way ANOVA with Tukey-Kramer post-hoc test. The outlier data point was excluded from the statistical calculations.

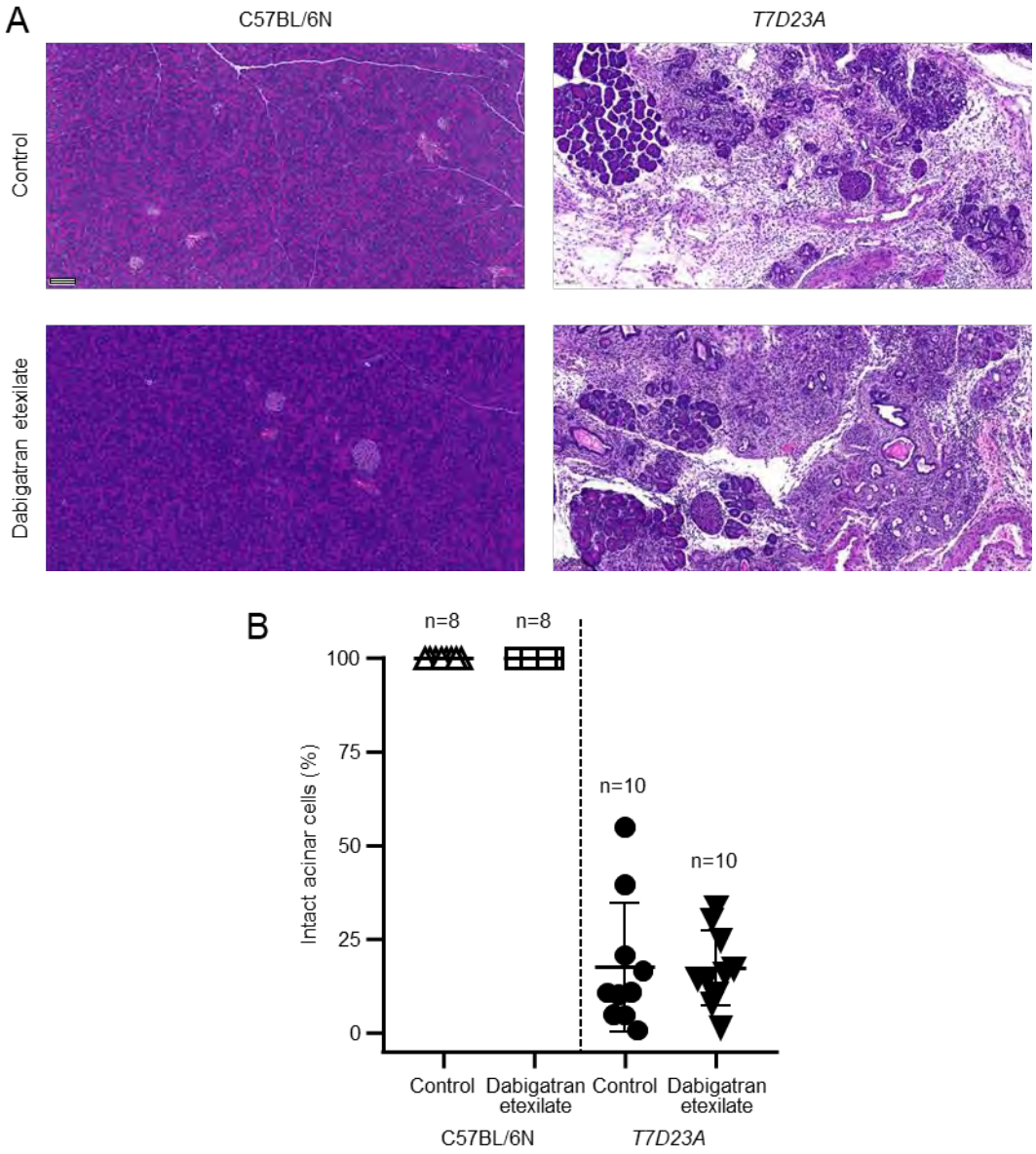

Figure 15. Effect of dabigatran etexilate feeding on spontaneous pancreatitis in *T7D23A* mice. C57BL/6N and *T7D23A* mice were given solid chow with or without 10 mg/g dabigatran etexilate from 21 to 28 days of age. Mice were euthanized at 28 days of age. **A**, Representative pancreas sections stained with hematoxylin-eosin. Scale bar corresponds to 100 µm. Histological details of the spontaneous pancreatitis in *T7D23A* mice are also shown in reference [29]. **B**, Histological evaluation of acinar cell loss. Pancreas sections were visually scored for the presence of intact acinar cells. The difference of means between the groups was analyzed by one-way ANOVA with Tukey-Kramer post-hoc test.

V. Discussion

CP is a complex inflammatory disorder associated with multiple environmental and genetic risk factors. No specific therapy is available for CP. Understanding the role of genetic risk in CP onset and progression should open up new avenues for the development of diagnostic, prognostic and therapeutic tools required for the treatment and prevention of CP. In our work, we investigated a potential new genetic risk factor for CP, and performed preclinical testing of a drug candidate in mouse models of hereditary pancreatitis.

V.1. Genetic analysis of the c.1074G>A (p.W358X) PNLIPRP2 variant in CP

In our experiments, we wanted to investigate whether a common genetic variant in *PNLIPRP2* increased risk for CP. The p.W358X variant introduces a premature stop codon that causes early translation termination, resulting in a truncated PNLIPRP2 protein. Previously reported cell culture studies suggested that the truncated protein undergoes misfolding and induces ER stress [24]. We found no association of variant p.W358X with CP when all cases were considered as a group, or in subgroup analyses when non-alcoholic and alcoholic CP were examined separately. These observations demonstrate that the *PNLIPRP2* variant p.W358X is not a genetic risk factor for CP. Besides p.W358X, we detected additional *PNLIPRP2* variants in exon 11 and the flanking intronic regions, which were linked in conserved haplotypes. When analyzed for disease association, we found enrichment of the CGGAA haplotype (see Figure 3) in the non-alcoholic CP cohort. However, despite apparent statistical significance, we interpret this result as a fortuitous association due to the small sample size.

Published data indicated that variant p.W358X might cause acinar cell damage and increase risk to CP by inducing ER stress and activating cell-death pathways [24]. However, this scenario would occur only if expression levels of the truncated PNLIPRP2 protein were high enough to cause ER stress. To characterize expression of the p.W358X allele relative to the full-length, wild-type *PNLIPRP2* allele, we PCR amplified *PNLIPRP2* from pancreatic cDNA of heterozygous and homozygous p.W358X carriers, and estimated mRNA expression by DNA sequencing (comparison of peak-heights in heterozygous samples), and by agarose gel electrophoresis (comparison of band intensities of amplicons amplified from the truncated and full-length alleles). Furthermore, we interrogated the GTEx Portal database, which provides data on the association of gene expression levels with common genetic variants (https://gtexportal.org). Both approaches indicated that mRNA levels encoding the p.W358X *PNLIPRP2* variant are diminished relative to those of full-length *PNLIPRP2*. In all likelihood, the mRNA encoding the p.W358X variant suffers nonsense-mediated decay [77], an mRNA

degradation mechanism commonly associated with transcripts containing premature stop codons. The previously published study that reported the cellular effects of the p.W358X variant used artificial expression plasmids containing a strong viral promoter and the coding DNA for wild-type and variant *PNLIPRP2* [24]. Because these constructs lack introns, the mRNA with the p.W358X variant does not undergo nonsense-mediated decay despite the presence of the premature stop codon. Consequently, protein expression levels in those experiments remained high enough to induce ER stress. Our new data convincingly demonstrates that this is not the case in human pancreatic acinar cells, where mRNA expression of *PNLIPRP2* variant p.W358X is markedly reduced. Thus, given the low levels of mRNA expression, it is unlikely that the p.W358X *PNLIPRP2* variant causes CP or increases disease risk through a gain of function, as suggested by prior studies in transfected tissue culture cells [24].

The very high prevalence of the *PNLIPRP2* p.W358X allele (allele frequency 48%) in the general population should suggest that this variant is unlikely to be relevant for CP or any other human disease. However, with respect to CP, other high-frequency variants have been shown to modify disease risk, such as the c.180C>T (p.G60=) *CTRC* variant (allele frequency ~30%) [78-81], a common inversion art the *CTRB1-CTRB2* locus (allele frequency ~28%) [28], and a large deletion in the trypsinogen locus commonly referred to as the *PRSS1-PRSS2* haplotype (allele frequency ~42-44% in Europeans) [27,82]. Even if CP risk is unaffected by *PNLIPRP2* p.W358X variant, it remains possible that loss of lipase function might have an impact on other human health conditions. In this regard, it is noteworthy that suckling *Pnliprp2*-deficient mice had fat malabsorption and poor growth but survived to adulthood and were fertile [83]. It is not known but conceivable that homozygosity for the p.W358X *PNLIPRP2* variant might have a similar effect in human infants. Alternatively, the p.W358X *PNLIPRP2* variant in humans may represent a completely benign loss-of-function lipase variant compensated by other lipases [21], a protective allele [84], or an allele that modifies adaptations to diet [57]. Future studies will determine whether any of these speculative scenarios regarding the biological significance of the p.W358X *PNLIPRP2* allele are valid.

V.2. Preclinical testing of dabigatran in trypsin-dependent pancreatitis

The aim of this study was to demonstrate that pancreatic trypsin inhibition is a viable therapeutic approach to treat, cure or prevent pancreatitis. Specifically, we tested the hypothesis that the recently reported therapeutic effect of dabigatran etexilate in experimental pancreatitis of transgenic PRSS1^{R122H} mice was due to the trypsin inhibitory activity of dabigatran [33].

First, we modeled the binding of the dabigatran molecule to trypsin using homology-based docking, followed by inhibition assays with dabigatran against a set of human, mouse, and bovine trypsin isoforms, and then we performed preclinical studies on mouse models of trypsin-dependent pancreatitis with the prodrug dabigatran etexilate. Our results demonstrate that dabigatran was readily docked into the substrate binding pocket of trypsin, and it inhibited all trypsin isoforms potently and with similar efficacy. Dabigatran exhibited several hundred-fold higher inhibitory activity compared to its parent compound benzamidine. The kinetics of inhibition was competitive, indicating that dabigatran impedes substrate binding to trypsin. In mouse experiments, we confirmed that oral administration of dabigatran etexilate produced high enough blood concentrations of dabigatran that can achieve full trypsin inhibition. A single gavage of dabigatran etexilate (100 mg/kg dose) yielded dabigatran concentrations (peak ~2.5 μg/mL) that were more than 100-fold higher than the K_i values against the various trypsin isoforms. However, under these conditions, plasma dabigatran levels decreased rapidly, and the drug was almost completely eliminated within a few hours. When dabigatran etexilate was administered to mice by feeding of solid chow containing the prodrug (10 mg/g), more steady plasma concentrations were observed (~300-400 ng/mL), which were about 10-fold higher than the K_i values against trypsins. An important caveat to these findings is that the site of trypsin inhibition to prevent pancreatitis is the pancreas, and pancreatic tissue levels of dabigatran may not reflect plasma concentrations. We were unable to measure dabigatran in the pancreas owing to interference of the pancreatic proteases with the Hemoclot assay. Previous studies showed that administration of 100 or 200 mg dabigatran etexilate 3 times daily to human volunteers resulted in steady-state plasma concentrations of dabigatran of approximately 50 and 100 ng/mL, respectively [54]. In clinical practice, the typical dosing of Pradaxa is two 150 mg capsules daily [53], which is unlikely to produce high enough dabigatran plasma concentrations that exert significant trypsin inhibitory activity in the pancreas.

To characterize the effect of dabigatran-etexilate on trypsin-dependent pancreatitis, we used two mouse models, *T7K24R* and *T7D23A*, that were developed recently in the Sahin-Tóth laboratory [29,30]. Homozygous *T7K24R* mice [30] carry the human hereditary-pancreatitis associated mutation p.K24R, which increases trypsinogen autoactivation by 5-fold. These mice are phenotypically similar to the PRSS1^{R122H} model [33], as they develop progressive CP after an acute episode of cerulein-induced pancreatitis [31]. Because cerulein-treated *T7K24R* mice exhibit high intrapancreatic trypsin activity (see Figure 9), therapeutic approaches targeting trypsin should be beneficial. Our results with *T7K24R* mice confirmed the published efficacy

of dabigatran etexilate against cerulein-induced progressive CP, and we made the following new observations. We found that a single gavage of dabigatran etexilate given shortly after the last cerulein injection was sufficient for therapeutic effect. Interestingly, we observed some variability with respect to the therapeutic activity of dabigatran etexilate. We speculate that efficient inhibition of intrapancreatic trypsin requires high enough plasma levels of dabigatran, which, in turn, may be determined by the success of the gavage procedure, and the intestinal absorption of the prodrug. The plasma dabigatran concentration after a single gavage of dabigatran etexilate showed significant variability at the 1 h peak (see Figure 8), reinforcing our view that bioavailability and peak drug concentrations may be the critical factors in therapeutic efficacy. Unfortunately, due to limitations in solubility and gavage volume, we were unable to test higher dabigatran etexilate doses. Our results with the *T7K24R* mice confirm and extend the proposed therapeutic benefit of dabigatran etexilate in trypsin-dependent pancreatitis when given shortly after the induction of disease. Owing to the anticoagulant activity of dabigatran, it was not feasible to test the effect of drug pre-treatment in our experiments, as cerulein injections would cause fatal bleeding in this setting.

In the next set of experiments, we used the trypsin-dependent mouse pancreatitis model *T7D23A*. Heterozygous *T7D23A* mice exhibit rapid, spontaneous CP development, and severe end-stage disease [29]. The relatively aggressive disease course is due to the p.D23A mutation that increases autoactivation of mouse cationic trypsinogen by 50-fold. In our studies, we tested the effect of dabigatran etexilate at an early age with incipient CP, utilizing 1- and 2-week drug dosing schemes, using either daily gavages of dabigatran etexilate or feeding with solid chow containing the prodrug. Surprisingly, neither method of drug treatment showed any therapeutic effect. It is likely that that dabigatran concentrations achieved in the pancreas of *T7D23A* mice were insufficient to exert a significant trypsin inhibitory effect. With the gavage treatment, only the short-lived peak concentrations might have been adequately high, whereas the use of drug-laced chow yielded much lower blood concentrations of dabigatran. We also note, that relative to *T7K24R* mice, *T7D23A* mice carry a trypsinogen mutation with a stronger biochemical effect and exhibit more aggressive pancreatitis phenotype. Therefore, *T7D23A* mice may require higher blood concentrations of dabigatran than *T7K24R* mice for successful inhibition of intrapancreatic trypsin activity and treatment of pancreatitis.

Dabigatran etexilate treatment of *T7D23A* mice also revealed some potentially problematic effects that will require further investigation in the future. Relative to the untreated controls, we observed worse pancreas atrophy and lower plasma amylase levels in the drug-treated mice

when using oral gavage. The largest effect was seen with twice-daily doses, suggesting a dose dependence. An explanation to this finding is not readily obvious; however, we speculate that fluctuations in dabigatran concentrations, as a result of the gavage method of oral drug administration, may be responsible for the phenomenon. Thus, we may witness a rebound effect after the transient trypsin inhibition in the pancreas, as plasma dabigatran levels fall. A similar scenario of rebound may also account for the elevated plasma amylase levels in a subset of dabigatran etexilate-treated *T7K24R* mice that had an incomplete therapeutic response (see Figure 10 and 11).

A small but measurable increase in the pancreas weight was observed when *T7D23A* mice were fed with dabigatran etexilate mixed in with chow. However, this effect was unrelated to pancreatitis treatment, as it also occurred with C57BL/6N mice. The trophic effect on the rodent pancreas caused by trypsin inhibitor consumption has been extensively documented [73-76], and our experiments seemed to replicate this phenomenon. Limited conversion of dabigatran etexilate to dabigatran in the gut would inhibit luminal trypsins, which, in turn, would increase plasma cholecystokinin levels that drive the trophic effect on the pancreas. This feedback mechanism may interfere with preclinical experiments that use orally administered trypsin inhibitors to rodents and measure pancreas size, weight, or function as treatment outcomes. In this context, a published study demonstrated that severity of experimental pancreatitis was increased after rats and mice were fed the trypsin inhibitor camostat for two weeks [85]. A similar functional adaptation may also exist in humans; however, it appears to have no clinical relevance [86].

The aim of our studies was to show that dabigatran inhibits trypsin, and thereby confers therapeutic benefit in pancreatitis. Although our results are fully consistent with this notion, we cannot rule out that dabigatran also acts via other pathways that may reduce pancreatic inflammation and/or ameliorate pancreas regeneration. In their original paper, the Ji laboratory proposed that the anticoagulant activity of dabigatran may be partly or largely responsible for its therapeutic efficacy in pancreatitis [33]. Their intriguing data showed that the factor Xa inhibitor apixaban (100 mg/kg), which is devoid of trypsin inhibitory activity, had no therapeutic activity. However, when apixaban and camostat (200 mg/kg) were administered together, the combination was highly effective, even though camostat showed only a partial effect when given alone. A possible interpretation of these published results is that anticoagulation may improve tissue penetration of the trypsin inhibitor camostat, and thereby renders it more effective. Other prior studies demonstrated that heparin improved pancreatitis

outcomes in cerulein-induced rodent models, possibly by eliminating fibrin deposits and improving circulation and oxygenation [87, 88]. More recently, a retrospective clinical cohort analysis offered further support for the use of anticoagulation in pancreatitis therapy by demonstrating that systemic anticoagulation was associated with decreased mortality and morbidity in acute pancreatitis [89]. Finally, we note that thrombin inhibition by dabigatran was shown to decrease the number of proinflammatory macrophages in atherosclerotic lesions [90], and to ameliorate organ fibrosis in various mouse models [91-93].

The goal of our study was to offer proof of concept that inhibition of trypsin activity in the pancreas can have a therapeutic effect in pancreatitis. We used dabigatran etexilate as a test case, because it is orally bioavailable and it is clinically approved and used worldwide. Furthermore, aside from the adverse effects related to anticoagulation, it has an excellent safety profile. Despite the somewhat mixed results, we view our experiments as strongly encouraging, because we demonstrated that benzamidine derivatives such as dabigatran are effective trypsin inhibitors with therapeutic efficacy in pancreatitis. Our results also warrant revisiting the potential therapeutic value of other trypsin inhibitory compounds, such as gabexate, camostat and nafamostat, in trypsin-dependent pancreatitis. Translation of the preclinical studies to human clinical trials in the future should focus on the utility of trypsin inhibitors against trypsin-mediated forms of CP, such as hereditary pancreatitis associated with trypsinogen mutations. Trial designs should consider that trypsin inhibition is expected to prevent or dampen disease initiation but not severity outcomes, such as organ failure, caused by lipotoxicity [94].

VI. Conclusions and new findings

VI.1. Genetic analysis of the c.1074G>A (p.W358X) PNLIPRP2 variant in CP

1. Our genetic case-control study found no association between the p.W358X *PNLIPRP2* variant and CP.

2. We demonstrated that the mRNA expression of the p.W358X *PNLIPRP2* variant allele was diminished in the human pancreas, relative to the full-length, wild-type *PNLIPRP2* allele. We propose that the variant allele mRNA undergoes nonsense-mediated decay.

VI.2. Preclinical testing of dabigatran in trypsin-dependent pancreatitis

1. We demonstrated that the anticoagulant dabigatran inhibited the enzyme activity of all human and mouse trypsin isoforms.

2. We showed that oral administration of dabigatran etexilate to mice either by gavage or by solid chow resulted in potentially therapeutic dabigatran concentrations in the blood.

3. We demonstrated that in the *T7K24R* mouse model of trypsin-dependent pancreatitis, a single oral dose of dabigatran etexilate prevented progression of cerulein-induced acute pancreatitis, and resulted in histologically verified healing of the pancreas.

4. We found that the development of spontaneous, trypsin-dependent CP in *T7D23A* mice was unaffected by chronic oral administration of dabigatran etexilate. The lack of efficacy in this model was likely due to the more aggressive CP phenotype, and the insufficient dabigatran levels attained in the pancreas.

VII. References

1. Yadav D, Lowenfels AB. The epidemiology of pancreatitis and pancreatic cancer. Gastroenterology. 2013 Jun;144(6):1252-61. doi: 10.1053/j.gastro.2013.01.068. PMID: 23622135; PMCID: PMC3662544.
2. Hall TC, Garcea G, Webb MA, Al-Leswas D, Metcalfe MS, Dennison AR. The socio-economic impact of chronic pancreatitis: a systematic review. J Eval Clin Pract. 2014 Jun;20(3):203-7. doi: 10.1111/jep.12117. Epub 2014 Mar 24. PMID: 24661411.
3. Ting J, Wilson L, Schwarzenberg SJ, Himes R, Barth B, Bellin MD, Durie PR, Fishman DS, Freedman SD, Gariepy CE, Giefer MJ, Gonska T, Husain SZ, Kumar S, Morinville VD, Lowe ME, Ooi CY, Pohl JF, Troendle D, Usatin D, Werlin SL, Wilschanski M, Heyman MB, Uc A. Direct Costs of Acute Recurrent and Chronic Pancreatitis in Children in the INSPPIRE Registry. J Pediatr Gastroenterol Nutr. 2016 Mar;62(3):443-9. doi: 10.1097/MPG.0000000000001057. PMID: 26704866; PMCID: PMC4767646.
4. Kleeff, J., Whitcomb, D., Shimosegawa, T. et al. Chronic pancreatitis. Nat Rev Dis Primers 3, 17060 (2017). https://doi.org/10.1038/nrdp.2017.60
5. Beyer G, Habtezion A, Werner J, Lerch MM, Mayerle J. Chronic pancreatitis. Lancet. 2020 Aug 15;396(10249):499-512. doi: 10.1016/S0140-6736(20)31318-0. PMID: 32798493.
6. Hegyi E, Sahin-Tóth M. Genetic Risk in Chronic Pancreatitis: The Trypsin-Dependent Pathway. Dig Dis Sci. 2017 Jul;62(7):1692-1701. doi: 10.1007/s10620-017-4601-3. Epub 2017 May 23. PMID: 28536777; PMCID: PMC5487703.
7. Mayerle J, Sendler M, Hegyi E, Beyer G, Lerch MM, Sahin-Tóth M. Genetics, Cell Biology, and Pathophysiology of Pancreatitis. Gastroenterology. 2019 May;156(7):1951-1968.e1. doi: 10.1053/j.gastro.2018.11.081. Epub 2019 Jan 18. PMID: 30660731; PMCID: PMC6903413.
8. Sahin-Tóth M. Genetic risk in chronic pancreatitis: the misfolding-dependent pathway. Curr Opin Gastroenterol. 2017 Sep;33(5):390-395. doi: 10.1097/MOG.0000000000000380. PMID: 28650851; PMCID: PMC5549634.
9. Toldi V, Kassay N, Szabó A. Missense PNLIP mutations impeding pancreatic lipase secretion cause protein misfolding and endoplasmic reticulum stress. Pancreatology. 2021 Oct;21(7):1317-1325. doi: 10.1016/j.pan.2021.07.008. Epub 2021 Aug 4. PMID: 34373204.
10. Masamune A, Kotani H, Sörgel FL, Chen JM, Hamada S, Sakaguchi R, Masson E, Nakano E, Kakuta Y, Niihori T, Funayama R, Shirota M, Hirano T, Kawamoto T, Hosokoshi A, Kume K, Unger L, Ewers M, Laumen H, Bugert P, Mori MX, Tsvilovskyy V, Weißgerber P, Kriebs U, Fecher-Trost C, Freichel M, Diakopoulos KN, Berninger A, Lesina M, Ishii K, Itoi T, Ikeura T, Okazaki K, Kaune T, Rosendahl J, Nagasaki M, Uezono Y, Algül H, Nakayama K, Matsubara Y, Aoki Y, Férec C, Mori Y, Witt H, Shimosegawa T. Variants That Affect Function of Calcium Channel TRPV6 Are Associated With Early-Onset Chronic Pancreatitis. Gastroenterology. 2020 May;158(6):1626-1641.e8. doi: 10.1053/j.gastro.2020.01.005. Epub 2020 Jan 10. PMID: 31930989.
11. Raeder H, Johansson S, Holm PI, Haldorsen IS, Mas E, Sbarra V, Nermoen I, Eide SA, Grevle L, Bjørkhaug L, Sagen JV, Aksnes L, Søvik O, Lombardo D, Molven A, Njølstad PR. Mutations in the CEL

VNTR cause a syndrome of diabetes and pancreatic exocrine dysfunction. Nat Genet. 2006 Jan;38(1):54-62. doi: 10.1038/ng1708. Epub 2005 Dec 20. PMID: 16369531.

12. Johansson BB, Torsvik J, Bjørkhaug L, Vesterhus M, Ragvin A, Tjora E, Fjeld K, Hoem D, Johansson S, Ræder H, Lindquist S, Hernell O, Cnop M, Saraste J, Flatmark T, Molven A, Njølstad PR. Diabetes and pancreatic exocrine dysfunction due to mutations in the carboxyl ester lipase gene-maturity onset diabetes of the young (CEL-MODY): a protein misfolding disease. J Biol Chem. 2011 Oct 7;286(40):34593-605. doi: 10.1074/jbc.M111.222679. Epub 2011 Jul 22. PMID: 21784842; PMCID: PMC3186416.
13. Xiao X, Jones G, Sevilla WA, Stolz DB, Magee KE, Haughney M, Mukherjee A, Wang Y, Lowe ME. A Carboxyl Ester Lipase (CEL) Mutant Causes Chronic Pancreatitis by Forming Intracellular Aggregates That Activate Apoptosis. J Biol Chem. 2016 Oct 28;291(44):23224-23236. doi: 10.1074/jbc.M116.734384. Epub 2016 Sep 20. Erratum in: J Biol Chem. 2017 May 12;292(19):7744. PMID: 27650499; PMCID: PMC5087739.
14. Fjeld K, Weiss FU, Lasher D, Rosendahl J, Chen JM, Johansson BB, Kirsten H, Ruffert C, Masson E, Steine SJ, Bugert P, Cnop M, Grützmann R, Mayerle J, Mössner J, Ringdal M, Schulz HU, Sendler M, Simon P, Sztromwasser P, Torsvik J, Scholz M, Tjora E, Férec C, Witt H, Lerch MM, Njølstad PR, Johansson S, Molven A. A recombined allele of the lipase gene CEL and its pseudogene CELP confers susceptibility to chronic pancreatitis. Nat Genet. 2015 May;47(5):518-522. doi: 10.1038/ng.3249. Epub 2015 Mar 16. PMID: 25774637; PMCID: PMC5321495.
15. Mao XT, Zou WB, Cao Y, Wang YC, Deng SJ, Cooper DN, Férec C, Li ZS, Chen JM, Liao Z. The CEL-HYB1 Hybrid Allele Promotes Digestive Enzyme Misfolding and Pancreatitis in Mice. Cell Mol Gastroenterol Hepatol. 2022;14(1):55-74. doi: 10.1016/j.jcmgh.2022.03.013. Epub 2022 Apr 7. PMID: 35398595; PMCID: PMC9117557.
16. Fjeld K, Gravdal A, Brekke RS, Alam J, Wilhelm SJ, El Jellas K, Pettersen HN, Lin J, Solheim MH, Steine SJ, Johansson BB, Njølstad PR, Verbeke CS, Xiao X, Lowe ME, Molven A. The genetic risk factor CEL-HYB1 causes proteotoxicity and chronic pancreatitis in mice. Pancreatology. 2022 Dec;22(8):1099-1111. doi: 10.1016/j.pan.2022.11.003. Epub 2022 Nov 9. PMID: 36379850.
17. Hegyi E, Sahin-Tóth M. Human CPA1 mutation causes digestive enzyme misfolding and chronic pancreatitis in mice. Gut. 2019 Feb;68(2):301-312. doi: 10.1136/gutjnl-2018-315994. Epub 2018 Jul 25. PMID: 30045879; PMCID: PMC6326849.
18. Behar DM, Basel-Vanagaite L, Glaser F, Kaplan M, Tzur S, Magal N, Eidlitz-Markus T, Haimi-Cohen Y, Sarig G, Bormans C, Shohat M, Zeharia A. Identification of a novel mutation in the PNLIP gene in two brothers with congenital pancreatic lipase deficiency. J Lipid Res. 2014 Feb;55(2):307-12. doi: 10.1194/jlr.P041103. Epub 2013 Nov 21. PMID: 24262094; PMCID: PMC3886669.
19. Szabó A, Xiao X, Haughney M, Spector A, Sahin-Tóth M, Lowe ME. A novel mutation in PNLIP causes pancreatic triglyceride lipase deficiency through protein misfolding. Biochim Biophys Acta. 2015 Jul;1852(7):1372-9. doi: 10.1016/j.bbadis.2015.04.002. Epub 2015 Apr 7. PMID: 25862608; PMCID: PMC4645278.
20. Zhu G, Wilhelm SJ, George LG, Cassidy BM, Zino S, Luke CJ, Hanna M, Stone S, Phan N, Matiwala N, Ballentine SJ, Lowe ME, Xiao X. Preclinical mouse model of a misfolded PNLIP variant develops

chronic pancreatitis. Gut. 2023 Jan 11:gutjnl-2022-327960. doi: 10.1136/gutjnl-2022-327960. Epub ahead of print. PMID: 36631248.

21. Lowe ME. The triglyceride lipases of the pancreas. J Lipid Res. 2002 Dec;43(12):2007-16. doi: 10.1194/jlr.r200012-jlr200. PMID: 12454260.
22. Cygler M, Schrag JD, Sussman JL, Harel M, Silman I, Gentry MK, Doctor BP. Relationship between sequence conservation and three-dimensional structure in a large family of esterases, lipases, and related proteins. Protein Sci. 1993 Mar;2(3):366-82. doi: 10.1002/pro.5560020309. PMID: 8453375; PMCID: PMC2142374.
23. Cao H, Hegele RA. DNA polymorphisms of lipase related genes. J Hum Genet. 2003;48(8):443-446. doi: 10.1007/s10038-003-0051-1. Epub 2003 Aug 1. PMID: 12898288.
24. Xiao X, Mukherjee A, Ross LE, Lowe ME. Pancreatic lipase-related protein-2 (PLRP2) can contribute to dietary fat digestion in human newborns. J Biol Chem. 2011 Jul 29;286(30):26353-63. doi: 10.1074/jbc.M111.249813. Epub 2011 Jun 7. PMID: 21652702; PMCID: PMC3143598.
25. Whitcomb DC, Gorry MC, Preston RA, Furey W, Sossenheimer MJ, Ulrich CD, Martin SP, Gates LK Jr, Amann ST, Toskes PP, Liddle R, McGrath K, Uomo G, Post JC, Ehrlich GD. Hereditary pancreatitis is caused by a mutation in the cationic trypsinogen gene. Nat Genet. 1996 Oct;14(2):141-5. doi: 10.1038/ng1096-141. PMID: 8841182
26. Witt H, Sahin-Tóth M, Landt O, Chen JM, Kähne T, Drenth JP, Kukor Z, Szepessy E, Halangk W, Dahm S, Rohde K, Schulz HU, Le Maréchal C, Akar N, Ammann RW, Truninger K, Bargetzi M, Bhatia E, Castellani C, Cavestro GM, Cerny M, Destro-Bisol G, Spedini G, Eiberg H, Jansen JB, Koudova M, Rausova E, Macek M Jr, Malats N, Real FX, Menzel HJ, Moral P, Galavotti R, Pignatti PF, Rickards O, Spicak J, Zarnescu NO, Böck W, Gress TM, Friess H, Ockenga J, Schmidt H, Pfützer R, Löhr M, Simon P, Weiss FU, Lerch MM, Teich N, Keim V, Berg T, Wiedenmann B, Luck W, Groneberg DA, Becker M, Keil T, Kage A, Bernardova J, Braun M, Güldner C, Halangk J, Rosendahl J, Witt U, Treiber M, Nickel R, Férec C. A degradation-sensitive anionic trypsinogen (PRSS2) variant protects against chronic pancreatitis. Nat Genet. 2006 Jun;38(6):668-73. doi: 10.1038/ng1797. Epub 2006 May 14. PMID: 16699518; PMCID: PMC2746914.
27. Masson E, Ewers M, Paliwal S, Kume K, Scotet V, Cooper DN, Rebours V, Buscail L, Rouault K; GREPAN (Genetic REsearch on PANcreatitis) Study Group; Abrantes A, Aguilera Munoz L, Albouys J, Alric L, Amiot X, Archambeaud I, Audiau S, Bastide L, Baudon J, Bellaiche G, Bellon S, Bertrand V, Bideau K, Billiemaz K, Billioud C, Bonnefoy S, Borderon C, Bournet B, Breton E, Brugel M, Buscail L, Cadiot G, Camus M, Carpentier-Pourquier M, Chamouard P, Chaput U, Chen JM, Cholet F, Ciocan DM, Clavel C, Coffin B, Coimet-Berger L, Cosconea S, Creveaux I, Culetto A, Daboussi O, De Mestier L, Degand T, D'engremont C, Denis B, Dermine S, Desgrippes, Drouet D'Aubigny A, Enaud R, Fabre A, Férec C, Gargot D, Gelsi E, Gentilcore E, Gincul R, Ginglinger-Favre E, Giovannini M, Gomercic C, Gondran H, Grainville T, Grandval P, Grasset D, Grimaldi S, Grimbert S, Hagege H, Heissat S, Hentic O, Herber-Mayne A, Hervouet M, Hoibian S, Jacques J, Jais B, Kaassis M, Koch S, Lacaze E, Lacroute J, Lamireau T, Laurent L, Le Guillou X, Le Rhun M, Leblanc S, Levy P, Lievre A, Lorenzo D, Maire F, Marcel K, Masson E, Mauillon J, Morgant S, Moussata D, Muller N, Nambot S, Napoleon B, Olivier A, Pagenault M, Pelletier AL, Pennec O, Pinard F, Pioche M, Prost B, Queneherve L, Rebours V, Reboux

N, Rekik S, Riachi G, Rohmer B, Roquelaure B, Rosa Hezode I, Rostain F, Saurin JC, Servais L, Stan-Iuga R, Subtil C, Tanneche J, Texier C, Thomassin L, Tougeron D, Vuitton L, Wallenhorst T, Wangerme M, Zanaldi H, Zerbib F, Bhaskar S, Kikuta K, Rao GV, Hamada S, Reddy DN, Masamune A, Chandak GR, Witt H, Férec C, Chen JM. The PRSS3P2 and TRY7 deletion copy number variant modifies risk for chronic pancreatitis. Pancreatology. 2022 Dec 5:S1424-3903(22)00822-5. doi: 10.1016/j.pan.2022.11.013. Epub ahead of print. PMID: 36517351.

28. Rosendahl J, Kirsten H, Hegyi E, Kovacs P, Weiss FU, Laumen H, Lichtner P, Ruffert C, Chen JM, Masson E, Beer S, Zimmer C, Seltsam K, Algül H, Bühler F, Bruno MJ, Bugert P, Burkhardt R, Cavestro GM, Cichoz-Lach H, Farré A, Frank J, Gambaro G, Gimpfl S, Grallert H, Griesmann H, Grützmann R, Hellerbrand C, Hegyi P, Hollenbach M, Iordache S, Jurkowska G, Keim V, Kiefer F, Krug S, Landt O, Leo MD, Lerch MM, Lévy P, Löffler M, Löhr M, Ludwig M, Macek M, Malats N, Malecka-Panas E, Malerba G, Mann K, Mayerle J, Mohr S, Te Morsche RHM, Motyka M, Mueller S, Müller T, Nöthen MM, Pedrazzoli S, Pereira SP, Peters A, Pfützer R, Real FX, Rebours V, Ridinger M, Rietschel M, Rösmann E, Saftoiu A, Schneider A, Schulz HU, Soranzo N, Soyka M, Simon P, Skipworth J, Stickel F, Strauch K, Stumvoll M, Testoni PA, Tönjes A, Werner L, Werner J, Wodarz N, Ziegler M, Masamune A, Mössner J, Férec C, Michl P, P H Drenth J, Witt H, Scholz M, Sahin-Tóth M; all members of the PanEuropean Working group on ACP. Genome-wide association study identifies inversion in the CTRB1-CTRB2 locus to modify risk for alcoholic and non-alcoholic chronic pancreatitis. Gut. 2018 Oct;67(10):1855-1863. doi: 10.1136/gutjnl-2017-314454. Epub 2017 Jul 28. PMID: 28754779; PMCID: PMC6145291.
29. Geisz A, Sahin-Tóth M. A preclinical model of chronic pancreatitis driven by trypsinogen autoactivation. Nat Commun. 2018 Nov 28;9(1):5033. doi: 10.1038/s41467-018-07347-y. PMID: 30487519; PMCID: PMC6261995.
30. Jancsó Z, Sahin-Tóth M. Mutation That Promotes Activation of Trypsinogen Increases Severity of Secretagogue-Induced Pancreatitis in Mice. Gastroenterology. 2020 Mar;158(4):1083-1094. doi: 10.1053/j.gastro.2019.11.020. Epub 2019 Nov 18. PMID: 31751559; PMCID: PMC7062587.
31. Jancsó Z, Sahin-Tóth M. Chronic progression of cerulein-induced acute pancreatitis in trypsinogen mutant mice. Pancreatology. 2022 Mar;22(2):248-257. doi: 10.1016/j.pan.2022.01.007. Epub 2022 Jan 14. PMID: 35063369; PMCID: PMC8941852.
32. Demcsák A, Sahin-Tóth M. Rate of autoactivation determines pancreatitis phenotype in trypsinogen mutant mice. Gastroenterology. 2022 Sep; 163(3):761–763. doi: 10.1053/j.gastro.2022.06.001
33. Gui F, Zhang Y, Wan J, Zhan X, Yao Y, Li Y, Haddock AN, Shi J, Guo J, Chen J, Zhu X, Edenfield BH, Zhuang L, Hu C, Wang Y, Mukhopadhyay D, Radisky ES, Zhang L, Lugea A, Pandol SJ, Bi Y, Ji B. Trypsin activity governs increased susceptibility to pancreatitis in mice expressing human PRSS1R122H. J Clin Invest. 2020 Jan 2;130(1):189-202. doi: 10.1172/JCI130172. PMID: 31550238; PMCID: PMC6934224.
34. Ascenzi P, Bocedi A, Bolognesi M, Spallarossa A, Coletta M, De Cristofaro R, Menegatti E. The bovine basic pancreatic trypsin inhibitor (Kunitz inhibitor): a milestone protein. Curr Protein Pept Sci. 2003 Jun;4(3):231-51. doi: 10.2174/1389203033487180. PMID: 12769721.

35. Tamura Y, Hirado M, Okamura K, Minato Y, Fujii S. Synthetic inhibitors of trypsin, plasmin, kallikrein, thrombin, C1r-, and C1 esterase. Biochim Biophys Acta. 1977 Oct 13;484(2):417-22. doi: 10.1016/0005-2744(77)90097-3. PMID: 143965.
36. Fujii S, Hitomi Y. New synthetic inhibitors of C1r, C1 esterase, thrombin, plasmin, kallikrein and trypsin. Biochim Biophys Acta. 1981 Oct 13;661(2):342-5. doi: 10.1016/0005-2744(81)90023-1. PMID: 6271224.
37. Takasugi S, Yonezawa H, Ikei N, Kanno T. Prevention of acute experimental pancreatitis in rats and dogs by intraduodenal infusion of a synthetic trypsin inhibitor. Digestion. 1982;24(1):36-41. doi: 10.1159/000198772. PMID: 6182046.
38. Lankisch PG, Pohl U, Göke B, Otto J, Wereszczynska-Siemiatkowska U, Gröne HJ, Rahlf G. Effect of FOY-305 (camostate) on severe acute pancreatitis in two experimental animal models. Gastroenterology. 1989 Jan;96(1):193-9. doi: 10.1016/0016-5085(89)90780-4. PMID: 2909420.
39. Wisner JR Jr, Ozawa S, Renner IG. The effects of nafamostat mesilate (FUT-175) on caerulein-induced acute pancreatitis in the rat. Int J Pancreatol. 1989 May;4(4):383-90. doi: 10.1007/BF02938474. PMID: 2732529.
40. Otsuki M, Tani S, Okabayashi Y, Fuji M, Nakamura T, Fujisawa T, Itoh H. Beneficial effects of the synthetic trypsin inhibitor camostate in cerulein-induced acute pancreatitis in rats. Dig Dis Sci. 1990 Feb;35(2):242-50. doi: 10.1007/BF01536770. PMID: 1689237.
41. Manabe T, Hirano T, Imanishi K, Ando K, Yotsumoto F, Tobe T. Protective effect of nafamostat mesilate on cellular and lysosomal fragility of acinar cells in rat cerulein pancreatitis. Int J Pancreatol. 1992 Oct;12(2):167-72. PMID: 1281204.
42. Kisfalvi K, Papp M, Friess H, Büchler M, Gorácz UG. Beneficial effects of preventive oral administration of camostate on cerulein-induced pancreatitis in rats. Dig Dis Sci. 1995 Mar;40(3):546-7. doi: 10.1007/BF02064366. PMID: 7741926.
43. Keck T, Balcom JH, Antoniu BA, Lewandrowski K, Warshaw AL, Fernández-del Castillo CF. Regional effects of nafamostat, a novel potent protease and complement inhibitor, on severe necrotizing pancreatitis. Surgery. 2001 Aug;130(2):175-81. doi: 10.1067/msy.2001.115827. PMID: 11490346.
44. Lee JK, Ryu JK, Park JK, Lee SH, Yoon WJ, Kim YT, Jung HC, Yoon YB. Effects of nafamostat mesilate on the prevention of cerulein-induced acute pancreatitis. Pancreas. 2008 Apr;36(3):255-60. doi: 10.1097/MPA.0b013e31815b6b10. PMID: 18362838.
45. Motoo Y. Antiproteases in the treatment of chronic pancreatitis. JOP. 2007 Jul 9;8(4 Suppl):533-7. PMID: 17625311.
46. Smith M, Kocher HM, Hunt BJ. Aprotinin in severe acute pancreatitis. Int J Clin Pract. 2010 Jan;64(1):84-92. doi: 10.1111/j.1742-1241.2008.01899.x. Epub 2009 Jan 28. PMID: 19178597.
47. Seta T, Noguchi Y, Shikata S, Nakayama T. Treatment of acute pancreatitis with protease inhibitors administered through intravenous infusion: an updated systematic review and meta-analysis. BMC Gastroenterol. 2014 May 30;14:102. doi: 10.1186/1471-230X-14-102. PMID: 24886242; PMCID: PMC4061927.

48. Yu G, Li S, Wan R, Wang X, Hu G. Nafamostat mesilate for prevention of post-ERCP pancreatitis: a meta-analysis of prospective, randomized, controlled trials. Pancreas. 2015 May;44(4):561-9. doi: 10.1097/MPA.0000000000000310. PMID: 25822153.
49. Hirota M, Shimosegawa T, Kitamura K, Takeda K, Takeyama Y, Mayumi T, Ito T, Takenaka M, Iwasaki E, Sawano H, Ishida E, Miura S, Masamune A, Nakai Y, Mitoro A, Maguchi H, Kimura K, Sanuki T, Ito T, Haradome H, Kozaka K, Gabata T, Kataoka K, Hirota M, Isaji S, Nakamura R, Yamagiwa K, Kayaba C, Ikeda K. Continuous regional arterial infusion versus intravenous administration of the protease inhibitor nafamostat mesilate for predicted severe acute pancreatitis: a multicenter, randomized, open-label, phase 2 trial. J Gastroenterol. 2020 Mar;55(3):342-352. doi: 10.1007/s00535-019-01644-z. Epub 2019 Nov 22. PMID: 31758329; PMCID: PMC7026212.
50. Matsumoto T, Okuwaki K, Imaizumi H, Kida M, Iwai T, Yamauchi H, Kaneko T, Hasegawa R, Masutani H, Tadehara M, Adachi K, Watanabe M, Kurosu T, Tamaki A, Kikuchi H, Ohno T, Koizumi W. Nafamostat Mesylate is Not Effective in Preventing Post-Endoscopic Retrograde Cholangiopancreatography Pancreatitis. Dig Dis Sci. 2021 Dec;66(12):4475-4484. doi: 10.1007/s10620-020-06782-6. Epub 2021 Jan 25. PMID: 33495919.
51. Hauel NH, Nar H, Priepke H, Ries U, Stassen JM, Wienen W. Structure-based design of novel potent nonpeptide thrombin inhibitors. J Med Chem. 2002 Apr 25;45(9):1757-66. doi: 10.1021/jm0109513. PMID: 11960487.
52. van Ryn J, Goss A, Hauel N, Wienen W, Priepke H, Nar H, Clemens A. The discovery of dabigatran etexilate. Front Pharmacol. 2013 Feb 12;4:12. doi: 10.3389/fphar.2013.00012. PMID: 23408233; PMCID: PMC3569592.
53. Ageno W, Eikelboom J, Lip GY. Dabigatran in clinical practice: Contemporary overview of the evidence. Int J Cardiol. 2016 Oct 1;220:417-28. doi: 10.1016/j.ijcard.2016.06.078. Epub 2016 Jun 23. Erratum in: Int J Cardiol. 2016 Nov 15;223:1074-1076. PMID: 27390965.
54. Stangier J, Clemens A. Pharmacology, pharmacokinetics, and pharmacodynamics of dabigatran etexilate, an oral direct thrombin inhibitor. Clin Appl Thromb Hemost. 2009 Sep-Oct;15 Suppl 1:9S-16S. doi: 10.1177/1076029609343004. Epub 2009 Aug 19. PMID: 19696042.
55. Wienen W, Stassen JM, Priepke H, Ries UJ, Hauel N. In-vitro profile and ex-vivo anticoagulant activity of the direct thrombin inhibitor dabigatran and its orally active prodrug, dabigatran etexilate. Thromb Haemost. 2007 Jul;98(1):155-62. PMID: 17598008.
56. Chase T Jr, Shaw E. p-Nitrophenyl-p'-guanidinobenzoate HCl: a new active site titrant for trypsin. Biochem Biophys Res Commun. 1967 Nov 30;29(4):508-14. doi: 10.1016/0006-291x(67)90513-x. PMID: 16496527
57. Király O, Guan L, Sahin-Tóth M. Expression of recombinant proteins with uniform N-termini. Methods Mol Biol. 2011;705:175-94. doi: 10.1007/978-1-61737-967-3_10. PMID: 21125386; PMCID: PMC3107599.
58. Katona G, Berglund GI, Hajdu J, Gráf L, Szilágyi L. Crystal structure reveals basis for the inhibitor resistance of human brain trypsin. J Mol Biol. 2002 Feb 1;315(5):1209-18. doi: 10.1006/jmbi.2001.5305. PMID: 11827488.

59. Alekseenko A, Kotelnikov S, Ignatov M, Egbert M, Kholodov Y, Vajda S, Kozakov D. ClusPro LigTBM: Automated Template-based Small Molecule Docking. J Mol Biol. 2020 May 15;432(11):3404-3410. doi: 10.1016/j.jmb.2019.12.011. Epub 2019 Dec 19. PMID: 31863748; PMCID: PMC7890944.
60. Brooks BR, Bruccoleri RE, Olafson BD, States DJ, Swaminathan S, Karplus M. CHARMM: A program for macromolecular energy, minimization, and dynamics calculations. J Comput Chem. 1983 Jun doi:10.1002/JCC.540040211
61. Lengyel Z, Pál G, Sahin-Tóth M. Affinity purification of recombinant trypsinogen using immobilized ecotin. Protein Expr Purif. 1998 Mar;12(2):291-4. doi: 10.1006/prep.1997.0837. PMID: 9518472.
62. Németh BC, Wartmann T, Halangk W, Sahin-Tóth M. Autoactivation of mouse trypsinogens is regulated by chymotrypsin C via cleavage of the autolysis loop. J Biol Chem. 2013 Aug 16;288(33):24049-62. doi: 10.1074/jbc.M113.478800. Epub 2013 Jun 27. PMID: 23814066; PMCID: PMC3745349.
63. Nemoda Z, Sahin-Tóth M. Chymotrypsin C (caldecrin) stimulates autoactivation of human cationic trypsinogen. J Biol Chem. 2006 Apr 28;281(17):11879-86. doi: 10.1074/jbc.M600124200. Epub 2006 Feb 27. PMID: 16505482; PMCID: PMC1586167.
64. Sahin-Tóth M, Kukor Z, Nemoda Z. Human cationic trypsinogen is sulfated on Tyr154. FEBS J. 2006 Nov;273(22):5044-50. doi: 10.1111/j.1742-4658.2006.05501.x. PMID: 17087724; PMCID: PMC2645268.
65. Mosztbacher D, Demcsák A, Sahin-Tóth M. Measuring digestive protease activation in the mouse pancreas. Pancreatology. 2020 Mar;20(2):288-292. doi: 10.1016/j.pan.2019.12.020. Epub 2019 Dec 26. PMID: 31899136; PMCID: PMC7103542.
66. Samoš M, Stančiaková L, Ivanková J, Staško J, Kovář F, Dobrotová M, Galajda P, Kubisz P, Mokáň M. Monitoring of dabigatran therapy using Hemoclot(®) Thrombin Inhibitor assay in patients with atrial fibrillation. J Thromb Thrombolysis. 2015 Jan;39(1):95-100. doi: 10.1007/s11239-014-1125-y. PMID: 25103614.
67. Cini M, Legnani C, Cosmi B, Testa S, Dellanoce C, Paoletti O, Marcucci R, Poli D, Paniccia R, Pengo V, Tripodi A, Palareti G; START-Laboratory Register. Comparison of five specific assays for determination of dabigatran plasma concentrations in patients enrolled in the START-Laboratory Register. Int J Lab Hematol. 2018 Apr;40(2):229-236. doi: 10.1111/ijlh.12772. Epub 2018 Jan 3. PMID: 29314632.
68. Cao H, Hegele RA. DNA polymorphisms of lipase related genes. J Hum Genet. 2003;48(8):443-446. doi: 10.1007/s10038-003-0051-1. Epub 2003 Aug 1. PMID: 12898288.
69. Hancock AM, Witonsky DB, Ehler E, Alkorta-Aranburu G, Beall C, Gebremedhin A, Sukernik R, Utermann G, Pritchard J, Coop G, Di Rienzo A. Colloquium paper: human adaptations to diet, subsistence, and ecoregion are due to subtle shifts in allele frequency. Proc Natl Acad Sci U S A. 2010 May 11;107 Suppl 2(Suppl 2):8924-30. doi: 10.1073/pnas.0914625107. Epub 2010 May 5. PMID: 20445095; PMCID: PMC3024024.
70. Giller T, Buchwald P, Blum-Kaelin D, Hunziker W. Two novel human pancreatic lipase related proteins, hPLRP1 and hPLRP2. Differences in colipase dependence and in lipase activity. J Biol Chem. 1992 Aug 15;267(23):16509-16. PMID: 1379598.

71. Nar H, Bauer M, Schmid A, Stassen JM, Wienen W, Priepke HW, Kauffmann IK, Ries UJ, Hauel NH. Structural basis for inhibition promiscuity of dual specific thrombin and factor Xa blood coagulation inhibitors. Structure. 2001 Jan 10;9(1):29-37. doi: 10.1016/s0969-2126(00)00551-7. PMID: 11342132.

72. Melmed RN, Bouchier IA. A further physiological role for naturally occurring trypsin inhibitors: the evidence for a trophic stimulant of the pancreatic acinar cell. Gut. 1969 Dec;10(12):973-9. doi: 10.1136/gut.10.12.973. PMID: 5391956; PMCID: PMC1553017.

73. Göke B, Printz H, Koop I, Rausch U, Richter G, Arnold R, Adler G. Endogenous CCK release and pancreatic growth in rats after feeding a proteinase inhibitor (camostate). Pancreas. 1986;1(6):509-15. doi: 10.1097/00006676-198611000-00008. PMID: 3562444.

74. Niederau C, Liddle RA, Williams JA, Grendell JH. Pancreatic growth: interaction of exogenous cholecystokinin, a protease inhibitor, and a cholecystokinin receptor antagonist in mice. Gut. 1987;28 Suppl(Suppl):63-9. doi: 10.1136/gut.28.suppl.63. PMID: 2446964; PMCID: PMC1434558.

75. Smith JC, Wilson FD, Allen PV, Berry DL. Hypertrophy and hyperplasia of the rat pancreas produced by short-term dietary administration of soya-derived protein and soybean trypsin inhibitor. J Appl Toxicol. 1989 Jun;9(3):175-9. doi: 10.1002/jat.2550090307. PMID: 2745924.

76. Crozier SJ, Sans MD, Lang CH, D'Alecy LG, Ernst SA, Williams JA. CCK-induced pancreatic growth is not limited by mitogenic capacity in mice. Am J Physiol Gastrointest Liver Physiol. 2008 May;294(5):G1148-57. doi: 10.1152/ajpgi.00426.2007. Epub 2008 Mar 20. PMID: 18356533.

77. Lykke-Andersen S, Jensen TH. Nonsense-mediated mRNA decay: an intricate machinery that shapes transcriptomes. Nat Rev Mol Cell Biol. 2015 Nov;16(11):665-77. doi: 10.1038/nrm4063. Epub 2015 Sep 23. PMID: 26397022.

78. Masson E, Chen JM, Scotet V, Le Maréchal C, Férec C. Association of rare chymotrypsinogen C (CTRC) gene variations in patients with idiopathic chronic pancreatitis. Hum Genet. 2008 Feb;123(1):83-91. doi: 10.1007/s00439-007-0459-3. Epub 2008 Jan 3. PMID: 18172691.

79. Paliwal S, Bhaskar S, Mani KR, Reddy DN, Rao GV, Singh SP, Thomas V, Chandak GR. Comprehensive screening of chymotrypsin C (CTRC) gene in tropical calcific pancreatitis identifies novel variants. Gut. 2013 Nov;62(11):1602-6. doi: 10.1136/gutjnl-2012-302448. Epub 2012 May 12. PMID: 22580415.

80. LaRusch J, Lozano-Leon A, Stello K, Moore A, Muddana V, O'Connell M, Diergaarde B, Yadav D, Whitcomb DC. The Common Chymotrypsinogen C (CTRC) Variant G60G (C.180T) Increases Risk of Chronic Pancreatitis But Not Recurrent Acute Pancreatitis in a North American Population. Clin Transl Gastroenterol. 2015 Jan 8;6(1):e68. doi: 10.1038/ctg.2014.13. PMID: 25569187; PMCID: PMC4418406.

81. Grabarczyk AM, Oracz G, Wertheim-Tysarowska K, Kujko AA, Wejnarska K, Kolodziejczyk E, Bal J, Koziel D, Kowalik A, Gluszek S, Rygiel AM. Chymotrypsinogen C Genetic Variants, Including c.180TT, Are Strongly Associated With Chronic Pancreatitis in Pediatric Patients. J Pediatr Gastroenterol Nutr. 2017 Dec;65(6):652-657. doi: 10.1097/MPG.0000000000001767. Erratum in: J Pediatr Gastroenterol Nutr. 2018 Feb;66(2):369. PMID: 28968289. Hancock AM, Witonsky DB, Ehler E, Alkorta-Aranburu G, Beall C, Gebremedhin A, Sukernik R, Utermann G, Pritchard J, Coop G, Di Rienzo A. Colloquium paper: human adaptations to diet, subsistence, and ecoregion are due to subtle shifts in allele frequency. Proc Natl Acad Sci U S A. 2010 May 11;107 Suppl 2(Suppl 2):8924-30. doi: 10.1073/pnas.0914625107. Epub 2010 May 5. PMID: 20445095; PMCID: PMC3024024.

82. Whitcomb DC, LaRusch J, Krasinskas AM, Klei L, Smith JP, Brand RE, Neoptolemos JP, Lerch MM, Tector M, Sandhu BS, Guda NM, Orlichenko L; Alzheimer's Disease Genetics Consortium; Alkaade S, Amann ST, Anderson MA, Baillie J, Banks PA, Conwell D, Coté GA, Cotton PB, DiSario J, Farrer LA, Forsmark CE, Johnstone M, Gardner TB, Gelrud A, Greenhalf W, Haines JL, Hartman DJ, Hawes RA, Lawrence C, Lewis M, Mayerle J, Mayeux R, Melhem NM, Money ME, Muniraj T, Papachristou GI, Pericak-Vance MA, Romagnuolo J, Schellenberg GD, Sherman S, Simon P, Singh VP, Slivka A, Stolz D, Sutton R, Weiss FU, Wilcox CM, Zarnescu NO, Wisniewski SR, O'Connell MR, Kienholz ML, Roeder K, Barmada MM, Yadav D, Devlin B. Common genetic variants in the CLDN2 and PRSS1-PRSS2 loci alter risk for alcohol-related and sporadic pancreatitis. Nat Genet. 2012 Dec;44(12):1349-54. doi: 10.1038/ng.2466. Epub 2012 Nov 11. PMID: 23143602; PMCID: PMC3510344.

83. Lowe ME, Kaplan MH, Jackson-Grusby L, D'Agostino D, Grusby MJ. Decreased neonatal dietary fat absorption and T cell cytotoxicity in pancreatic lipase-related protein 2-deficient mice. J Biol Chem. 1998 Nov 20;273(47):31215-21. doi: 10.1074/jbc.273.47.31215. PMID: 9813028; PMCID: PMC3690502.

84. Harper AR, Nayee S, Topol EJ. Protective alleles and modifier variants in human health and disease. Nat Rev Genet. 2015 Dec;16(12):689-701. doi: 10.1038/nrg4017. Epub 2015 Oct 27. PMID: 26503796.

85. Leonhardt U, Seidensticker F, Stöckmann F, Creutzfeldt W. Effect of camostate administration for two weeks on experimental pancreatitis in mice and rats. Pancreas. 1993 Jan;8(1):98-102. doi: 10.1097/00006676-199301000-00017. PMID: 7678329.

86. Friess H, Kleeff J, Isenmann R, Malfertheiner P, Büchler MW. Adaptation of the human pancreas to inhibition of luminal proteolytic activity. Gastroenterology. 1998 Aug;115(2):388-96. doi: 10.1016/s0016-5085(98)70205-7. PMID: 9679044.

87. Hackert T, Werner J, Gebhard MM, Klar E. Effects of heparin in experimental models of acute pancreatitis and post-ERCP pancreatitis. Surgery. 2004 Feb;135(2):131-8. doi: 10.1016/j.surg.2003.08.001. PMID: 14739847.

88. Park MJ, Iyer S, Xue X, Bragazzi Cunha J, Gu S, Moons D, Pipe SW, Williams JA, Simeone DM, Shah YM, Omary MB. HIF1-alpha Regulates Acinar Cell Function and Response to Injury in Mouse Pancreas. Gastroenterology. 2018 May;154(6):1630-1634.e3. doi: 10.1053/j.gastro.2018.01.037. Epub 2018 Feb 1. PMID: 29409830; PMCID: PMC5927829.

89. Kröner PT, Wallace MB, Raimondo M, Antwi SO, Ma Y, Li Z, Ji B, Bi Y. Systemic anticoagulation is associated with decreased mortality and morbidity in acute pancreatitis. Pancreatology. 2021 Dec;21(8):1428-1433. doi: 10.1016/j.pan.2021.09.003. Epub 2021 Sep 8. PMID: 34518096.

90. Feldmann K, Grandoch M, Kohlmorgen C, Valentin B, Gerfer S, Nagy N, Hartwig S, Lehr S, Fender AC, Fischer JW. Decreased M1 macrophage polarization in dabigatran-treated Ldlr-deficient mice: Implications for atherosclerosis and adipose tissue inflammation. Atherosclerosis. 2019 Aug;287:81-88. doi: 10.1016/j.atherosclerosis.2019.06.897. Epub 2019 Jun 8. PMID: 31233979.

91. Bogatkevich GS, Ludwicka-Bradley A, Nietert PJ, Akter T, van Ryn J, Silver RM. Antiinflammatory and antifibrotic effects of the oral direct thrombin inhibitor dabigatran etexilate in a murine model of interstitial lung disease. Arthritis Rheum. 2011 May;63(5):1416-25. doi: 10.1002/art.30255. PMID: 21312187; PMCID: PMC3086970.

92. Dong A, Mueller P, Yang F, Yang L, Morris A, Smyth SS. Direct thrombin inhibition with dabigatran attenuates pressure overload-induced cardiac fibrosis and dysfunction in mice. Thromb Res. 2017 Nov;159:58-64. doi: 10.1016/j.thromres.2017.09.016. Epub 2017 Sep 21. PMID: 28982031; PMCID: PMC5722681.

93. Saifi MA, Annaldas S, Godugu C. A direct thrombin inhibitor, dabigatran etexilate protects from renal fibrosis by inhibiting protease activated receptor-1. Eur J Pharmacol. 2021 Feb 15;893:173838. doi: 10.1016/j.ejphar.2020.173838. Epub 2020 Dec 24. PMID: 33359646.

94. Navina S, et al. Lipotoxicity causes multisystem organ failure and exacerbates acute pancreatitis in obesity. Sci Transl Med. 2011;3(107):107ra110.

VIII. Acknowledgements

I would like to express my greatest gratitude to my supervisors and mentors, Prof. Dr. Miklós Sahin-Tóth and Dr. Eszter Hegyi, who have created the opportunity for me to work, learn and develop throughout my doctoral years. I genuinely appreciate and respect their infinite support and essential knowledge which guided me and made my research work possible.

I would like to express my special thanks Dr. Balázs Németh who guided, encouraged and supported me unconditionnally through the years of being a medical and doctoral student, introduced me to basic experimental methodology and taught me scientific attitude.

I am truly thankful for Dr. Zsanett Jancsó and Dr. Alexandra Demcsák for their valuable contribution, advice and help during my work in the United States.

I wish to say thanks to Prof. Dr. Péter Hegyi and to the coworkers of the Hungarian Pancreatic Study Group, whose support and assistance I could always count on.

I dedicate this thesis to my amazing family and friends, especially my parents Beatrix Horváth and Zsolt László Pesei, and my sister, Fruzsina Beatrix Pesei, who always kept me going with their belief.

ANNEX

PLOS ONE

RESEARCH ARTICLE

The common truncation variant in pancreatic lipase related protein 2 (PNLIPRP2) is expressed poorly and does not alter risk for chronic pancreatitis

Balázs Csaba Németh[1,2☯], Zsófia Gabriella Pesei[1,2☯], Eszter Hegyi[1,3], Ákos Szücs[4], Andrea Szentesi[2,3], Péter Hegyi[3,5], Mark E. Lowe[6], Miklós Sahin-Tóth[1]*

1 Center for Exocrine Disorders, Department of Molecular and Cell Biology, Boston University Henry M. Goldman School of Dental Medicine, Boston, MA, United States of America, **2** First Department of Medicine, University of Szeged, Szeged, Hungary, **3** Institute for Translational Medicine, University of Pécs, Pécs, Hungary, **4** First Department of Surgery, Semmelweis University, Budapest, Hungary, **5** First Department of Medicine, University of Pécs, Pécs, Hungary, **6** Department of Pediatrics, Washington University School of Medicine, St Louis, MO, United States of America

☯ These authors contributed equally to this work.
* miklos@bu.edu

Check for updates

OPEN ACCESS

Citation: Németh BC, Pesei ZG, Hegyi E, Szücs Á, Szentesi A, Hegyi P, et al. (2018) The common truncation variant in pancreatic lipase related protein 2 (PNLIPRP2) is expressed poorly and does not alter risk for chronic pancreatitis. PLoS ONE 13(11): e0206869. https://doi.org/10.1371/journal.pone.0206869

Editor: Jeffrey L. Brodsky, University of Pittsburgh, UNITED STATES

Received: September 9, 2018

Accepted: October 19, 2018

Published: November 8, 2018

Copyright: © 2018 Németh et al. This is an open access article distributed under the terms of the Creative Commons Attribution License, which permits unrestricted use, distribution, and reproduction in any medium, provided the original author and source are credited.

Data Availability Statement: All relevant data are within the manuscript.

Funding: The studies were supported by NIH grants R01 DK082412 and R01 DK058088 (to MST), R01 DK097241 and R01 DK080820 (to MEL) and the Hungarian National Research, Development and Innovation Fund grant #FK124632 (to BCN). The registry of the Hungarian Pancreatic Study Group was supported by the Hungarian Scientific Research Fund (K116634 to

Abstract

A nonsense variant (p.W358X) of human pancreatic lipase related protein 2 (PNLIPRP2) is present in different ethnic populations with a high allele frequency. In cell culture experiments, the truncated protein mainly accumulates inside the cells and causes endoplasmic reticulum stress. Here, we tested the hypothesis that variant p.W358X might increase risk for chronic pancreatitis through acinar cell stress. We sequenced exon 11 of *PNLIPRP2* in a cohort of 256 subjects with chronic pancreatitis (152 alcoholic and 104 non-alcoholic) and 200 controls of Hungarian origin. We observed no significant difference in the distribution of the truncation variant between patients and controls. We analyzed mRNA expression in human pancreatic cDNA samples and found the variant allele markedly reduced. We conclude that the p.W358X truncation variant of *PNLIPRP2* is expressed poorly and has no significant effect on the risk of chronic pancreatitis.

Introduction

Recurrent acute pancreatitis and chronic pancreatitis are inflammatory diseases of the pancreas with significant health and economic burdens [1, 2]. After an initial episode of acute pancreatitis, 10 to 30% of adults and children have additional episodes and, of those, a large fraction develop chronic pancreatitis (CP) [3, 4]. Progression of a single episode to chronic pancreatitis often associates with genetic risk factors in genes encoding digestive enzymes expressed in pancreatic acinar cells [5–7]. Since the discovery that a genetic variant in *PRSS1* (cationic trypsinogen) causes hereditary pancreatitis, most investigations to identify additional genetic risk factors focused on proteases and their inhibitors [8, 9].

PH) and the Momentum Grant of the Hungarian Academy of Sciences (LP2014-10/2014 to PH). The funders had no role in study design, data collection and analysis, decision to publish, or preparation of the manuscript.

Competing interests: The authors have declared that no competing interests exist.

More recent studies linked genetic variants in pancreatic lipases to increased risk for CP. The first report described variants in the gene encoding carboxyl ester lipase (*CEL*) that result in a form of autosomal dominant CP characterized by early-onset pancreatic insufficiency and diabetes [10]. A subsequent study found that a hybrid allele resulting from recombination of *CEL* and a neighboring pseudogene, *CELP*, increased risk for CP in northern Europeans [11]. Additionally, a report of two brothers who had a deficiency of pancreatic lipase (PNLIP) and evidence of CP showed they were homozygous for a missense mutation in *PNLIP* [12]. Follow-up studies indicated that the genetic variants of CEL and PNLIP likely cause disease through increased protein misfolding and maladaptive activation of unfolded protein response pathways [11, 13–15]. Importantly, these studies suggest that genetic variants in other pancreatic lipases, such as the pancreatic lipase related protein 2 (PNLIPRP2), might increase the risk for CP.

PNLIPRP2 is homologous with PNLIP and both belong to the same large lipase gene family [16–18]. Unlike PNLIP, which only digests triglycerides, PNLIPRP2 has lipase activity against triglycerides, phospholipids and galactolipids [16]. In newborn mice, PNLIPRP2 plays a critical role in fat digestion [19]. Its role in humans remains unclear. Intriguingly, a nonsense variant (p.W358X) in human *PNLIPRP2* is present in different ethnic populations at a high allele frequency of 0.3 to 0.5 [20]. When expressed in transfected HEK 293T cells, the truncated protein largely accumulated inside the cells as a detergent-insoluble aggregate and only a small amount was secreted into the medium [21]. The intracellular aggregates activated the unfolded protein response. The findings show that p.W358X PNLIPRP2 can alter cellular physiology through two mechanisms. First, the secretory defect results in a loss of function that might affect dietary fat digestion. Second, the intracellular aggregates of truncated PNLIPRP2 may result in a gain of function by placing pancreatic acinar cells at increased risk for injury through a maladaptive unfolded protein response. In combination with other stressors, the presence of PNLIPRP2 aggregates could activate cell death and inflammatory pathways leading to pancreatitis. A similar mechanism was reported for misfolding PRSS1 and carboxypeptidase A1 (CPA1) mutants, which appear to cause pancreatitis through endoplasmic reticulum stress [22]. Herein, we investigated whether the p.W358X *PNLIPRP2* allele is a genetic risk factor for CP in patients with alcohol-related and non-alcohol-related CP.

Materials and methods

Nomenclature

Nucleotide numbering follows coding DNA numbering with the first nucleotide of the ATG translation initiation codon designated as +1. Amino acids are numbered starting with the initiator methionine of the primary translation product of *PNLIPRP2*. The NCBI genomic reference sequence for *PNLIPRP2* (NC_000010.11, *Homo sapiens* chromosome 10, GRCh38.p12 primary assembly) and the NCBI coding DNA reference sequence (NM_005396.4) correspond to the minor truncation allele. In the present study, we used the major full-length *PNLIPRP2* allele as reference for the designation of all *PNLIPRP2* variants. In this manner, the nonsense p.W358X variant becomes the "effect" allele, which is the only biologically meaningful representation. Table 1 compares *PNLIPRP2* variant designations using the two different reference sequences and lists the dbSNP numbers for unambiguous identification.

Study subjects

This study used de-identified genomic DNA samples from the registry of the Hungarian Pancreatic Study Group (ethical approval number TUKEB 22254-1/2012/EKU; biobanking approval number IF702-19/2012). Subjects were recruited from 11 Hungarian centers between

Table 1. Designation of *PNLIPRP2* variants with respect to the NCBI reference sequence corresponding to the minor truncation allele and the full-length major allele used as the reference in this study.

		NCBI reference minor truncation allele		Reference used in this work major full-length allele	
***PNLIPRP2* region**	**dbSNP number**	**Nucleotide change**	**Amino acid change**	**Nucleotide change**	**Amino acid change**
Intron 10		c.1070-379delG		c.1070-379delG	
Intron 10	rs4751994	c.1070-321C>T		c.1070-321T>C	
Exon 11	rs4751995	c.1074A>G	p.X358W	**c.1074G>A**	**p.W358X**
Exon 11	rs4751996	c.1084A>G	p.I362V	c.1084G>A	p.V362I
Exon 11	rs10885997	c.1161A>G	p.S387 =	c.1161G>A	p.S387 =
Intron 11	rs7910135	c.1181+55C>A		c.1181+55A>C	

The truncation variant is highlighted in bold type.

https://doi.org/10.1371/journal.pone.0206869.t001

2012 and 2018 and all gave informed consent according to the ethical guidelines of the Declaration of Helsinki. The current study was also approved by the Institutional Review Board at Boston University ("Analysis of susceptibility genes in patients with chronic pancreatitis"; IRB number H-35382). A total of 256 unrelated patients with CP, including 152 with alcoholic CP and 104 with non-alcoholic CP and 200 control subjects with no pancreatic disease were analyzed. The CP study cohort included patients with a history of recurrent acute pancreatitis and/or pathological imaging findings consistent with CP, such as pancreatic calcifications, duct dilatation or irregularities, with or without exocrine pancreatic insufficiency or diabetes. Patient characteristics are described in Table 2. Alcoholic CP was diagnosed in CP cases with alcohol consumption of more than 80 g/day (men) or 60 g/day (women) for at least two years. De-identified pancreatic cDNA and matching genomic DNA samples (n = 9) from cadaveric donors were obtained from the University of Szeged, Hungary.

DNA sequencing

Primer sequences and amplicon sizes are listed in Table 3. PCR reactions were performed using 1.0 U HotStar Taq DNA polymerase (Qiagen, Valencia, CA), 0.2 mM dNTP, 2.0 μL 10x PCR buffer (Qiagen), 0.5 μM primers, and 10–50 ng genomic DNA or cDNA template in a total volume of 20 μL. Cycling conditions were as follows: 15-min initial heat activation at 95 °C; 40 cycles of 30 s denaturation at 94 °C, 30 s annealing at 60 °C, and 60 s extension at 72 °C; and final extension for 5 min at 72 °C. Products were verified by 1.5% agarose gel electrophoresis. PCR amplicons (5 μL) were treated with 1 μL FastAP Thermosensitive Alkaline Phosphatase and 0.5 μL Exonuclease I (Thermo Fisher Scientific, Waltham, MA) for 15 min at 37 °C and the reaction was stopped by heating the samples to 85 °C for 15 min. Sanger sequencing was performed using the forward PCR primers as sequencing primer. Amplicons containing the heterozygous c.1070-379delG variant were also sequenced with the reverse primer.

Table 2. Study population.

	All CP *n = 256*		**NACP n = 104**		**ACP n = 152**		**Controls *n = 200***	
	Male	**Female**	**Male**	**Female**	**Male**	**Female**	**Male**	**Female**
number	194	62	60	44	134	18	113	87
mean age at recruitment	56±10	56±14	57±12	57±16	55±10	53±9	52±12	52±13
mean age of disease onset	48±12	48±16	47±12	48±18	48±12	48±9	-	-

Age values indicate mean ± S.D. in years. CP, chronic pancreatitis, NACP, non-alcoholic chronic pancreatitis, ACP, alcoholic chronic pancreatitis.

https://doi.org/10.1371/journal.pone.0206869.t002

Table 3. Oligonucleotide primers used for PCR amplification of exon 11 of *PNLIPRP2* from genomic DNA (e11 primers) and a portion of the *PNLIPRP2* coding sequence from pancreatic cDNA (RT primers).

Primer name	Sequence (5'>3')	Amplicon	Annealing temperature
PNLIPRP2 e11 forward PNLIPRP2 e11 reverse	GTT CTG GAG GAT GGA AAT CTG CAA AAG GAG TTA GCA CAT GAC T	836 bp	60 °C
PNLIPRP2 RT forward PNLIPRP2 RT reverse	CAT CTG GAT TTC TTT CCA AAT GG CGA GTG CAT TAA AGA TTT TAT TAC CG	732 bp	60 °C

https://doi.org/10.1371/journal.pone.0206869.t003

Results

A common truncation variant in *PNLIPRP2*

The common truncation variant c.1074G>A (p.W358X) in *PNLIPRP2* was first described in 2003 as W357X in European, African and Chinese populations with allele frequencies of 0.53, 0.55 and 0.33, respectively [20]. A 2010 study on the association of common gene variants and human dietary habits described the variant as W358X (rs4751995) with similar allele frequencies [23]. The discrepancy in numbering is because the original cloning study of *PNLIPRP2* missed one of the two consecutive Met codons at the start of the coding sequence [18]. Interestingly, the first Met is encoded by a separate upstream exon, which should be counted as exon 1 of the *PNLIPRP2* gene; placing the truncation variant in exon 11. The NCBI reference sequence for *PNLIPRP2* corresponds to the minor truncation allele. To describe the truncation variant in a biologically meaningful manner, in this study we used the major full-length *PNLIPRP2* allele as reference (Table 1).

DNA sequence analysis of exon 11 of human *PNLIPRP2*

We genotyped 152 subjects with alcoholic CP, 104 subjects with non-alcoholic CP and 200 control subjects, recruited from the registry of the Hungarian Pancreatic Study Group. We used direct DNA sequencing after PCR amplification of exon 11 and flanking intronic regions of *PNLIPRP2*. Within the amplified 793 nt sequence, we found 6 nucleotide variants, which included three intronic variants (c.1070-379delG, c.1070-321T>C and c.1181+55A>C), one synonymous variant (c.1161G>A, p.S387 =), one missense variant (c.1084G>A, p.V362I) and the truncation variant c.1074G>A (p.W358X) (Fig 1). The commonly occurring variants c.1070-321T>C, p.W358X, p.V362I, p.S387 = and c.1181+55A>C were found in linkage disequilibrium as a conserved haplotype (CAAAC in Fig 1). Another common haplotype (CGGAA in Fig 1) was formed by variants c.1070-321T>C and p.S387 = .

When allele frequency was considered, distribution of the variants between patients and controls showed no significant difference (Table 4). Subgroup analysis for alcoholic and non-alcoholic CP patients versus controls revealed no association either (Tables 5 and 6). We also analyzed genotypes using dominant and recessive models but found no significant differences in genotype frequencies between all CP patients or the alcoholic and non-alcoholic cohorts versus controls (Tables 7, 8 and 9). Finally, comparison of the three haplotypes between patients and controls yielded no significant differences with the exception of the CGGAA haplotype (see Fig 1), which was overrepresented in the non-alcoholic CP cohort relative to controls (OR 1.6, *P* 0.04) (Tables 10, 11 and 12). We consider this a spurious association due to limited sample size and chance.

Expression of the *PNLIPRP2* truncation allele

To estimate the relative mRNA expression of the full-length and truncation alleles of *PNLIPRP2*, we used direct sequencing of pancreatic cDNA after PCR amplification of a 732 nt

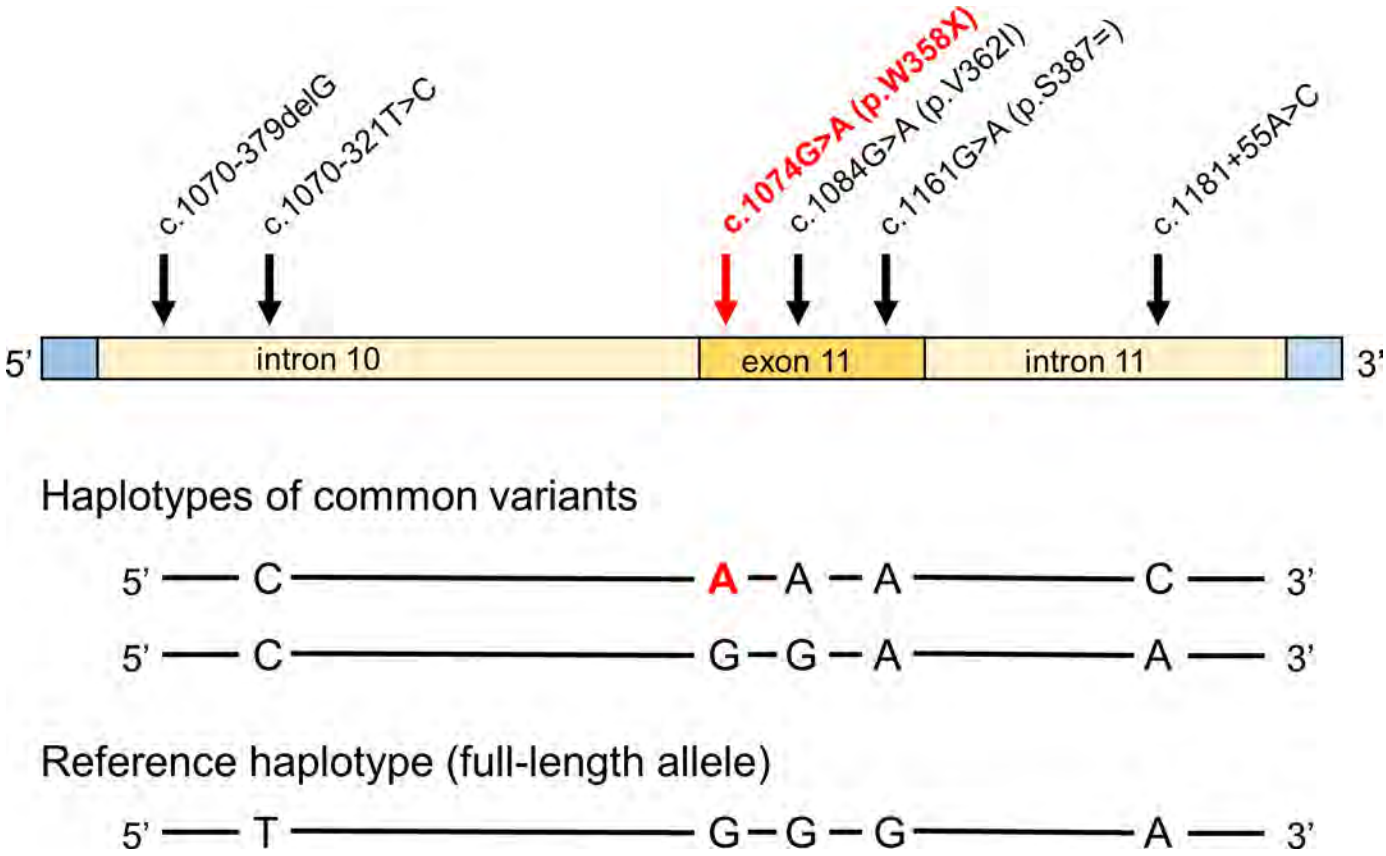

Fig 1. *PNLIPRP2* variants in exon 11 and the flanking intronic regions identified in the present study. The truncation variant is in bold type. The three haplotypes formed by the five commonly occurring variants are also shown.

https://doi.org/10.1371/journal.pone.0206869.g001

fragment of the coding DNA. We obtained nine de-identified cDNA samples with matching genomic DNA from cadaveric donors. Sequencing of the genomic DNA revealed five heterozygous samples and one sample homozygous for the truncation allele. The electropherograms of the heterozygous genomic sequences showed two signals at the position of variants p.W358X and p.V362I, with comparable peak heights (Fig 2A). Surprisingly, when heterozygous cDNA samples were sequenced, only one peak was visible at these positions, which corresponded to the major full-length allele, whereas no signal was apparent for the minor truncation allele (Fig 2B). PCR amplification of the pancreatic cDNA sample with the homozygous truncation allele confirmed the absence of detectable mRNA expression (Fig 2C). Taken

Table 4. Allele frequency of *PNLIPRP2* variants in patients with chronic pancreatitis (CP) and controls without pancreatic disease.

PNLIPRP2	Nucleotide change	Amino acid change	CP patient alleles	Control alleles	OR	*P* value	95% CI
Intron 10	c.1070-379delG		2/512 (0.4%)	1/400 (0.3%)	1.6	0.72	0.14–17.3
Intron 10	c.1070-321T>C		319/512 (62.3%)	240/400 (60%)	1.1	0.48	0.84–1.4
Exon 11	**c.1074G>A**	**p.W358X**	**245/512 (47.9%)**	**192/400 (48%)**	**0.99**	**0.97**	**0.77–1.3**
Exon 11	c.1084G>A	p.V362I	245/512 (47.9%)	192/400 (48%)	0.99	0.97	0.77–1.3
Exon 11	c.1161G>A	p.S387 =	321/512 (62.7%)	240/400 (60%)	1.1	0.4	0.86–1.5
Intron 11	c.1181+55A>C		246/512 (48%)	192/400 (48%)	1	0.99	0.77–1.3

The truncation variant is highlighted in bold type. OR, odds ratio; CI, confidence interval.

https://doi.org/10.1371/journal.pone.0206869.t004

Table 5. Allele frequency of *PNLIPRP2* variants in patients with non-alcoholic chronic pancreatitis (NACP) and controls without pancreatic disease.

PNLIPRP2	Nucleotide change	Amino acid change	NACP patient alleles	Control alleles	OR	*P* value	95% CI
Intron 10	c.1070-379delG		1/208 (0.5%)	1/400 (0.3%)	1.9	0.64	0.12–31
Intron 10	c.1070-321T>C		131/208 (63%)	240/400 (60%)	1.1	0.48	0.8–1.6
Exon 11	**c.1074G>A**	**p.W358X**	**93/208 (44.7%)**	**192/400 (48%)**	**0.88**	**0.44**	**0.63–1.2**
Exon 11	c.1084G>A	p.V362I	93/208 (44.7%)	192/400 (48%)	0.88	0.44	0.63–1.2
Exon 11	c.1161G>A	p.S387 =	131/208 (63%)	240/400 (60%)	1.1	0.48	0.8–1.6
Intron 11	c.1181+55A>C		94/208 (45.2%)	192/400 (48%)	0.89	0.51	0.64–1.3

The truncation variant is highlighted in bold type. OR, odds ratio; CI, confidence interval.

https://doi.org/10.1371/journal.pone.0206869.t005

Table 6. Allele frequency of *PNLIPRP2* variants in patients with alcoholic chronic pancreatitis (ACP) and controls without pancreatic disease.

PNLIPRP2	Nucleotide change	Amino acid change	ACP patient alleles	Control alleles	OR	*P* value	95% CI
Intron 10	c.1070-379delG		1/304 (0.3%)	1/400 (0.3%)	1.3	0.85	0.08–21.1
Intron 10	c.1070-321T>C		188/304 (61.8%)	240/400 (60%)	1.1	0.62	0.8–1.5
Exon 11	**c.1074G>A**	**p.W358X**	**152/304 (50%)**	**192/400 (48%)**	**1.1**	**0.6**	**0.8–1.5**
Exon 11	c.1084G>A	p.V362I	152/304 (50%)	192/400 (48%)	1.1	0.6	0.8–1.5
Exon 11	c.1161G>A	p.S387 =	190/304 (62.5%)	240/400 (60%)	1.1	0.5	0.82–1.5
Intron 11	c.1181+55A>C		152/304 (50%)	192/400 (48%)	1.1	0.6	0.8–1.5

The truncation variant is highlighted in bold type. OR, odds ratio; CI, confidence interval.

https://doi.org/10.1371/journal.pone.0206869.t006

Table 7. Genotype distribution of *PNLIPRP2* variants in patients with chronic pancreatitis (CP) and in controls.

PNLIPRP2	Nucleotide change	Genotype	CP patients	Controls	OR	*P* value	95% CI
Intron 10	c.1070-379delG	GG delG deldel	254/256 (99.2%) 2/256 (0.8%) 0/256 (0%)	199/200 (99.5%) 1/200 (0.5%) 0/200 (0%)	*1.6* 0.78	*0.72* 0.9	*0.14–17.4* 0.02–39.6
Intron 10	c.1070-321T>C	TT TC CC	37/256 (14.5%) 119/256 (46.5%) 100/256 (39%)	27/200 (13.5%) 106/200 (53%) 67/200 (33.5%)	*0.92* 1.3	*0.77* 0.22	*0.54–1.6* 0.87–1.9
Exon 11	**c.1074G>A**	GG GA AA	68/256 (26.6%) 131/256 (51.2%) 57/256 (22.2%)	50/200 (25%) 108/200 (54%) 42/200 (21%)	*0.92* 1.1	*0.7* 0.75	*0.6–1.4* 0.69–1.7
Exon 11	c.1084G>A	GG GA AA	68/256 (26.6%) 131/256 (51.2%) 57/256 (22.2%)	50/200 (25%) 108/200 (54%) 42/200 (21%)	*0.92* 1.1	*0.7* 0.75	*0.6–1.4* 0.69–1.7
Exon 11	c.1161G>A	GG GA AA	37/256 (14.5%) 117/256 (45.7%) 102/256 (39.8%)	27/200 (13.5%) 106/200 (53%) 67/200 (33.5%)	*0.92* 1.3	*0.77* 0.16	*0.54–1.6* 0.89–1.9
Intron 11	c.1181+55A>C	AA AC CC	68/256 (26.6%) 130/256 (50.8%) 58/256 (22.6%)	50/200 (25%) 108/200 (54%) 42/200 (21%)	*0.92* 1.1	*0.7* 0.67	*0.6–1.4* 0.7–1.7

Data were analyzed assuming dominant (shown in italics) or recessive models of inheritance. The truncation variant is highlighted in bold type. OR, odds ratio; CI, confidence interval.

https://doi.org/10.1371/journal.pone.0206869.t007

together, our observations indicate that the truncation allele is not expressed at the mRNA level to a significant extent, in all likelihood due to nonsense-mediated mRNA decay.

We also consulted the Genotype-Tissue Expression (GTEx) Portal (www.gtexportal.org/home) and found that all five common variants within the truncation haplotype were

Table 8. Genotype distribution of *PNLIPRP2* variants in patients with non-alcoholic chronic pancreatitis (NACP) and in controls.

PNLIPRP2	Nucleotide change	Genotype	NACP patients	Controls	OR	*P* value	95% CI
Intron 10	c.1070-379delG	GG delG deldel	103/104 (99%) 1/104 (1%) 0/104 (0%)	199/200 (99.5%) 1/200 (0.5%) 0/200 (0%)	*1.9* 1.9	*0.64* 0.75	*0.12–31.2* 0.04–97.4
Intron 10	c.1070-321T>C	TT TC CC	12/104 (11.5%) 53/104 (51%) 39/104 (37.5%)	27/200 (13.5%) 106/200 (53%) 67/200 (33.5%)	*1.2* 1.2	*0.63* 0.49	*0.58–2.5* 0.73–2
Exon 11	**c.1074G>A**	GG GA AA	26/104 (25%) 63/104 (60.6%) 15/104 (14.4%)	50/200 (25%) 108/200 (54%) 42/200 (21%)	*1* 0.63	*1* 0.17	*0.58–1.7* 0.33–1.2
Exon 11	c.1084G>A	GG GA AA	26/104 (25%) 63/104 (60.6%) 15/104 (14.4%)	50/200 (25%) 108/200 (54%) 42/200 (21%)	*1* 0.63	*1* 0.17	*0.58–1.7* 0.33–1.2
Exon 11	c.1161G>A	GG GA AA	12/104 (11.5%) 53/104 (51%) 39/104 (37.5%)	27/200 (13.5%) 106/200 (53%) 67/200 (33.5%)	*1.2* 1.2	*0.63* 0.49	*0.58–2.5* 0.73–2
Intron 11	c.1181+55A>C	AA AC CC	26/104 (25%) 62/104 (59.6%) 16/104 (15.4%)	50/200 (25%) 108/200 (54%) 42/200 (21%)	*1* 0.68	*1* 0.24	*0.58–1.7* 0.36–1.3

Data were analyzed assuming dominant (shown in italics) or recessive models of inheritance. The truncation variant is highlighted in bold type. OR, odds ratio; CI, confidence interval.

https://doi.org/10.1371/journal.pone.0206869.t008

Table 9. Genotype distribution of *PNLIPRP2* variants in patients with alcoholic chronic pancreatitis (ACP) and in controls.

PNLIPRP2	Nucleotide change	Genotype	ACP patients	Controls	OR	*P* value	95% CI
Intron 10	c.1070-379delG	GG delG deldel	151/152 (99.3%) 1/152 (0.7%) 0/152 (0%)	199/200 (99.5%) 1/200 (0.5%) 0/200 (0%)	*1.3* 1.3	*0.85* 0.89	*0.08–21.2* 0.03–66.6
Intron 10	c.1070-321T>C	TT TC CC	25/152 (16.5%) 66/152 (43.4%) 61/152 (40.1%)	27/200 (13.5%) 106/200 (53%) 67/200 (33.5%)	*0.79* 1.3	*0.44* 0.2	*0.44–1.4* 0.86–2.1
Exon 11	**c.1074G>A**	GG GA AA	42/152 (27.6%) 68/152 (44.8%) 42/152 (27.6%)	50/200 (25%) 108/200 (54%) 42/200 (21%)	*0.87* 1.4	*0.58* 0.15	*0.54–1.4* 0.88–2.4
Exon 11	c.1084G>A	GG GA AA	42/152 (27.6%) 68/152 (44.8%) 42/152 (27.6%)	50/200 (25%) 108/200 (54%) 42/200 (21%)	*0.87* 1.4	*0.58* 0.15	*0.54–1.4* 0.88–2.4
Exon 11	c.1161G>A	GG GA AA	25/152 (16.5%) 64/152 (42.1%) 63/152 (41.4%)	27/200 (13.5%) 106/200 (53%) 67/200 (33.5%)	*0.79* 1.4	*0.44* 0.13	*0.44–1.4* 0.9–2.2
Intron 11	c.1181+55A>C	AA AC CC	42/152 (27.6%) 68/152 (44.8%) 42/152 (27.6%)	50/200 (25%) 108/200 (54%) 42/200 (21%)	*0.87* 1.4	*0.58* 0.15	*0.54–1.4* 0.88–2.4

Data were analyzed assuming dominant (shown in italics) or recessive models of inheritance. The truncation variant is highlighted in bold type. OR, odds ratio; CI, confidence interval.

https://doi.org/10.1371/journal.pone.0206869.t009

Table 10. Distribution of common *PNLIPRP2* haplotype alleles in patients with chronic pancreatitis (CP) and in controls.

Haplotype	All CP patients	Controls	OR	*P* value	95% CI
CAAAC	**244/512 (47.7%)**	**191/400 (47.8%)**	**1**	**0.98**	**0.77–1.3**
CGGAA	73/512 (14.3%)	48/400 (12.0%)	1.2	0.32	0.83–1.8
TGGGA	191/512 (37.3%)	160/400 (40.0%)	0.89	0.41	0.68–1.2

The truncation haplotype is highlighted in bold type. OR, odds ratio; CI, confidence interval. See Fig 1 for more details.

https://doi.org/10.1371/journal.pone.0206869.t010

Table 11. Distribution of common *PNLIPRP2* haplotype alleles in patients with non-alcoholic chronic pancreatitis (NACP) and in controls.

Haplotype	NACP patients	Controls	OR	*P* value	95% CI
CAAAC	**92/208 (44.2%)**	**191/400 (47.8%)**	**0.87**	**0.41**	**0.62–1.2**
CGGAA	38/208 (18.3%)	48/400 (12.0%)	1.6	0.040*	1.0–2.6
TGGGA	77/208 (37.0%)	160/400 (40.0%)	0.88	0.48	0.62–1.3

The truncation haplotype is highlighted in bold type. OR, odds ratio; CI, confidence interval. See Fig 1 for more details. The asterisk indicates significant association.

https://doi.org/10.1371/journal.pone.0206869.t011

associated with diminished *PNLIPRP2* mRNA expression (Fig 3). The GTEx database is an open-access public resource to study tissue-specific gene expression and its relationship to genetic variation. The project analyzes global RNA expression within individual human tissues from deeply genotyped donors and correlates variations in gene expression with genetic alterations.

Discussion

Physicians have increasingly recognized that CP is a complex disorder associated with multiple risk factors [24]. For many, particularly children, genetic variants in genes encoding pancreatic digestive enzymes contribute to the pathophysiology of CP [6]. In this study, we sought to determine if a common genetic variant in *PNLIPRP2* increased the risk for CP. The variant introduces a premature stop codon, p.W358X, resulting in a truncated protein and *in vitro* evidence suggests the expressed protein misfolds and activates the unfolded protein response [21]. We found no correlation of variant p.W358X with CP as a group or sub-grouped into alcoholic CP or non-alcoholic CP. This finding demonstrates that p.W358X is not a significant genetic risk factor for CP. We identified additional variants within exon 11 and the flanking intronic regions of *PNLIPRP2*, which formed conserved haplotypes. When these haplotypes were analyzed for disease association, we observed enrichment of the CGGAA haplotype (see Fig 1) in the non-alcoholic CP cohort. However, statistical significance was barely reached and we interpret this finding as fortuitous association due to the small sample size.

Because the presumed mechanism whereby variant p.W358X would contribute to CP is by activating maladaptive unfolded protein response and cell death pathways, we sought to determine if expression of the p.W358X allele was lower than expression of full length *PNLIPRP2*. If so, the levels of truncated protein may not be sufficient to activate the unfolded protein response. We accomplished this goal in two ways. First, we PCR amplified *PNLIPRP2* from pancreatic cDNA of heterozygous and homozygous p.W358X carriers and analyzed expression by DNA sequencing and agarose gel electrophoresis. Second, we interrogated the GTEx Portal database. Both methods confirmed that the amount of mRNA encoding p.W358X PNLIPRP2 is quite low compared to the mRNA amounts for full-length PNLIPRP2. The results suggest that the mRNA encoding the p.W358X variant undergoes nonsense-mediated decay [25]. In the previous study that characterized the cellular effects of the p.W358X variant the authors

Table 12. Distribution of common *PNLIPRP2* haplotype alleles in patients with alcoholic chronic pancreatitis (ACP) and in controls.

Haplotype	ACP patients	Controls	OR	*P* value	95% CI
CAAAC	**152/304 (50.0%)**	**191/400 (47.8%)**	**1.1**	**0.55**	**0.81–1.5**
CGGAA	35/304 (11.5%)	48/400 (12.0%)	0.95	0.84	0.60–1.5
TGGGA	114/304 (37.5%)	160/400 (40.0%)	0.90	0.5	0.66–1.2

The truncation haplotype is highlighted in bold type OR, odds ratio; CI, confidence interval. See Fig 1 for more details.

https://doi.org/10.1371/journal.pone.0206869.t012

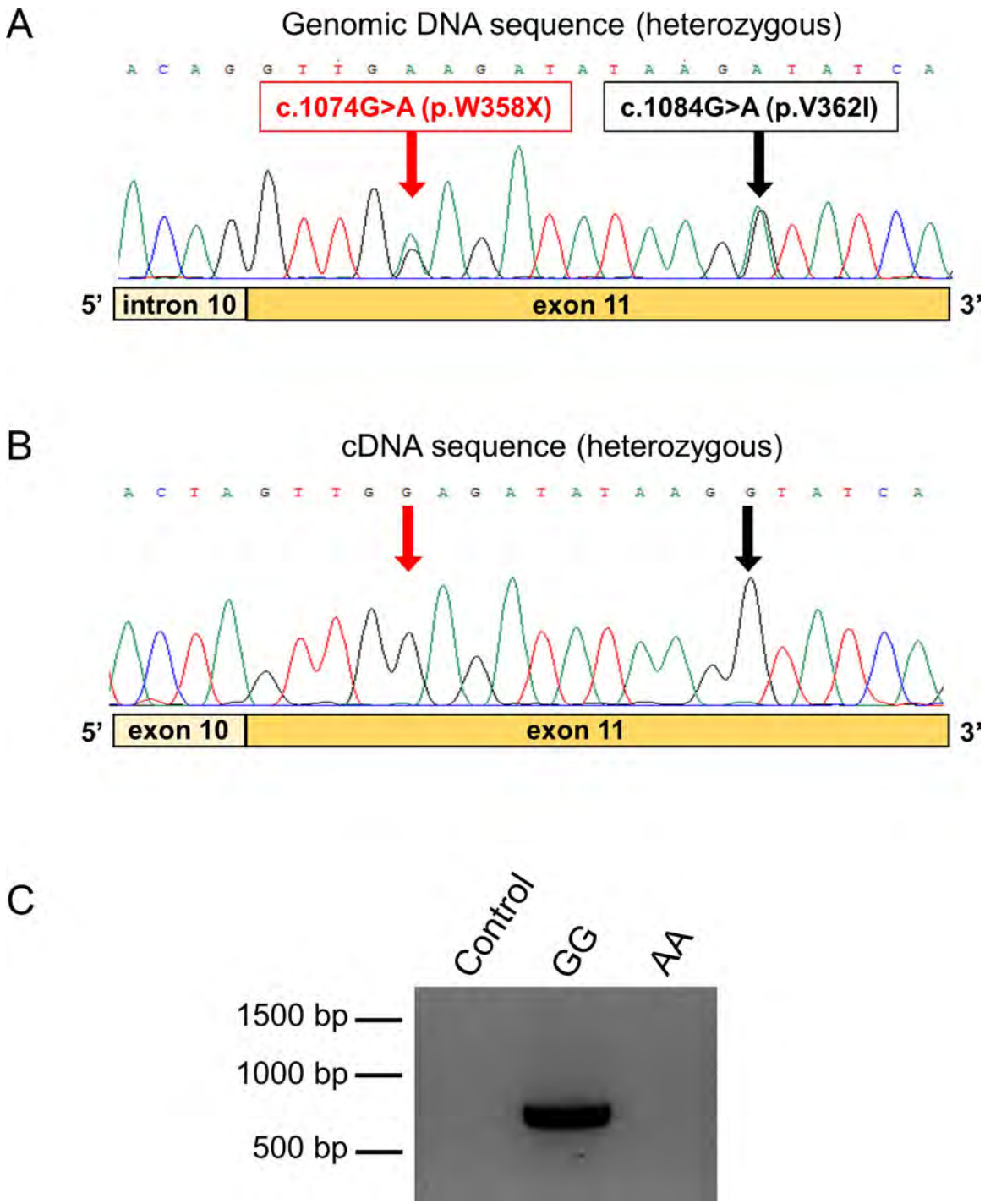

Fig 2. Expression of the *PNLIPRP2* p.W358X truncation variant. A, Electropherogram of the genomic DNA sequence of a heterozygous carrier showing the double signal at the position of variants p.W358X and p.V362I. **B**, Electropherogram of the pancreatic cDNA sequence of the same heterozygous subject. Note the absence of the signal corresponding to the minor truncation allele at the position of the variants. **C**, Agarose gel electrophoresis of PCR amplicons from pancreatic cDNA samples of subjects with homozygous A (minor truncation allele) and G (full-length allele) genotypes. Control reaction was performed with no added template.

https://doi.org/10.1371/journal.pone.0206869.g002

used artificial cDNA expression constructs, which lacked introns [21]. Consequently, the *PNLIPRP2* mRNA encoding the truncation variant did not suffer degradation and protein

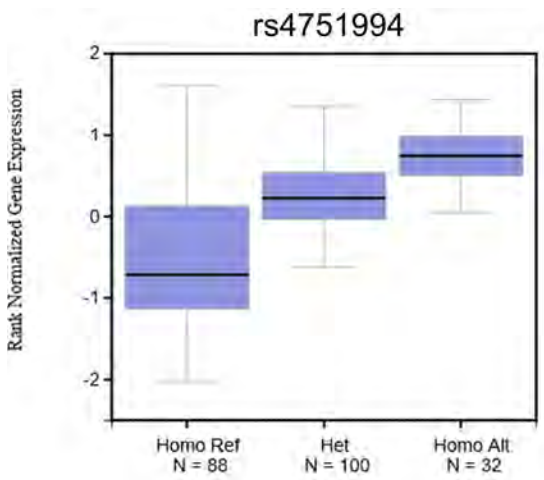
rs4751994
Rank Normalized Gene Expression
2
1
0
-1
-2
Homo Ref
N = 88
Het
N = 100
Homo Alt
N = 32

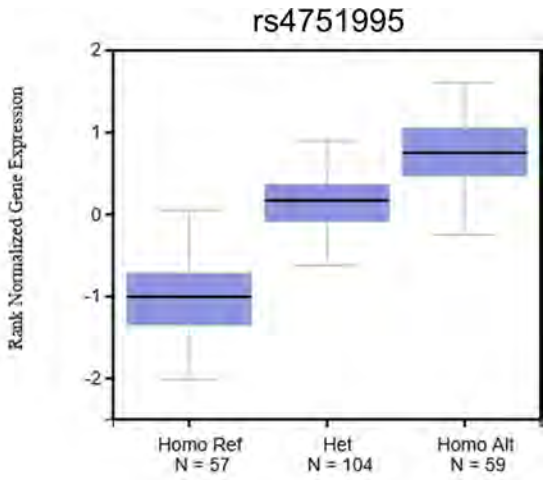
rs4751995
Rank Normalized Gene Expression
2
1
0
-1
-2
Homo Ref
N = 57
Het
N = 104
Homo Alt
N = 59

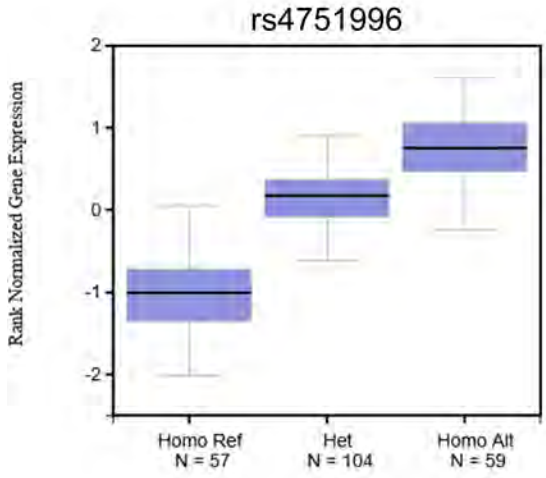
rs4751996
Rank Normalized Gene Expression
2
1
0
-1
-2
Homo Ref
N = 57
Het
N = 104
Homo Alt
N = 59

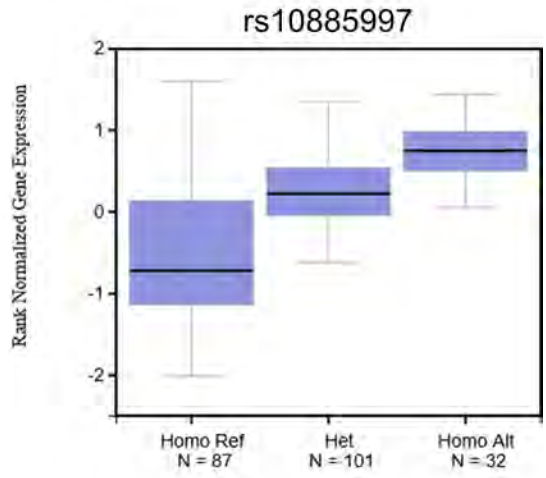
rs10885997
Rank Normalized Gene Expression
2
1
0
-1
-2
Homo Ref
N = 87
Het
N = 101
Homo Alt
N = 32

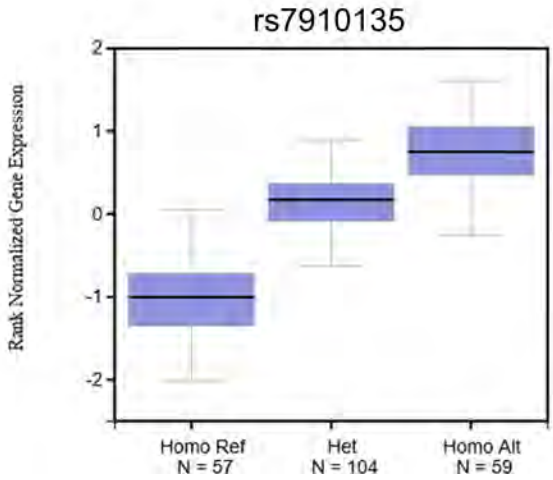
rs7910135
Rank Normalized Gene Expression
2
1
0
-1
-2
Homo Ref
N = 57
Het
N = 104
Homo Alt
N = 59

Fig 3. The effect of common *PNLIPRP2* variants on mRNA expression in the pancreas. Box plots were taken from the GTEx Portal (GTEx Analysis Release V7 - www.gtexportal.org). Note the diminished expression of the reference alleles (Ref), which correspond to the truncation haplotype in this database. See Table 1 for variant designation.

https://doi.org/10.1371/journal.pone.0206869.g003

expression levels achieved were high enough to induce the unfolded protein response. The present data strongly argue that this cannot be the case when variant p.W358X is expressed from its native gene in the acinar cells.

Given the low levels of mRNA expression, it is unlikely that p.W358X PNLIPRP2 causes disease through gain-of-function as suggested by studies in transfected tissue culture cells [21]. In retrospect, it seems reasonable to have predicted that p.W358X PNLIPRP2 should not be a significant risk factor for CP or another disease since it is so prevalent. More likely, any effect of p.W358X PNLIPRP2 on human health should result from loss-of-function. Humans harbor many genetic variants predicted to cause loss-of-function [26]. Homozygosity for loss-of-function variants either results in a non-fatal phenotype or represent benign variations in redundant genes. A non-fatal loss-of-function phenotype was found in *Pnliprp2*-deficient mice [19]. Suckling *Pnliprp2*-deficient mice had fat malabsorption and poor growth but survived to adulthood and were fertile. It is not known if a similar effect occurs in human infants homozygous for p.W358X PNLIPRP2. In humans, p.W358X PNLIPRP2 may represent a loss-of-function tolerant genetic variant with the loss of its lipase activity compensated by other lipases [16]. Alternatively, p.W358X PNLIPRP2 may represent a protective or disease modifying allele [27]. That is, homozygosity for this allele may confer protection against disease or modify adaptations to diet [23]. Determination of the importance of the common p.W358X *PNLIPRP2* allele in human health will require additional investigations.

Author Contributions

Conceptualization: Mark E. Lowe, Miklós Sahin-Tóth.

Data curation: Balázs Csaba Németh, Zsófia Gabriella Pesei, Eszter Hegyi, Ákos Szücs.

Formal analysis: Balázs Csaba Németh, Zsófia Gabriella Pesei, Eszter Hegyi, Mark E. Lowe, Miklós Sahin-Tóth.

Funding acquisition: Péter Hegyi, Mark E. Lowe, Miklós Sahin-Tóth.

Investigation: Balázs Csaba Németh.

Project administration: Andrea Szentesi, Péter Hegyi, Miklós Sahin-Tóth.

Resources: Ákos Szücs, Andrea Szentesi, Péter Hegyi, Miklós Sahin-Tóth.

Supervision: Miklós Sahin-Tóth.

Writing – original draft: Mark E. Lowe, Miklós Sahin-Tóth.

Writing – review & editing: Balázs Csaba Németh, Zsófia Gabriella Pesei, Eszter Hegyi, Ákos Szücs, Andrea Szentesi, Péter Hegyi, Mark E. Lowe, Miklós Sahin-Tóth.

References

1. Hall TC, Garcea G, Webb MA, Al-Leswas D, Metcalfe MS, Dennison AR. The socio-economic impact of chronic pancreatitis: a systematic review. J Eval Clin Pract 2014; 20:203–207. https://doi.org/10.1111/jep.12117 PMID: 24661411
2. Ting J, Wilson L, Schwarzenberg SJ, Himes R, Barth B, Bellin MD, et al. Direct costs of acute recurrent and chronic pancreatitis in children in the INSPPIRE registry. J Pediatr Gastroenterol Nutr 2016; 62:443–449. https://doi.org/10.1097/MPG.0000000000001057 PMID: 26704866

3. Bai HX, Lowe ME, Husain SZ. What have we learned about acute pancreatitis in children? J Pediatr Gastroenterol Nutr 2011; 52:262–270. https://doi.org/10.1097/MPG.0b013e3182061d75 PMID: 21336157
4. Yadav D, O'Connell M, Papachristou GI. Natural history following the first attack of acute pancreatitis. Am J Gastroenterol 2012; 107:1096–1103. https://doi.org/10.1038/ajg.2012.126 PMID: 22613906
5. Giefer MJ, Lowe ME, Werlin SL, Zimmerman B, Wilschanski M, Troendle D, et al. Early-onset acute recurrent and chronic pancreatitis is associated with *PRSS1* or *CTRC* gene mutations. J Pediatr 2017; 186:95–100. https://doi.org/10.1016/j.jpeds.2017.03.063 PMID: 28502372
6. Schwarzenberg SJ, Bellin M, Husain SZ, Ahuja M, Barth B, Davis H, et al. Pediatric chronic pancreatitis is associated with genetic risk factors and substantial disease burden. J Pediatr 2015; 166:890–896. https://doi.org/10.1016/j.jpeds.2014.11.019 PMID: 25556020
7. Conwell DL, Banks PA, Sandhu BS, Sherman S, Al-Kaade S, Gardner TB, et al. Validation of demographics, etiology, and risk factors for chronic pancreatitis in the USA: A report of the North American Pancreas Study (NAPS) Group. Dig Dis Sci 2017; 62:2133–2140. https://doi.org/10.1007/s10620-017-4621-z PMID: 28600657
8. Whitcomb DC, Gorry MC, Preston RA, Furey W, Sossenheimer MJ, Ulrich CD, et al. Hereditary pancreatitis is caused by a mutation in the cationic trypsinogen gene. Nat Genet 1996; 14:141–145. https://doi.org/10.1038/ng1096-141 PMID: 8841182
9. Weiss FU, Skube ME, Lerch MM. Chronic pancreatitis: an update on genetic risk factors. Curr Opin Gastroenterol 2018; 34:322–329. https://doi.org/10.1097/MOG.0000000000000461 PMID: 29901518
10. Raeder H, Johansson S, Holm PI, Haldorsen IS, Mas E, Sbarra V, et al. Mutations in the CEL VNTR cause a syndrome of diabetes and pancreatic exocrine dysfunction. Nat Genet 2006; 38:54–62. https://doi.org/10.1038/ng1708 PMID: 16369531
11. Fjeld K, Weiss FU, Lasher D, Rosendahl J, Chen JM, Johansson BB, et al. A recombined allele of the lipase gene *CEL* and its pseudogene *CELP* confers susceptibility to chronic pancreatitis. Nat Genet 2015; 47:518–522. https://doi.org/10.1038/ng.3249 PMID: 25774637
12. Behar DM, Basel-Vanagaite L, Glaser F, Kaplan M, Tzur S, Magal N, et al. Identification of a novel mutation in the *PNLIP* gene in two brothers with congenital pancreatic lipase deficiency. J Lipid Res 2014; 55:307–312. https://doi.org/10.1194/jlr.P041103 PMID: 24262094
13. Johansson BB, Torsvik J, Bjorkhaug L, Vesterhus M, Ragvin A, Tjora E, et al. Diabetes and pancreatic exocrine dysfunction due to mutations in the carboxyl ester lipase gene-maturity onset diabetes of the young (CEL-MODY): a protein misfolding disease. J Biol Chem 2011; 286:34593–4605. https://doi.org/10.1074/jbc.M111.222679 PMID: 21784842
14. Szabó A, Xiao X, Haughney M, Spector A, Sahin-Tóth M, Lowe ME. A novel mutation in PNLIP causes pancreatic triglyceride lipase deficiency through protein misfolding. Biochim Biophys Acta 2015; 1852:1372–1379. https://doi.org/10.1016/j.bbadis.2015.04.002 PMID: 25862608
15. Xiao X, Jones G, Sevilla WA, Stolz DB, Magee KE, Haughney M, et al. A carboxyl ester lipase (CEL) mutant causes chronic pancreatitis by forming intracellular aggregates that activate apoptosis. J Biol Chem 2016; 291:23224–23236. https://doi.org/10.1074/jbc.M116.734384 PMID: 27650499
16. Lowe ME. The triglyceride lipases of the pancreas. J Lipid Res 2002; 43:2007–2016. PMID: 12454260
17. Cygler M, Schrag JD, Sussman JL, Harel M, Silman I, Gentry MK, et al. Relationship between sequence conservation and three-dimensional structure in a large family of esterases, lipases, and related proteins. Protein Sci 1993; 2:366–382. https://doi.org/10.1002/pro.5560020309 PMID: 8453375
18. Giller T, Buchwald P, Blum-Kaelin D, Hunziker W. Two novel human pancreatic lipase related proteins, hPLRP1 and hPLRP2: differences in colipase dependency and in lipase activity. J Biol Chem 1992; 267:16509–16516. PMID: 1379598
19. Lowe ME, Kaplan MH, Jackson-Grusby L, D'Agostino D, Grusby MJ. Decreased neonatal dietary fat absorption and T cell cytotoxicity in pancreatic lipase-related protein 2-deficient mice. J Biol Chem 1998; 273:31215–31221. PMID: 9813028
20. Cao H, Hegele RA. DNA polymorphisms of lipase related genes. J Hum Genet 2003; 48:443–446. https://doi.org/10.1007/s10038-003-0051-1 PMID: 12898288
21. Xiao X, Mukherjee A, Ross LE, Lowe ME. Pancreatic lipase-related protein-2 (PLRP2) can contribute to dietary fat digestion in human newborns. J Biol Chem 2011; 286:26353–26363. https://doi.org/10.1074/jbc.M111.249813 PMID: 21652702
22. Sahin-Tóth M. Genetic risk in chronic pancreatitis: the misfolding-dependent pathway. Curr Opin Gastroenterol 2017; 33:390–395. https://doi.org/10.1097/MOG.0000000000000380 PMID: 28650851
23. Hancock AM, Witonsky DB, Ehler E, Alkorta-Aranburu G, Beall C, Gebremedhin A, et al. Colloquium paper: human adaptations to diet, subsistence, and ecoregion are due to subtle shifts in allele frequency. Proc Natl Acad Sci USA 2010; 107 Suppl 2:8924–8930.

24. Kleeff J, Whitcomb DC, Shimosegawa T, Esposito I, Lerch MM, Gress T, et al. Chronic pancreatitis. Nat Rev Dis Primers 2017; 3:17060. https://doi.org/10.1038/nrdp.2017.60 PMID: 28880010

25. Lykke-Andersen S, Jensen TH. Nonsense-mediated mRNA decay: an intricate machinery that shapes transcriptomes. Nat Rev Mol Cell Biol 2015; 16:665–677. https://doi.org/10.1038/nrm4063 PMID: 26397022

26. MacArthur DG, Balasubramanian S, Frankish A, Huang N, Morris J, Walter K, et al. A systematic survey of loss-of-function variants in human protein-coding genes. Science 2012; 335:823–828. https://doi.org/10.1126/science.1215040 PMID: 22344438

27. Harper AR, Nayee S, Topol EJ. Protective alleles and modifier variants in human health and disease. Nat Rev Genet 2015; 16:689–701. https://doi.org/10.1038/nrg4017 PMID: 26503796

JCI insight

Preclinical testing of dabigatran in trypsin-dependent pancreatitis

Zsófia Gabriella Pesei, … , Sandor Vajda, Miklós Sahin-Tóth

JCI Insight. 2022;7(21):e161145. https://doi.org/10.1172/jci.insight.161145.

Research Article **Inflammation** **Therapeutics**

Pancreatitis, the inflammatory disorder of the pancreas, has no specific therapy. Genetic, biochemical, and animal model studies revealed that trypsin plays a central role in the onset and progression of pancreatitis. Here, we performed biochemical and preclinical mouse experiments to offer proof of concept that orally administered dabigatran etexilate can inhibit pancreatic trypsins and shows therapeutic efficacy in trypsin-dependent pancreatitis. We found that dabigatran competitively inhibited all human and mouse trypsin isoforms (K_i range 10–79 nM) and dabigatran plasma concentrations in mice given oral dabigatran etexilate well exceeded the K_i of trypsin inhibition. In the *T7K24R* trypsinogen mutant mouse model, a single oral gavage of dabigatran etexilate was effective against cerulein-induced progressive pancreatitis, with a high degree of histological normalization. In contrast, spontaneous pancreatitis in *T7D23A* mice, which carry a more aggressive trypsinogen mutation, was not ameliorated by dabigatran etexilate, given either as daily gavages or by mixing it with solid chow. Taken together, our observations showed that benzamidine derivatives such as dabigatran are potent trypsin inhibitors and show therapeutic activity against trypsin-dependent pancreatitis in *T7K24R* mice. Lack of efficacy in *T7D23A* mice is probably related to the more severe pathology and insufficient drug concentrations in the pancreas.

Find the latest version:

https://jci.me/161145/pdf

JCI insight

RESEARCH ARTICLE

Preclinical testing of dabigatran in trypsin-dependent pancreatitis

Zsófia Gabriella Pesei,[1] Zsanett Jancsó,[1] Alexandra Demcsák,[1] Balázs Csaba Németh,[1] Sandor Vajda,[2] and Miklós Sahin-Tóth[1]

[1]Department of Surgery, University of California Los Angeles, Los Angeles, California, USA. [2]Department of Biomedical Engineering, Boston University, Boston, Massachusetts, USA.

Pancreatitis, the inflammatory disorder of the pancreas, has no specific therapy. Genetic, biochemical, and animal model studies revealed that trypsin plays a central role in the onset and progression of pancreatitis. Here, we performed biochemical and preclinical mouse experiments to offer proof of concept that orally administered dabigatran etexilate can inhibit pancreatic trypsins and shows therapeutic efficacy in trypsin-dependent pancreatitis. We found that dabigatran competitively inhibited all human and mouse trypsin isoforms (K_i range 10–79 nM) and dabigatran plasma concentrations in mice given oral dabigatran etexilate well exceeded the K_i of trypsin inhibition. In the *T7K24R* trypsinogen mutant mouse model, a single oral gavage of dabigatran etexilate was effective against cerulein-induced progressive pancreatitis, with a high degree of histological normalization. In contrast, spontaneous pancreatitis in *T7D23A* mice, which carry a more aggressive trypsinogen mutation, was not ameliorated by dabigatran etexilate, given either as daily gavages or by mixing it with solid chow. Taken together, our observations showed that benzamidine derivatives such as dabigatran are potent trypsin inhibitors and show therapeutic activity against trypsin-dependent pancreatitis in *T7K24R* mice. Lack of efficacy in *T7D23A* mice is probably related to the more severe pathology and insufficient drug concentrations in the pancreas.

Introduction

There is no specific pharmacological therapy for the inflammatory disorders of the exocrine pancreas, which include acute pancreatitis (AP), recurrent acute pancreatitis (RAP), and chronic pancreatitis (CP) (1). Pancreatitis often presents as a progressive, relapsing-recurring disease, in which a sentinel episode of AP progresses to RAP, and eventually to CP, driven by underlying genetic and environmental risk factors (1, 2). Studies on genetic risk factors associated with the AP-RAP-CP sequence (denoted as CP from here on out) revealed that ectopic, intrapancreatic activation of the digestive protease precursor trypsinogen to its active form trypsin is responsible for disease onset and progression (3–5). Genetic alterations increase intrapancreatic trypsin activity by accelerating trypsinogen autoactivation, and/or by diminishing protective mechanisms, such as trypsinogen degradation by chymotrypsin C and trypsin inhibition by the serine protease inhibitor Kazal type 1. This disease model has been designated as the trypsin-dependent pathway of genetic risk in CP, which not only formulates a mechanistic framework for CP development but also identifies a clear therapeutic target, i.e., trypsin (4, 5).

Considering the long history of biochemical investigations into the function of trypsin, and the availability of a large number of natural and synthetic trypsin inhibitors, it seems surprising that no effective antitrypsin therapy has been developed so far to treat or prevent pancreatitis. Although bovine pancreatic trypsin inhibitor (aprotinin) (6) and the *p*-guanidino-benzoate derivatives gabexate (FOY), camostat (FOY-305) (7), and nafamostat (FUT-175) (8) seemed effective in rodent experiments (9–16), their clinical efficacy has been either variable or disappointing (17–22 and references therein). This apparent contradiction can be largely explained by the fact that early preclinical experiments did not use mouse models of trypsin-dependent pancreatitis. Similarly, clinical trials did not focus on trypsin-dependent disease, which could be verified by appropriate genetic testing. Finally, the compounds evaluated had inhibitory activity against a range of proteases other than trypsin, which further confounds interpretation of the results from preclinical and clinical trials. Despite their dubious efficacy, nafamostat and gabexate infusions are approved to treat AP, and oral camostat is used for the management of pain associated with CP in Japan. More recently, the COVID-19 pandemic

Conflict of interest: The authors have declared that no conflict of interest exists.

Copyright: © 2022, Pesei et al. This is an open access article published under the terms of the Creative Commons Attribution 4.0 International License.

Submitted: April 18, 2022
Accepted: September 13, 2022
Published: November 8, 2022

Reference information: *JCI Insight*. 2022;7(21):e161145. https://doi.org/10.1172/jci.insight.161145.

sparked revived awareness in these drugs, as camostat and nafamostat have been identified as strong inhibitors of the transmembrane serine protease 2, which is required for cellular entry of the SARS-CoV-2 virus (23, 24). Several clinical trials have been initiated to test efficacy against COVID-19, and the results may also inform future clinical trials in pancreatitis with respect to dosing and side effects (25–28).

In addition to the renewed interest in small–molecular weight trypsin inhibitors, novel mouse models of trypsin-dependent pancreatitis have been developed recently. Our laboratory generated several knockin mouse lines carrying human pancreatitis-associated mutations in the native mouse cationic trypsinogen (isoform T7) (29–32). Concurrently, the laboratory of Baoan Ji created transgenic models harboring wild-type or mutated forms of the serine protease 1 and 2 (*PRSS1* and *PRSS2*) genes that encode human cationic and anionic trypsinogens, respectively (33–36). All published mouse models develop either spontaneous, progressive pancreatitis driven by trypsinogen autoactivation or exhibit heightened sensitivity to cerulein-induced experimental pancreatitis. Remarkably, in their 2020 publication (34), the Ji group reported that the anticoagulant dabigatran etexilate markedly improved cerulein-induced pancreatitis in transgenic mice carrying human *PRSS1* with the p.R122H mutation (named PRSS1^{R122H} mice by the authors). Dabigatran etexilate (brand name Pradaxa) is routinely used worldwide as an orally active, reversible thrombin inhibitor for the anticoagulation of patients with venous thromboembolism or increased risk of stroke due to atrial fibrillation (37–39). It is a prodrug, which is absorbed from the gastrointestinal tract and becomes converted in the blood by nonspecific esterases to its active form, dabigatran (Figure 1A) (40). Dabigatran is a benzamidine derivative, and it has been reported to inhibit human thrombin reversibly with a K_i of 4.5 nM and bovine trypsin with a K_i of 50.3 nM (41). We hypothesized that the observed therapeutic effect of dabigatran in the PRSS1^{R122H} transgenic mice was due to trypsin inhibition in the pancreas rather than inhibition of thrombin in the circulation. To test this notion, here we compared the inhibitory activity of dabigatran against a panel of human and mouse trypsin isoforms in vitro and performed preclinical drug testing studies using 2 mouse models of trypsin-dependent pancreatitis. *T7D23A* and *T7K24R* mice carry the p.D23A and p.K24R mutations in mouse T7 trypsinogen, which are analogous to the human pancreatitis-associated *PRSS1* mutations p.D22G and p.K23R, respectively (29, 30). The p.D23A and p.K24R mutations increase autoactivation of mouse cationic trypsinogen by 50-fold and 5-fold, respectively. *T7D23A* mice are born with a normal pancreas but develop spontaneous, progressive pancreatitis at an early age (29). In contrast, *T7K24R* mice have no spontaneous phenotype, but they develop severe cerulein-induced AP followed by a progressive, CP-like disease (30, 31). These 2 models allowed us to test the effect of dabigatran etexilate under various conditions, i.e., cerulein-induced pancreatitis (*T7K24R*) versus spontaneous disease (*T7D23A*). Furthermore, we measured the plasma concentration of dabigatran after oral administration of dabigatran etexilate, in an attempt to correlate drug levels with trypsin-inhibitory activity and therapeutic efficacy. The results support and extend the potential utility of dabigatran and other benzamidine derivatives in pancreatitis therapy and highlight specific challenges the drug development process must overcome before advancement to clinical practice.

Results

Inhibition of trypsin by dabigatran. We hypothesized that the reported efficacy of dabigatran etexilate in pancreatitis (34) is related to the trypsin-inhibitory activity of dabigatran. As a benzamidine derivative (Figure 1A), dabigatran is expected to inhibit trypsin-like enzymes competitively; however, this inhibitory activity against human and mouse trypsin isoforms has not been demonstrated before to our knowledge.

First, we used homology-based docking to demonstrate that dabigatran can bind to the specificity pocket of trypsin. In our model, showing dabigatran docked to human mesotrypsin (Protein Data Bank [PDB] 1H4W) (42), the amidine moiety of dabigatran interacts with the side chain of Asp194 at the bottom of the specificity pocket, and the *N*-methyl-benzimidazole scaffold that bridges the benzamidine and the distal pyridine ring and propanoic acid end is positioned above the catalytic triad (Figure 1B). The benzamidine moiety of dabigatran overlaps with the bound benzamidine of the 1H4W mesotrypsin structure (Figure 1C). The docked conformation of dabigatran is also similar to that of the benzamidine-derivative dual-specificity thrombin and factor Xa inhibitor R11 (PubChem SID 820345) cocrystallized with bovine trypsin (PDB structure 1G36) (43). The latter compound and dabigatran both have the benzamidine group deep in the specificity pocket, connected to an *N*-methyl-benzimidazole moiety. Dabigatran and R11 differ in the groups at the distal end. R11 has a second methyl-benzimidazole group that lies flat on the protein surface. In contrast, in the docked structure of dabigatran, the carboxyl group of the distal propanoic acid

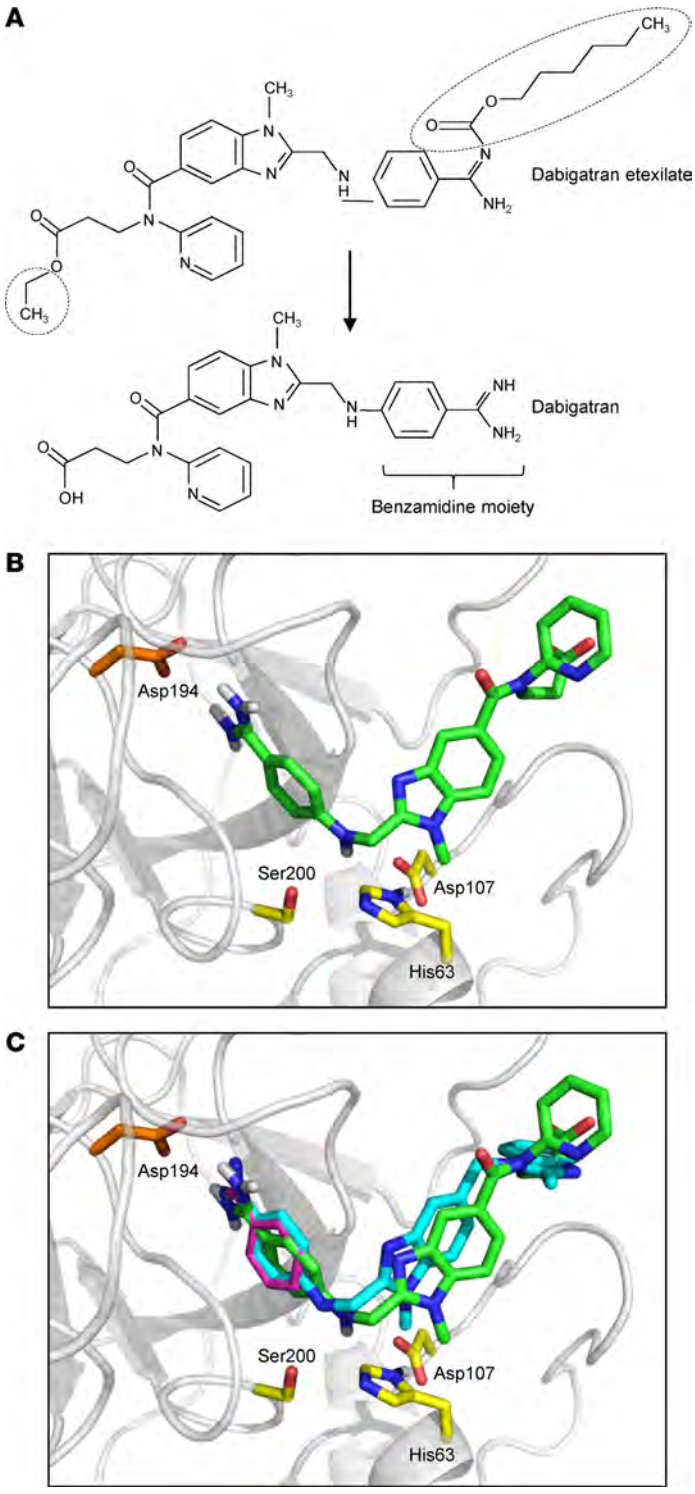

Figure 1. Modeling dabigatran binding to trypsin. (**A**) Chemical structure of dabigatran and its prodrug dabigatran etexilate. Differences are encircled. The benzamidine moiety of dabigatran is indicated. (**B**) Dabigatran (shown as green sticks) docked to human mesotrypsin (PDB structure 1H4W, shown as gray cartoon). Also indicated are the side chains of the catalytic triad His63, Asp107, and Ser200 (corresponding to His57, Asp102, and Ser195 in conventional crystallographic numbering) and Asp194 (Asp189) at the bottom of the specificity pocket (yellow and orange sticks, respectively). (**C**) Superimposition of trypsin-bound dabigatran, with benzamidine (from PDB structure 1H4W, magenta) and the benzamidine-derivative, dual-specificity thrombin and factor Xa inhibitor R11 cocrystallized with bovine trypsin (from PDB structure 1G36, cyan). The figures were created with the PyMOL Molecular Graphics System (https://pymol.org/2/).

is partially solvent exposed, and the pyridine ring is perpendicular to the plain of the methyl-benzimidazole in R11. Most atoms of dabigatran, including the benzamidine group, are shifted by 0.6–0.8 Å toward the catalytic triad relative to the same atoms in R11 (Figure 1C).

Next, we performed enzymatic measurements to compare the effect of benzamidine and dabigatran against human trypsin isoforms PRSS1 (serine protease 1, cationic trypsin), PRSS2 (serine protease 2, anionic trypsin), and PRSS3 (serine protease 3, mesotrypsin) and mouse trypsin isoforms T7 (cationic trypsin), T8, T9, and T20 (anionic trypsins). The trypsin isoforms were produced recombinantly, but human PRSS1 and PRSS2 were also purified from pancreatic juice in their native form, which contains a sulfate group on Tyr154. As a universal reference molecule, commercial bovine cationic trypsin was also assayed. Figure 2A demonstrates a representative experiment for the determination of the competitive inhibitory constant (K_i). As described in Methods, we calculated the K_i values by either individually (Figure 2B) or globally (Figure 2C) fitting the substrate saturation curves and obtained comparable results. Table 1 and Table 2 indicate the K_m and k_{cat} values determined in the absence and presence of increasing benzamidine and dabigatran concentrations. We show these data to demonstrate that the k_{cat} values remained constant within experimental error across all inhibitor concentrations tested, supporting the competitive nature of the inhibition. Table 3 lists the K_i values for benzamidine and dabigatran. Benzamidine inhibited trypsin with micromolar K_i values (range 3.3–20.6 μM and 4.2–22.6 μM by individual and global fit analysis, respectively), while dabigatran was an about 200- to 400-fold stronger inhibitor, exhibiting nanomolar K_i values (range 10–65 nM and 10.3–78.9 nM by individual and global fit analysis, respectively). Anionic trypsin isoforms were inhibited slightly stronger by benzamidine than cationic trypsins; however, this trend was less conspicuous with dabigatran. Reassuringly, the K_i values reported for dabigatran against bovine trypsin (41) and measured in our experiments were essentially identical. Dabigatran inhibited human trypsins as well as or slightly better than mouse trypsins, suggesting that results from preclinical mouse experiments should be relevant to human clinical trials. The experiments demonstrate that derivatives of benzamidine, such as dabigatran, can have highly improved inhibitory activity against trypsin and are universally effective against various trypsin paralogs.

Plasma levels of dabigatran after oral administration of dabigatran etexilate. Before embarking on experiments with trypsin-dependent pancreatitis models, we measured plasma concentrations of dabigatran in C57BL/6N mice after oral administration of the prodrug dabigatran etexilate. First, we performed intragastric gavage of a single dose (100 mg/kg) and followed plasma levels up to 8 hours. As shown in Figure 3A, dabigatran levels sharply rose to micromolar values within 30 minutes of oral gavage and peaked around 1 hour, after which time levels steadily decreased, with very little dabigatran measurable at the 4- and 8-hour time points. Importantly, peak concentrations of dabigatran were more than 2 orders of magnitude above the K_i values measured for trypsin inhibition. Second, we fed mice with solid chow containing dabigatran etexilate (10 mg/g) for 1 week and measured their plasma dabigatran concentration. Compared with acute administration of the prodrug by gavage, chronic feeding resulted in lower but steadier plasma concentrations (Figure 3B), with most values falling in the 600–800 nM range. This drug level is still more than 10-fold higher than K_i values of dabigatran against mouse trypsins.

Effect of dabigatran etexilate on cerulein-induced pancreatitis in T7K24R mice. The *T7K24R* mouse strain carries the p.K24R mutation in mouse cationic trypsinogen (isoform T7), which is analogous to the p.K23R pancreatitis-associated human *PRSS1* mutation (30). The mutation increases autoactivation of trypsinogen about 5-fold and thereby sensitizes the pancreas to experimental pancreatitis. We recently demonstrated that cerulein-induced pancreatitis in *T7K24R* mice is progressive; and after the acute episode, marked acinar atrophy develops with fibrosis and macrophage infiltration (31). The acinar cell dropout is most prominent on days 4–6 and involves essentially the entire pancreas. This trypsin-dependent outcome is convenient to monitor and quantify. Before testing the effect of dabigatran etexilate, we characterized intrapancreatic trypsin and chymotrypsin activity in *T7K24R* mice after 8 hourly injections of saline or cerulein (Figure 4A). Protease activities were measured at 1 hour, 1 day, 2 days, and 3 days after the cerulein injections. Relative to cerulein-treated C57BL/6N mice, pancreatic trypsin activity in *T7K24R* mice was at least 10-fold elevated (Figure 4B), and this high value persisted on days 1 and 2, finally diminishing on day 3, as acinar atrophy develops (31). Pancreatic chymotrypsin activity was also significantly higher in *T7K24R* mice, with peak activity (20-fold higher than in C57BL/6N mice) seen on day 1, which sharply declined by days 2 and 3 (Figure 4C). The different temporal kinetics of intrapancreatic trypsin and chymotrypsin activities are intriguing, although an explanation is not readily apparent.

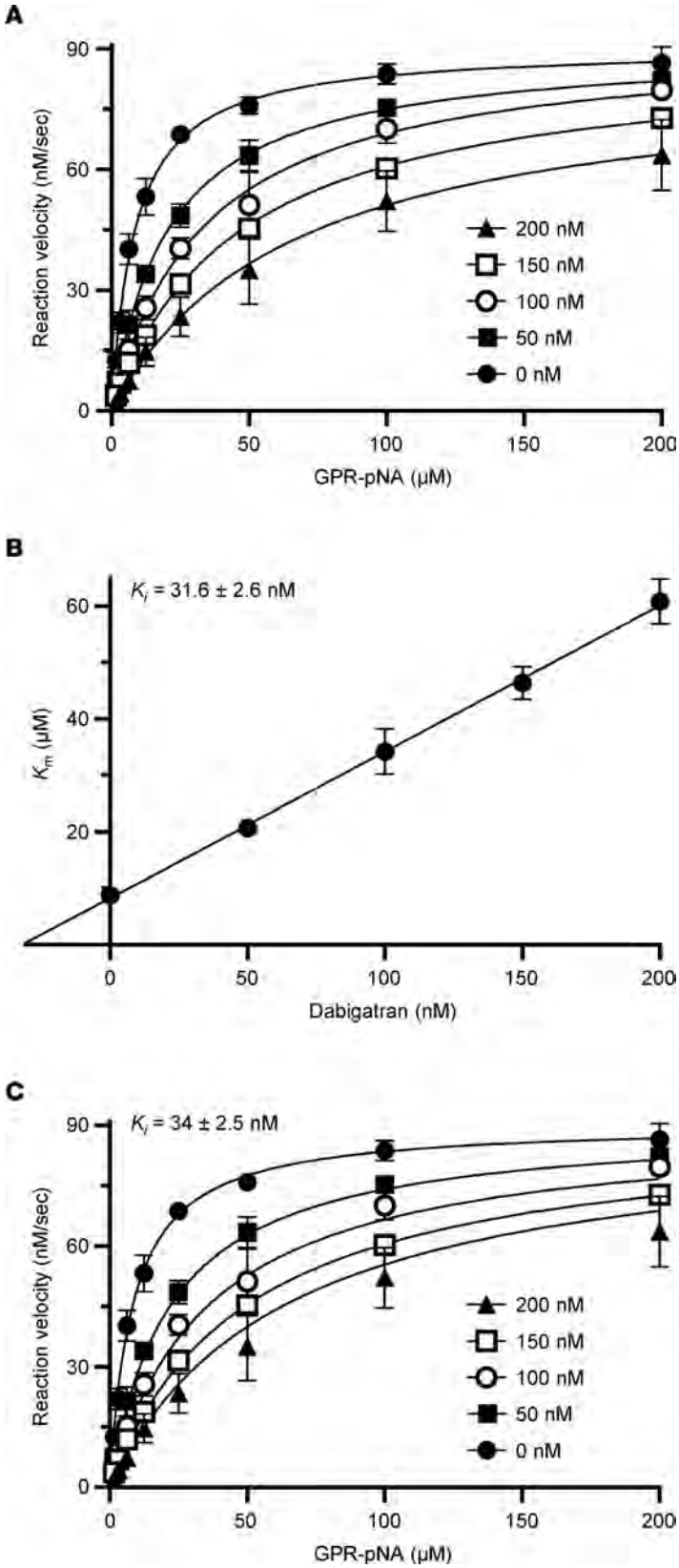

Figure 2. Inhibition of trypsin by dabigatran. Representative graphs of the kinetic assays using mouse anionic trypsin (isoform T8) are shown. Three experiments were performed. For clarity and convenience, the mean of the data points was plotted with standard deviation error bars, even though each experiment was analyzed separately. (**A**) Initial rate of trypsin activity as a function of substrate concentration in the absence and presence of increasing dabigatran concentrations. Rates were measured with 1 nM trypsin and the indicated concentrations of the *N*-CBZ-Gly-Pro-Arg-*p*-nitroanilide (GPR-pNA) trypsin substrate. Data sets for given dabigatran concentrations were *individually fitted* to the Michaelis-Menten equation. (**B**) Calculation of the competitive inhibitory constant (K_i) of dabigatran (mean ± standard deviation, n = 3). The K_m values derived from the saturation curves in **A** were plotted as a function of the dabigatran concentration. The K_i was then determined by dividing the y axis intercept with the slope of the linear fit. This value corresponds to the negative of the x axis intercept. (**C**) Calculation of the K_i of dabigatran by global fitting (mean ± standard deviation, n = 3). The data points from **A** were *globally fitted* to the competitive inhibition equation, as described in Methods.

As expected, no intrapancreatic protease activation was observed in saline-treated control mice. The high trypsin activity in the pancreas of cerulein-treated *T7K24R* mice suggests that trypsin-inhibitory therapy should be efficacious against pancreatitis in this model.

Table 1. Effect of benzamidine on the enzyme kinetics of human trypsin isoforms PRSS1, PRSS2, and PRSS3; mouse trypsin isoforms T7, T8, T9, and T20; and bovine trypsin

PRSS1	**0 μM**	**25 μM**	**50 μM**	**75 μM**	**100 μM**
k_{cat} (per second)	128.3 ± 10.4	134.8 ± 1.7	121 ± 3.3	136.3 ± 9.2	143.2 ± 8.1
K_m (μM)	18.3 ± 1.6	39.1 ± 0.9	59.6 ± 2.5	92 ± 4.4	115.3 ± 9.3
PRSS1-SO$_4$	**0 μM**	**12.5 μM**	**25 μM**	**37.5 μM**	**50 μM**
k_{cat} (per second)	106.4 ± 2.1	104.1 ± 2.8	112.1 ± 4.9	108.4 ± 5.3	113.6 ± 7.2
K_m (μM)	10.5 ± 0.5	22.3 ± 1.2	41.8 ± 2.8	49.5 ± 1.7	69.7 ± 7.2
PRSS2	**0 μM**	**25 μM**	**50 μM**	**75 μM**	**100 μM**
k_{cat} (per second)	82.5 ± 2.3	78.7 ± 1.7	78.4 ± 1.8	82.1 ± 2.4	78.3 ± 4.5
K_m (μM)	7.5 ± 0.1	15.5 ± 1.5	23.8 ± 0.9	37.5 ± 2	44.5 ± 2.9
PRSS2-SO$_4$	**0 μM**	**12.5 μM**	**25 μM**	**37.5 μM**	**50 μM**
k_{cat} (per second)	67.5 ± 0.7	64.8 ± 1.6	64.3 ± 1.4	64.5 ± 1.5	69.3 ± 0.3
K_m (μM)	4.5 ± 0.3	15.2 ± 0.5	26.4 ± 0.8	38.2 ± 1.4	54.1 ± 2.8
PRSS3	**0 μM**	**25 μM**	**50 μM**	**75 μM**	**100 μM**
k_{cat} (per second)	206.1 ± 5	211.9 ± 8.6	214.2 ± 4.7	201.3 ± 8	205.7 ± 6.3
K_m (μM)	22.2 ± 2.4	64.4 ± 4.8	114.2 ± 2.6	151.4 ± 6.7	182.9 ± 7.8
T7	**0 μM**	**12.5 μM**	**25 μM**	**37.5 μM**	**50 μM**
k_{cat} (per second)	118.6 ± 2.1	125.4 ± 2.7	125.5 ± 3.5	135 ± 3.9	127.9 ± 7.5
K_m (μM)	37 ± 3.2	74.9 ± 2	110.6 ± 7.6	165.5 ± 6	200.5 ± 6.3
T8	**0 μM**	**12.5 μM**	**25 μM**	**37.5 μM**	**50 μM**
k_{cat} (per second)	106.5 ± 0.5	103.9 ± 7.9	105.6 ± 4.9	100.2 ± 0.8	105.5 ± 7
K_m (μM)	8.1 ± 0.4	20.9 ± 3.5	37.7 ± 2.4	45 ± 0.6	66.7 ± 3.2
T9	**0 μM**	**12.5 μM**	**25 μM**	**37.5 μM**	**50 μM**
k_{cat} (per second)	112.6 ± 0.4	110 ± 3.4	111.4 ± 2.8	114.8 ± 2.8	112.3 ± 4.5
K_m (μM)	8.8 ± 0.4	23.7 ± 1.5	40 ± 1.4	59.9 ± 2.7	73.6 ± 2.2
T20	**0 μM**	**12.5 μM**	**25 μM**	**37.5 μM**	**50 μM**
k_{cat} (per second)	61.3 ± 3.8	65 ± 1	62.1 ± 1.8	64.7 ± 2.1	65.6 ± 2.1
K_m (μM)	1.4 ± 0.2	4.2 ± 0.7	7 ± 0.7	8.7 ± 0.4	12.4 ± 0.1
Bovine trypsin	**0 μM**	**25 μM**	**50 μM**	**75 μM**	**100 μM**
k_{cat} (per second)	114 ± 16.2	109 ± 9.5	115.8 ±.9	108.4 ± 5.3	113.6 ± 7.2
K_m (μM)	22.2 ± 1.2	48.9 ± 2.5	87.9 ± 14.5	121.8 ± 13.9	151.7 ± 6.3

Michaelis-Menten parameters (mean ± standard deviation, n = 3) were determined in the presence of the indicated inhibitor concentrations with the *N*-CBZ-Gly-Pro-Arg-*p*-nitroanilide (GPR-pNA) trypsin substrate at 24°C. See Methods for details. Sulfated human trypsins (PRSS1-SO$_4$ and PRSS2-SO$_4$) were purified from pancreatic juice. k_{cat}, catalytic rate constant (turnover number).

Therefore, in our experiments, we induced pancreatitis in *T7K24R* mice by 8 hourly injections of cerulein and euthanized the mice 96 hours (i.e., 4 days) later. To test the effect of dabigatran etexilate, a single dose of the prodrug was administered 30 minutes after the last injection (Figure 5A). Negative control mice without pancreatitis and vehicle-treated positive control mice with pancreatitis served for comparison. When the body weight of mice at the beginning and at the end of the experiment was compared, vehicle-treated mice with pancreatitis showed a slight decrease (Figure 5B). This phenomenon is due to a transient digestive dysfunction associated with the rapid development of acinar atrophy (31). In contrast, dabigatran etexilate–treated *T7K24R* mice with pancreatitis showed no change in body weight by the end of the experiment, suggesting a protective effect of the drug. The pancreas weight of vehicle-treated *T7K24R* mice with pancreatitis was significantly reduced, to almost half the normal pancreas size (Figure 5C). The atrophic weight loss of the pancreas remained prominent even after the pancreas weight was normalized to body weight (Figure 5D). Remarkably, however, the pancreas weight of the dabigatran etexilate–treated mice with pancreatitis was significantly higher, in some cases approaching the values of control mice with no pancreatitis, suggesting that the drug prevented and/or reversed

Table 2. Effect of dabigatran on the enzyme kinetics of human trypsin isoforms PRSS1, PRSS2, and PRSS3; mouse trypsin isoforms T7, T8, T9, and T20; and bovine trypsin

PRSS1	**0 nM**	**25 nM**	**50 nM**	**75 nM**	**100 nM**
k_{cat} (per second)	92.1 ± 3.4	90.8 ± 2.8	91.6 ± 4.8	95 ± 2.3	99.8 ± 3.3
K_m (μM)	17.4 ± 1.3	31.3 ± 3.6	50.2 ± 2.5	71.1 ± 4.2	88.7 ± 3.1
PRSS1-SO$_4$	**0 nM**	**25 nM**	**50 nM**	**75 nM**	**100 nM**
k_{cat} (per second)	103.2 ± 0.4	101 ± 2.3	105.5 ± 5.1	103.2 ± 4.2	104.7 ± 2.1
K_m (μM)	10.1 ± 0.6	21.4 ± 1.5	32.7 ± 3	42.8 ± 7.8	57 ± 2.1
PRSS2	**0 nM**	**25 nM**	**50 nM**	**75 nM**	**100 nM**
k_{cat} (per second)	91.7 ± 0.9	90.6 ± 2.6	89.1 ± 1.7	90.2 ± 2.3	87.5 ± 4.4
K_m (μM)	8 ± 0.5	23 ± 1.3	37.6 ± 0.6	46.8 ± 1.5	61.1 ± 6.1
PRSS2-SO$_4$	**0 nM**	**25 nM**	**50 nM**	**75 nM**	**100 nM**
k_{cat} (per second)	65.8 ± 0.7	63.4 ± 0.4	66.8 ± 1.6	63.8 ± 0.9	67.2 ± 1.9
K_m (μM)	3.9 ± 0.2	13 ± 0.5	23.5 ± 1.3	31.5 ± 0.4	42.4 ± 3.5
PRSS3	**0 nM**	**50 nM**	**100 nM**	**150 nM**	**200 nM**
k_{cat} (per second)	202.8 ± 4.2	214.6 ± 4.9	215.5 ± 4.6	217.5 ± 10.8	220.5 ± 4.1
K_m (μM)	7.5 ± 0.1	15.5 ± 1.5	23.8 ± 0.9	37.5 ± 2	44.5 ± 2.9
T7	**0 nM**	**50 nM**	**100 nM**	**150 nM**	**200 nM**
k_{cat} (per second)	118.6 ± 2.1	48.1 ± 0.9	47.5 ± 2	50.1 ± 1.5	49.3 ± 1.7
K_m (μM)	37 ± 3.2	63.5 ± 1.7	87.2 ± 1.1	130.7 ± 8,9	144.3 ±10.2
T8	**0 nM**	**50 nM**	**100 nM**	**150 nM**	**200 nM**
k_{cat} (per second)	90.9 ± 3.5	90.4 ± 1	92.3 ± 1.6	88.9 ± 1.3	85.1 ± 7.2
K_m (μM)	8.8 ± 1.6	20.6 ± 1.5	34.2 ± 4.1	46.3 ± 3	60.8 ± 4
T9	**0 nM**	**50 nM**	**100 nM**	**150 nM**	**200 nM**
k_{cat} (per second)	74 ± 0.7	75.8 ± 2	72.5 ± 2.6	78.4 ± 0.1	77.6 ± 2.5
K_m (μM)	7.9 ± 0.4	19.8 ± 2.7	28.3 ± 2.8	46.1 ± 2.4	56.7 ± 7.3
T20	**0 nM**	**50 nM**	**100 nM**	**150 nM**	**200 nM**
k_{cat} (per second)	52.1 ± 2.1	52 ± 4	51.1 ± 1.7	48.7 ± 3.3	50 ± 6.3
K_m (μM)	3.7 ± 0.3	9.5 ± 1.3	19.5 ± 0.5	22.5 ± 2.5	28.5 ± 2.2
Bovine trypsin	**0 nM**	**50 nM**	**100 nM**	**150 nM**	**200 nM**
k_{cat} (per second)	122.8 ± 2.1	127.7 ± 0.8	126.6 ± 3.5	123.8 ± 2.9	130.1 ± 1.4
K_m (μM)	24.8 ± 2.3	49.5 ± 3.3	71.6 ± 3.5	91.9 ± 4.9	125.8 ± 7

Michaelis-Menten parameters (mean ± standard deviation, n = 3) were determined in the presence of the indicated inhibitor concentrations with the GPR-pNA trypsin substrate at 24°C. See Methods for details. Sulfated human trypsins (PRSS1-SO$_4$ and PRSS2-SO$_4$) were purified from pancreatic juice.

acinar atrophy to a large extent. *T7K24R* mice exhibited low plasma amylase activity 4 days after the induction of cerulein-induced pancreatitis, close to the levels seen in control mice without pancreatitis (Figure 5E). Interestingly, in a subset of dabigatran etexilate–treated mice with pancreatitis (4 of 15), we observed more than 3-fold higher plasma amylase activity values, suggesting ongoing acinar cell injury. Histological analysis of pancreata from 10 vehicle-treated and 15 dabigatran etexilate–treated mice with hematoxylin-eosin staining demonstrated widespread loss of intact acini in vehicle-treated mice (for higher magnification of pathological details, see ref. 31). A dramatic, complete protective effect of dabigatran etexilate was observed in almost 50% of the drug-treated mice (Figure 6A). A significant yet incomplete (30%–50% normal histology) effect was seen in about 20% of the mice, whereas in the remaining 30% of mice dabigatran showed limited efficacy, with less than 25% of normal acini preserved (Figure 6B). This group included 2 cases with no detectable effect. Notably, the 4 drug-treated mice with the elevated plasma amylase activity all had partial histological responses, with 13%, 15%, 35%, and 45% intact acini visible on pancreas sections. Overall, the proportion of intact acini in the dabigatran etexilate–treated group was significantly higher than in the vehicle-treated group, indicating that dabigatran is effective in this model of trypsin-dependent pancreatitis.

Table 3. K_i values (mean ± standard deviation, n = 3) of benzamidine and dabigatran against human trypsin isoforms PRSS1, PRSS2, and PRSS3; mouse trypsin isoforms T7, T8, T9, and T20; and bovine trypsin

Enzyme	K_i benzamidine (μM)		K_i dabigatran (nM)		K_i ratio	
	Individual fit	Global fit	Individual fit	Global fit	Individual fit	Global fit
PRSS1	15.7 ± 4.7	22.5 ± 4	21 ± 2.3	28.2 ± 4.5	748	798
PRSS1-SO_4	8.3 ± 2.2	10.5 ± 0.9	21.2 ± 0.9	23.3 ± 2	392	451
PRSS2	8.6 ± 2.2	8.9 ± 0.7	17.9 ± 3.3	14.1 ± 1.1	480	631
PRSS2-SO_4	3.3 ± 0.5	4.2 ± 0.7	10 ± 3.2	10.3 ± 0.5	330	408
PRSS3	15.5 ± 2.3	13.3 ± 0.8	35.1 ± 2.4	51.6 ± 2.1	442	258
T7	20.6 ± 3	14.9 ± 0.3	65 ± 0.6	78.9 ± 9.5	317	189
T8	6.7 ± 1.3	6.7 ± 0.5	31.6 ± 2.6	30.4 ± 2.5	212	220
T9	6.8 ± 1	6.8 ± 0.1	28.4 ± 7.1	35.8 ± 3.5	239	190
T20	6.9 ± 1.1	7.6 ± 0.5	33.6 ± 4.8	22.6 ± 0.7	205	336
Bovine trypsin	15.2 ± 3.6	17.8 ± 0.6	48.7± 1.7	56.7 ± 3.6	312	314

Kinetic measurements with the GPR-pNA trypsin substrate in the presence of increasing inhibitor concentrations were analyzed by individually or globally fitting the substrate saturation curves, as indicated. See Methods for details. Sulfated human trypsins (PRSS1-SO_4 and PRSS2-SO_4) were purified from pancreatic juice.

Effect of orally gavaged dabigatran etexilate on spontaneous pancreatitis in T7D23A mice. Next, we tested the effect of dabigatran etexilate in a more aggressive, spontaneous pancreatitis model. The *T7D23A* mouse strain carries the p.D23A mutation in mouse cationic trypsinogen (isoform T7), which is analogous to the p.D22G pancreatitis-associated human *PRSS1* mutation (29). The mutation increases autoactivation of trypsinogen about 50-fold and elicits spontaneous, early-onset (3–5 weeks of age), and progressive pancreatitis. In the first experiment, we treated 3-week-old *T7D23A* mice with various doses of dabigatran etexilate via intragastric gavage for 2 weeks (Figure 7A). The dosages used were once daily 100 mg/kg, twice daily 100 mg/kg, and once daily 200 mg/kg. As controls, untreated *T7D23A* and C57BL/6N mice were used. Mice were euthanized at 5 weeks of age. Based on prior experience, at the beginning of the experiment, the pancreas of 3-week-old *T7D23A* mice was either normal or may have had incipient AP (29). Conversely, by 5 weeks of age, all *T7D23A* mice were expected to have developed early CP. The body weight of mice was measured at the beginning (3 weeks) and at the end (5 weeks) of the experiment (Figure 7B). As expected, during this period, the mice gained weight, and this was unaffected by gavage treatment. The weight gain of *T7D23A* mice was slightly lower relative to the C57BL/6N parent strain. Compared with untreated C57BL/6N mice, the pancreas weight of untreated *T7D23A* mice was markedly lower, due to the massive pancreas atrophy associated with their early CP (Figure 7C) (29). This large difference persisted even after normalization of the pancreas weight to the body weight of the mice (Figure 7D). In stark contrast to the effect seen with *T7K24R* mice, dabigatran etexilate treatment did not improve the pancreas weight of *T7D23A* mice. Curiously, a clear trend of worsening atrophy emerged with increasing dabigatran dosages, even though the differences did not reach statistical significance. As expected, plasma amylase activity was reduced in untreated *T7D23A* mice relative to C57BL/6N mice, though the difference did not reach statistical significance (Figure 7E). In agreement with their smaller pancreas weights, drug-treated *T7D23A* mice had significantly lower amylase levels relative to the untreated *T7D23A* controls. Histological analysis of pancreata revealed comparable CP-like disease in all groups of *T7D23A* mice whereas C57BL/6N controls showed normal pancreas morphology (Figure 8A). For details of the histological phenotype of pancreatitis in *T7D23A* mice, the reader is referred to the original publication (29). Quantitative analysis of intact acini per visual field showed the expected dramatic cell loss in the pancreata of *T7D23A* mice, but no appreciable difference was seen between the untreated and treated groups (Figure 8B). Taken together, the results from this experiment indicated that dabigatran etexilate introduced by intragastric gavage did not ameliorate the spontaneous pancreatitis of *T7D23A* mice. Furthermore, under certain dosing protocols, the drug seemed to worsen the disease slightly.

Effect of feeding with dabigatran etexilate–containing chow on spontaneous pancreatitis in T7D23A mice. Based on the results of the gavage experiments described above, we speculated that the *T7D23A* mouse model may require sustained drug levels in the blood to achieve full inhibition of pancreatic trypsins

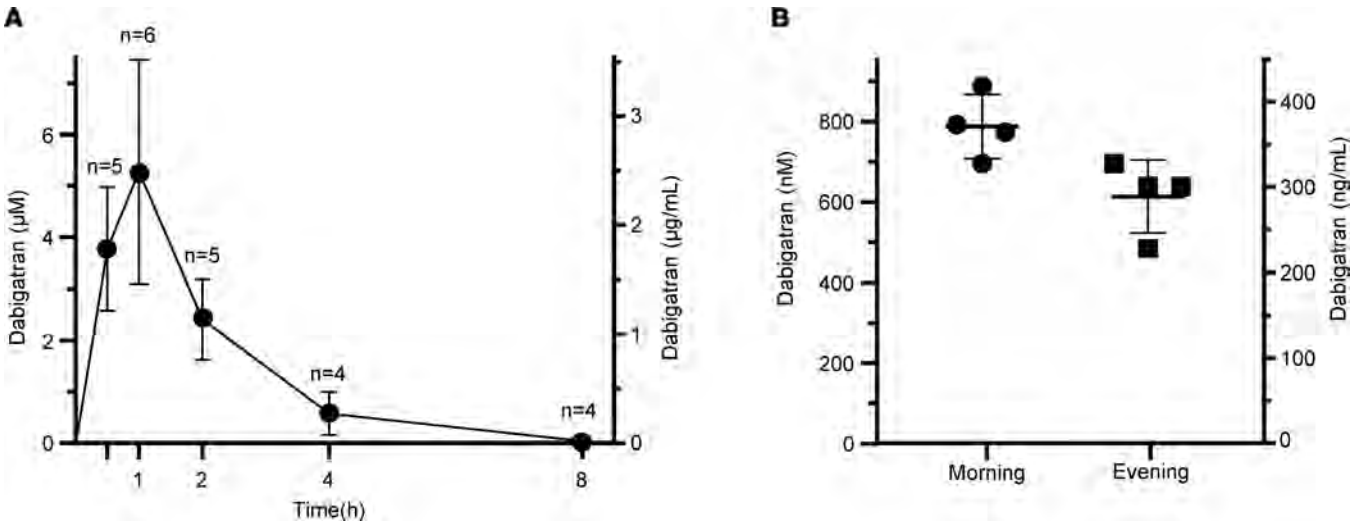

Figure 3. Dabigatran plasma concentrations in C57BL/6N mice following oral administration of dabigatran etexilate. Dabigatran levels were measured as described in Methods. (**A**) Mice (6–8 weeks of age) were given a single dose of 100 mg/kg dabigatran etexilate by oral gavage. Mice were euthanized at the indicated times. Data represent mean ± standard deviation (n = 4–6, as indicated). (**B**) Mice (12 weeks of age) were fed regular chow containing dabigatran etexilate at 10 mg/g concentration for 7 days. Mice were euthanized on day 8 either in the morning (9 am) or in the evening (5 pm). Mean dabigatran concentrations (± standard deviation, n = 4) measured at these time points were 787 ± 79 and 614 ± 91 nM, respectively.

and prevention/reversal of disease. Therefore, we tested whether feeding the mice with solid chow containing dabigatran etexilate would be efficacious. We fed 3 week-old-mice for 1 week and euthanized the mice at the age of 4 weeks (Figure 9A). There were 4 experimental groups, treated and untreated C57BL/6N controls, and treated and untreated *T7D23A* mice. Each group gained weight similarly during the 1-week treatment, indicating that mice readily consumed the dabigatran etexilate–containing chow (Figure 9B). When comparing the pancreas weight of treated and untreated mice, we observed a small increase in the drug-treated groups of both strains, indicating that this change is likely unrelated to a drug effect on pancreatitis (Figure 9C). The difference in pancreas weights reached statistical significance when normalized to body weight (Figure 9D). Long-term feeding of mice with trypsin inhibitors causes the pancreas weight to increase, due to luminal trypsin inhibition and a feedback mechanism that increases plasma cholecystokinin levels (44–48). Presumably, in our experiments, some of the unabsorbed dabigatran etexilate was converted to active dabigatran in the gut lumen and inhibited intestinal trypsins. Plasma amylase activities were comparable in all 4 groups of mice (Figure 9E). Finally, histological analysis showed normal pancreata in C57BL/6N mice and early CP in *T7D23A* mice (Figure 10A). Quantitative assessment of intact acini demonstrated no effect of dabigatran etexilate treatment on pancreatitis severity (Figure 10B). Taken together, the results indicate that feeding *T7D23A* mice with solid chow containing dabigatran etexilate did not prevent or improve their spontaneous pancreatitis.

Discussion

In the present study, we tested the hypothesis that the recently reported therapeutic effect of dabigatran etexilate in experimental pancreatitis of transgenic PRSS1^{R122H} mice was due to the trypsin-inhibitory activity of dabigatran (34). To this end, first we modeled binding of dabigatran to trypsin by homology-based docking, then performed inhibition assays with dabigatran against a panel of human, mouse, and bovine trypsin paralogs, followed by preclinical studies with dabigatran etexilate on mouse models of trypsin-dependent pancreatitis. We found that dabigatran was readily docked into the substrate binding pocket of trypsin, and it potently inhibited all trypsin isoforms tested with similar efficacy. Compared with its parent compound, benzamidine, dabigatran showed several hundred-fold improved inhibitory activity. The inhibition was competitive, confirming that dabigatran blocks substrate binding to trypsin. Before the preclinical mouse studies, we confirmed that oral administration of dabigatran etexilate in mice can produce high enough dabigatran levels in the blood to achieve trypsin inhibition. A single gavage of dabigatran etexilate (100 mg/kg dose) resulted in peak dabigatran concentrations (~2.5 μg/mL) more

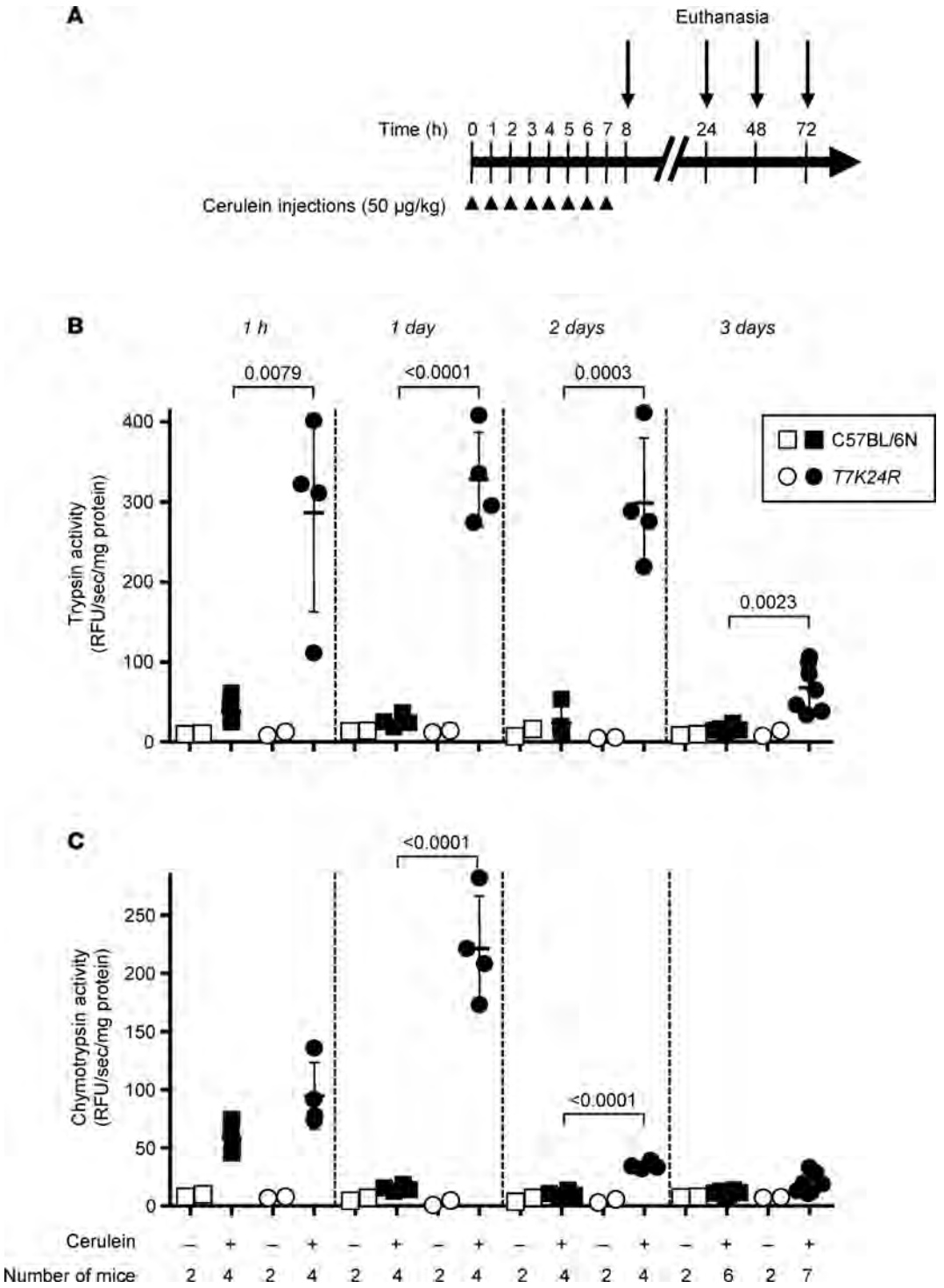

Figure 4. Intrapancreatic trypsin and chymotrypsin activity in *T7K24R* mice given saline or cerulein. (**A**) Experimental design. C57BL/6N and *T7K24R* mice (8–9 weeks of age) were treated with 8 hourly injections of saline or cerulein (arrowheads). Animals were euthanized at the indicated times (arrows), and the pancreas was freshly homogenized and assayed, as described in Methods. (**B**) Trypsin activity. (**C**) Chymotrypsin activity. Individual data points with mean and standard deviation are shown. The difference of means between the groups was analyzed by 1-way ANOVA with Tukey-Kramer post hoc test.

than 100-fold higher than the K_i values against trypsin isoforms. However, dabigatran levels fell rapidly under these conditions, and the inhibitory activity was almost completely lost within a few hours. When dabigatran etexilate was introduced to mice by chronic feeding of solid chow containing the prodrug (10 mg/g dose), relatively steady plasma concentrations were achieved (~300–400 ng/mL), which were about

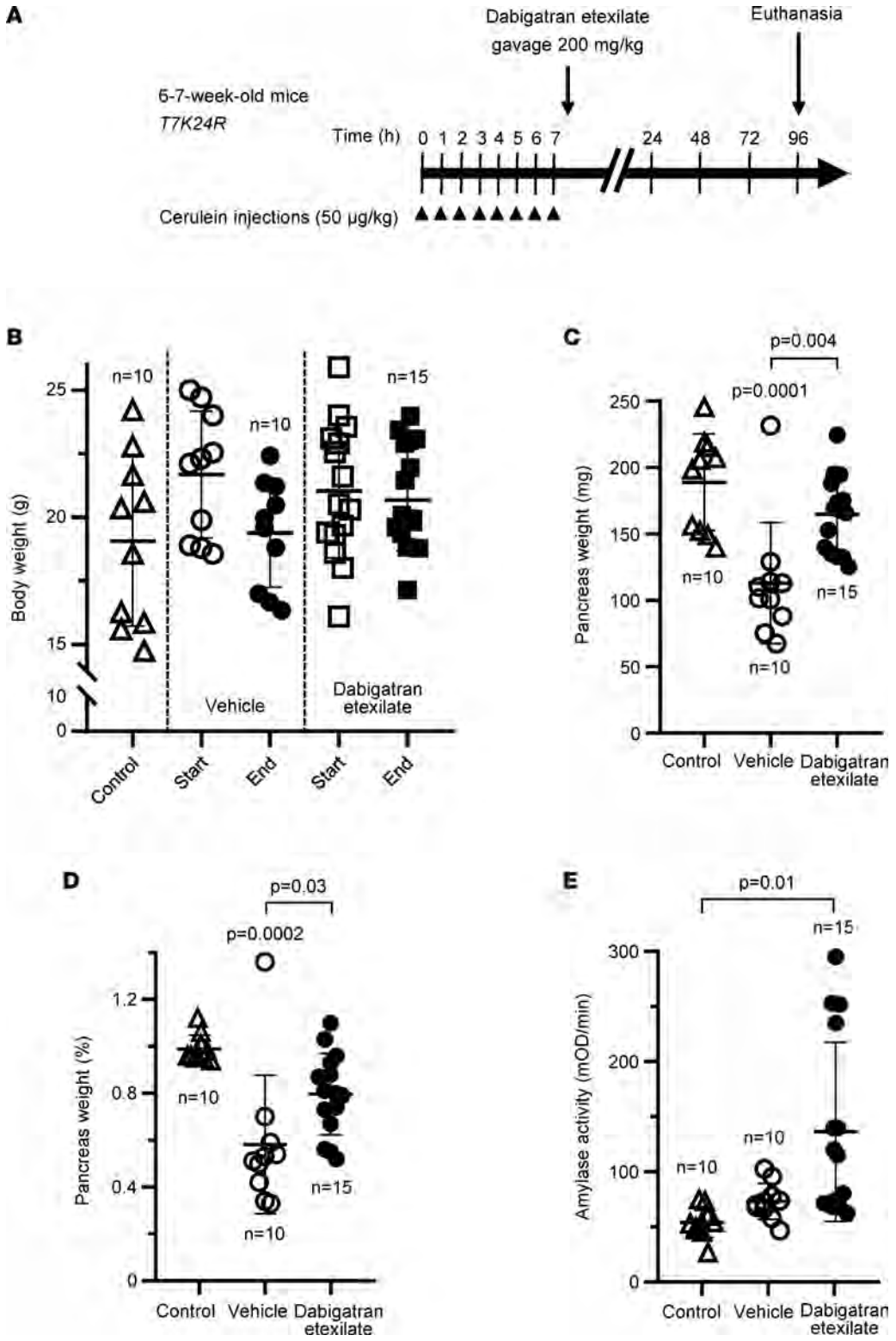

Figure 5. Effect of dabigatran etexilate on cerulein-induced pancreatitis in *T7K24R* mice. (**A**) Experimental design. Mice were given 8 hourly injections of cerulein (arrowheads), followed by a single oral gavage of 200 mg/kg dabigatran etexilate or vehicle administered 30 minutes after the last cerulein injection. Mice were euthanized 96 hours from the first cerulein injection. (**B**) Body weight at the start and end of the experiment. (**C**) Pancreas weight in milligrams. (**D**) Pancreas weight as percentage of body weight. (**E**) Plasma amylase activity (4 μL assayed). Control mice represent age-matched *T7K24R* mice without pancreatitis. Individual data points with mean and standard deviation are shown. The difference of means between the groups was analyzed by 1-way ANOVA with Tukey-Kramer post hoc test. mOD, milli–optical density.

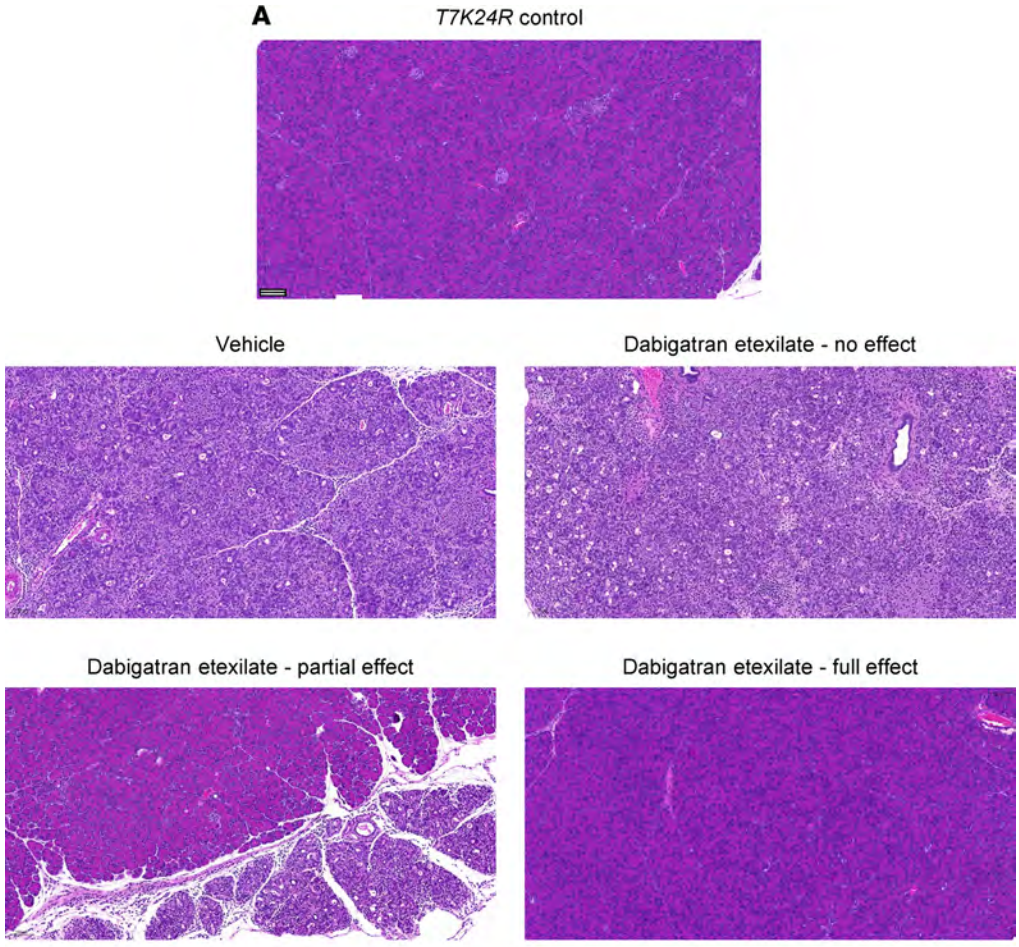

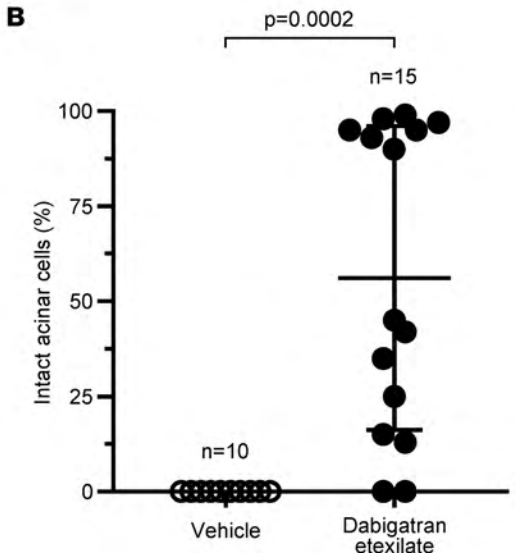

Figure 6. Effect of dabigatran etexilate on pancreas histology in cerulein-induced pancreatitis of *T7K24R* mice. Mice were given 8 hourly injections of cerulein, followed by a single oral gavage of 200 mg/kg dabigatran etexilate or vehicle administered 30 minutes after the last cerulein injection. Mice were euthanized 96 hours from the first cerulein injection. (**A**) Representative pancreas sections stained with hematoxylin-eosin from *T7K24R* mice given vehicle or dabigatran etexilate after the cerulein injections. For comparison, the normal pancreas histology of a control *T7K24R* mouse is shown. Scale bar corresponds to 100 μm. Higher magnification pictures of cerulein-induced pancreas pathology in *T7K24R* mice are shown in ref. 31. (**B**) Histological evaluation of acinar cell loss. Pancreas sections from mice given vehicle or dabigatran were visually scored for the presence of intact acinar cells. Individual data points with mean and standard deviation are shown. The difference of means between 2 groups was analyzed by 2-tailed unpaired *t* test.

10-fold higher than the K_i values against trypsins. We add, as a caveat, that we do not know how well dabigatran penetrates the pancreas, which is the site of trypsin inhibition to prevent pancreatitis. We were unable to measure dabigatran levels in the pancreas due to interference of pancreatic proteases with the HEMOCLOT functional assay. It is important to note that 3 times daily administration of 100 or 200 mg

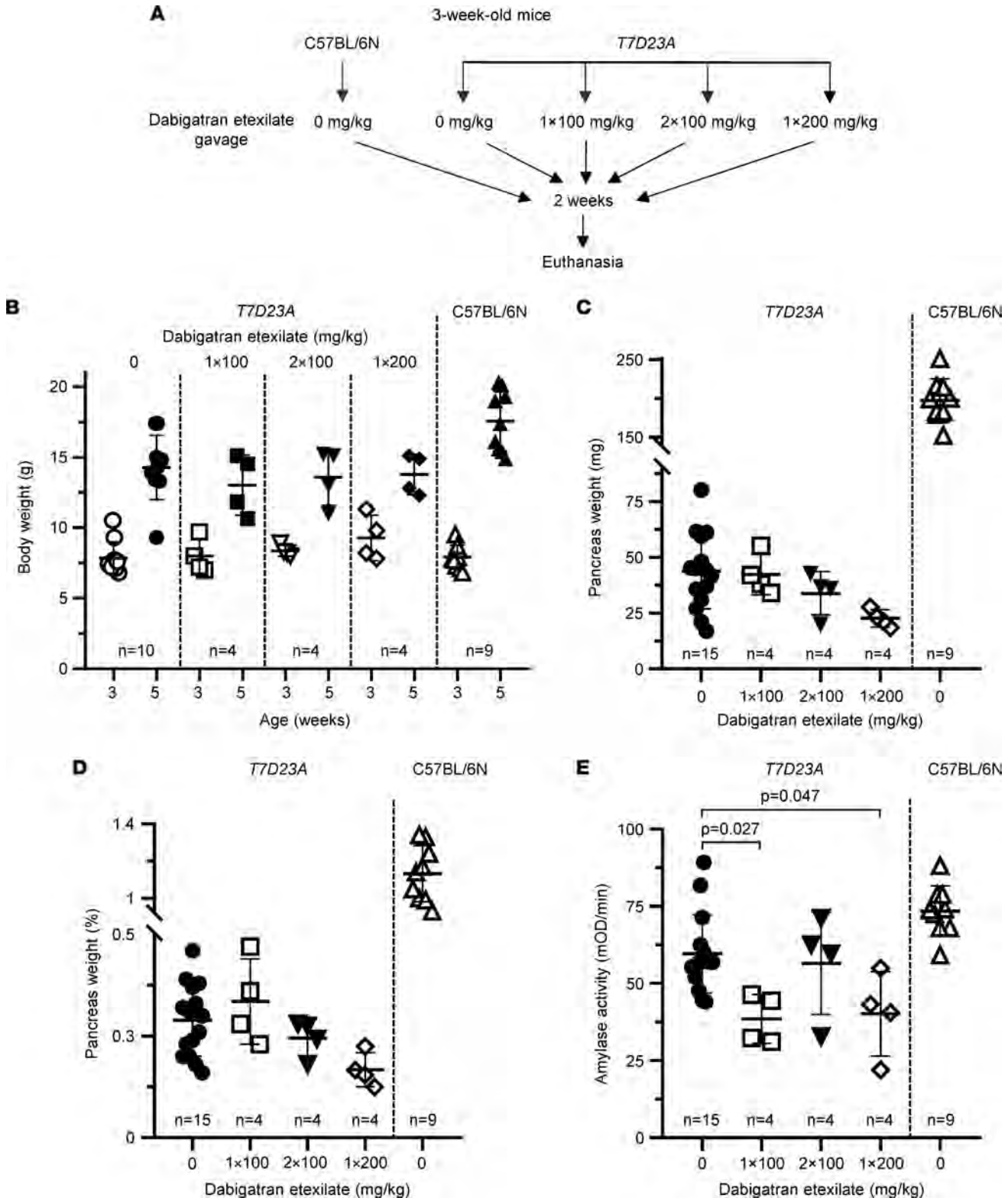

Figure 7. Effect of orally gavaged dabigatran etexilate on spontaneous pancreatitis in *T7D23A* mice. (**A**) Experimental design. Mice (3 weeks of age) were given 1 × 100 mg/kg, 2 × 100 mg/kg, or 1 × 200 mg/kg daily dose of dabigatran etexilate by intragastric gavage for 2 weeks. Untreated *T7D23A* and C57BL/6N mice served as controls. Mice were euthanized at 5 weeks of age. (**B**) Body weight of mice at the beginning (3 weeks) and end (5 weeks) of the experiment. (**C**) Pancreas weight in milligrams. (**D**) Pancreas weight as percentage of body weight. (**E**) Plasma amylase activity at 5 weeks of age (4 μL assayed). Individual data points with mean and standard deviation are shown. The difference of means between the groups was analyzed by 1-way ANOVA with Tukey-Kramer post hoc test.

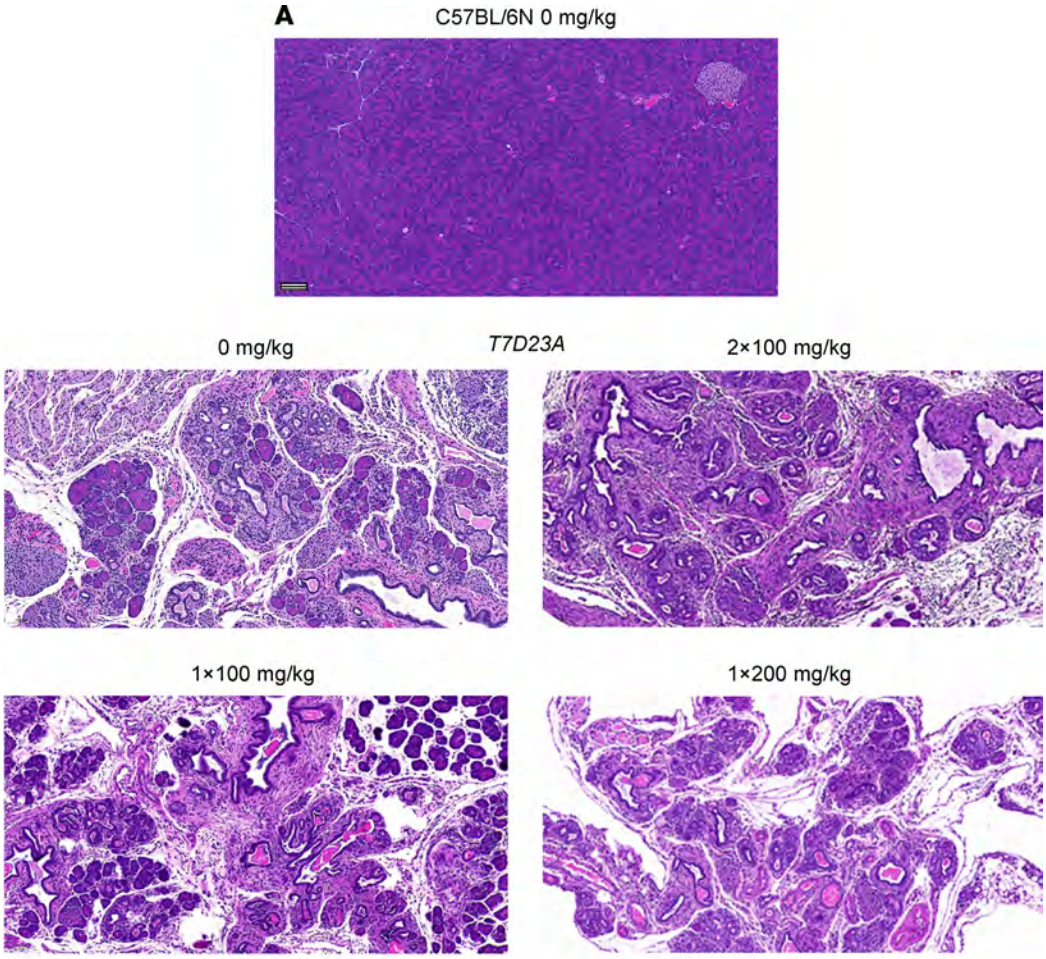

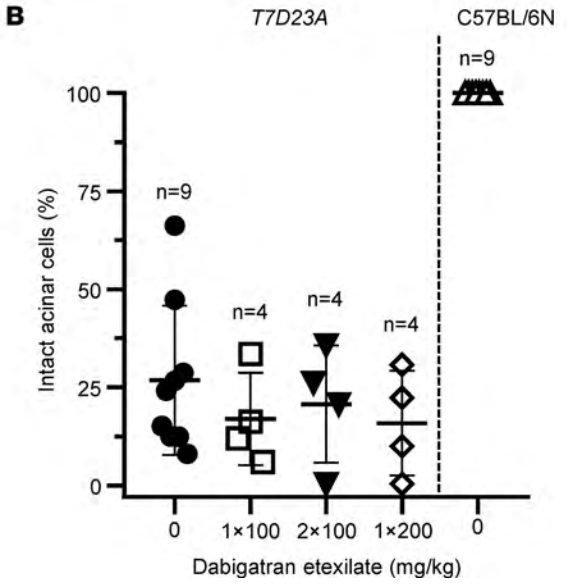

Figure 8. Effect of orally gavaged dabigatran etexilate on spontaneous pancreatitis in *T7D23A* mice. Mice (3 weeks of age) were given 1 × 100 mg/kg, 2 × 100 mg/kg, or 1 × 200 mg/kg daily dose of dabigatran etexilate by intragastric gavage for 2 weeks. Untreated *T7D23A* and C57BL/6N mice served as controls. Mice were euthanized at 5 weeks of age. (**A**) Representative pancreas sections stained with hematoxylin-eosin from untreated C57BL/6N and *T7D23A* control mice and *T7D23A* mice given dabigatran etexilate. Scale bar corresponds to 100 μm. Histological details of the spontaneous pancreatitis in *T7D23A* mice are also shown in ref. 29. (**B**) Histological evaluation of acinar cell loss. Pancreas sections were visually scored for the presence of intact acinar cells. Individual data points with mean and standard deviation are shown. The difference of means between the groups was analyzed by 1-way ANOVA with Tukey-Kramer post hoc test.

dabigatran etexilate to human volunteers resulted in steady-state plasma levels of dabigatran of around 50 and 100 ng/mL, respectively (40). Since the common dosing of Pradaxa in clinical practice is two 150 mg capsules daily (39), the resultant dabigatran plasma concentrations are unlikely to exert significant trypsin-inhibitory activity in the pancreas.

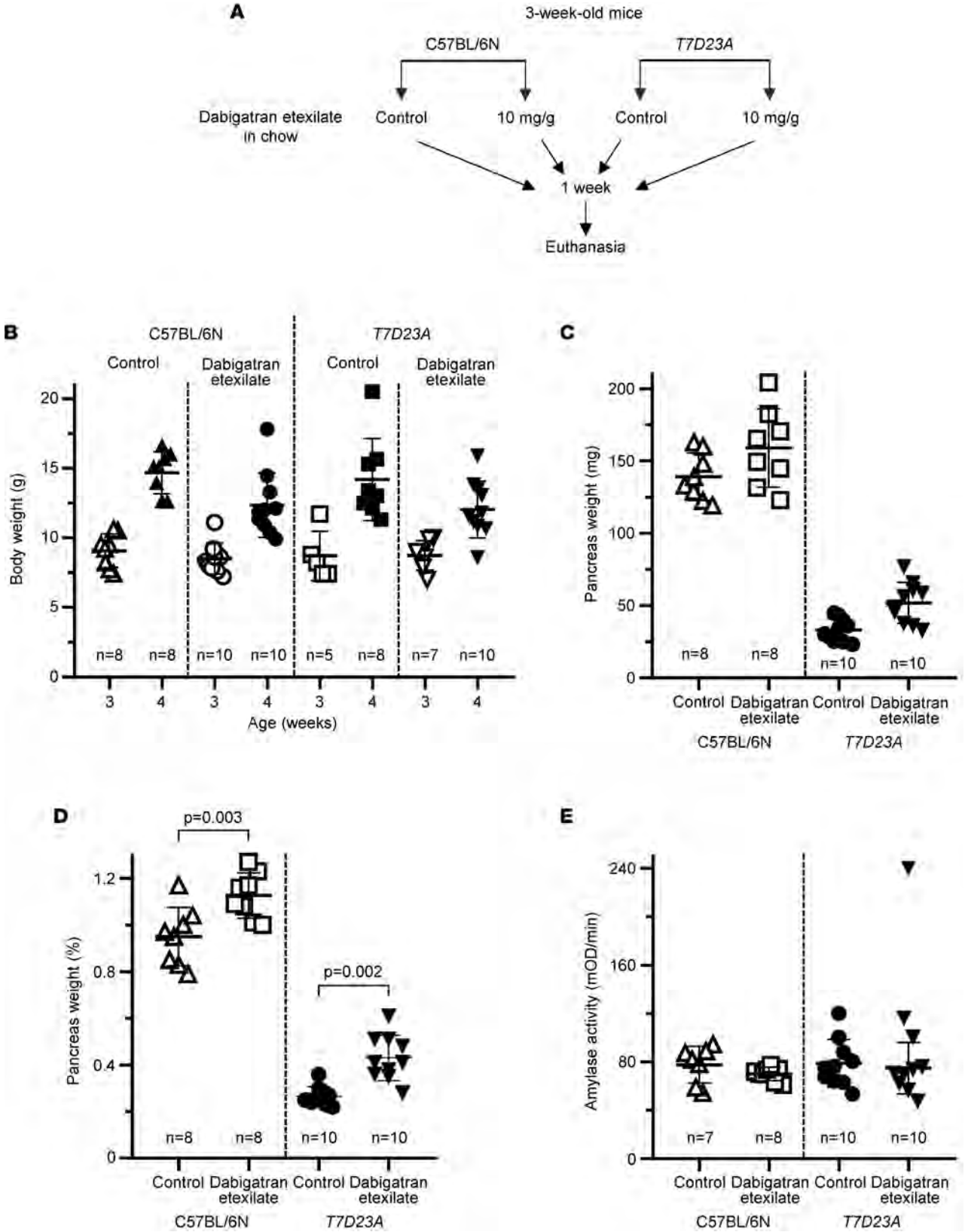

Figure 9. Effect of dabigatran etexilate feeding on spontaneous pancreatitis in *T7D23A* mice. (**A**) Experimental design. C57BL/6N and *T7D23A* mice were given solid chow with or without 10 mg/g dabigatran etexilate from 21 to 28 days of age. Mice were euthanized at 28 days of age. (**B**) Body weight at the beginning (3 weeks) and end (4 weeks) of the experiment. (**C**) Pancreas weight in milligrams. (**D**) Pancreas weight as percentage of body weight. (**E**) Plasma amylase activity (4 μL assayed). Individual data points with mean and standard deviation are shown. The difference of means between 2 groups was analyzed by 1-way ANOVA with Tukey-Kramer post hoc test. The outlier data point was excluded from the statistical calculations.

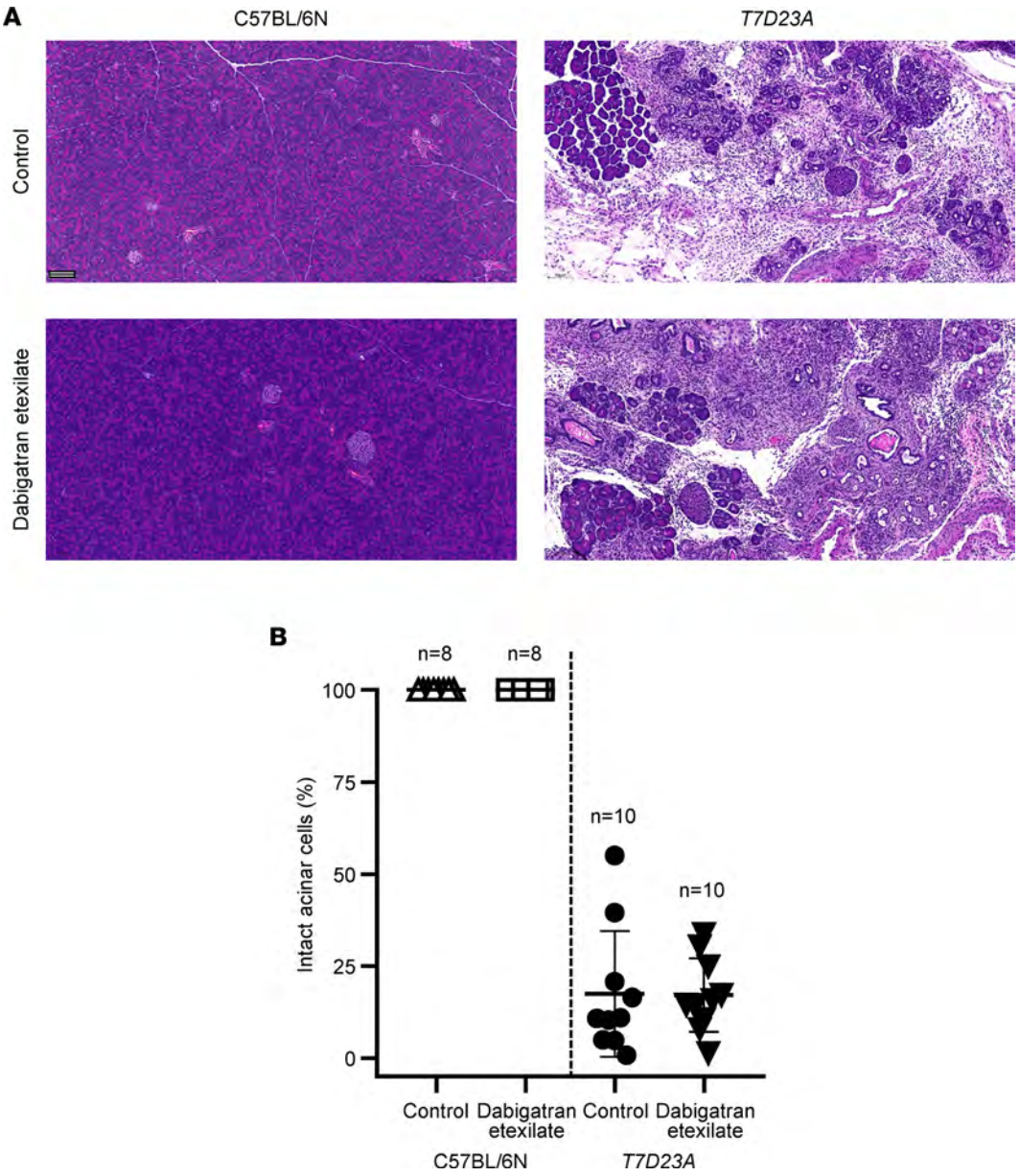

Figure 10. Effect of dabigatran etexilate feeding on spontaneous pancreatitis in *T7D23A* mice. C57BL/6N and *T7D23A* mice were given solid chow with or without 10 mg/g dabigatran etexilate from 21 to 28 days of age. Mice were euthanized at 28 days of age. (**A**) Representative pancreas sections stained with hematoxylin-eosin. Scale bar corresponds to 100 μm. Histological details of the spontaneous pancreatitis in *T7D23A* mice are also shown in ref. 29. (**B**) Histological evaluation of acinar cell loss. Pancreas sections were visually scored for the presence of intact acinar cells. Individual data points with mean and standard deviation are shown. The difference of means between the groups was analyzed by 1-way ANOVA with Tukey-Kramer post hoc test.

We tested the effect of dabigatran etexilate on trypsin-dependent pancreatitis in 2 mouse models we recently developed. First, homozygous *T7K24R* mice were used (30), which are phenotypically similar to the PRSS1^{R122H} model (34) in that they develop progressive, CP-like pancreatitis after an acute episode of cerulein-induced pancreatitis (31). We observed high intrapancreatic trypsin activity in cerulein-treated *T7K24R* mice, suggesting that trypsin-inhibitory therapy would be beneficial. Our experiments supported the published efficacy of dabigatran etexilate against cerulein-induced progressive CP, with the following observations. We found that a single gavage of the prodrug given within an hour after the last cerulein injection was sufficient for therapeutic activity. Furthermore, we observed variability with respect to the therapeutic effect. We speculate that cerulein-induced pathological trypsin activity in the pancreas has

to be inhibited within a short time frame before disease progression is inevitable. Efficient inhibition depends on high enough plasma concentrations of dabigatran, which, in turn, are determined by the technical success of the gavage and the rate of prodrug absorption. The 1-hour peak concentration of plasma dabigatran after a single gavage of the prodrug showed significant variability (see Figure 3A), supporting our notion that this may be the critical factor in therapeutic variability. Due to limitations in solubility and gavage volume, we were unable to test higher dabigatran etexilate doses in this experimental setting. Taken together, the observations verify the proposed therapeutic potential of dabigatran etexilate in trypsin-dependent pancreatitis. Finally, we note that it was not feasible to pretreat mice with dabigatran etexilate before induction of pancreatitis, because subsequent cerulein injections would cause fatal bleeding due to the anticoagulant activity of dabigatran.

Next, we used heterozygous *T7D23A* mice, which is a relatively aggressive, trypsin-dependent CP model with rapid, spontaneous disease development and severe end-stage disease (29). We tested the effect of dabigatran etexilate early in the disease course, utilizing 1–2 week treatment protocols. The prodrug was either introduced by daily gavages or mixed with solid chow. Unexpectedly, we found no therapeutic effect whatsoever with either method. Based on our observations with the *T7K24R* mice discussed above, we believe that dabigatran concentrations we achieved in *T7D23A* mice were insufficient to exert a meaningful trypsin-inhibitory effect in the pancreas. With once or twice daily gavage treatment, only the short-lived peak levels might have been sufficiently high, while feeding solid chow mixed with the prodrug resulted in relatively steady but much lower blood concentrations of dabigatran. We also note that *T7K24R* and *T7D23A* mice carry trypsinogen mutants that exhibit 5-fold and 50-fold increased autoactivation, respectively. Thus, due to the stronger biochemical and pathological phenotype, *T7D23A* mice may require higher dabigatran levels than *T7K24R* mice for successful treatment of pancreatitis.

We observed potentially problematic effects of dabigatran etexilate treatment in *T7D23A* mice that will require further investigation in the future. In the gavage experiments, there was a clear trend for the pancreas atrophy to show worse parameters relative to the untreated controls. A dose dependence was also apparent, with the largest effect seen with twice daily doses. Plasma amylase activities were also lower in the drug-treated groups, in agreement with the more pronounced pancreas atrophy. While an explanation to this observation is not readily apparent, we believe that the relatively rapid fluctuations in dabigatran levels may be responsible for the phenomenon. The transient trypsin inhibition in the pancreas may produce a rebound effect once dabigatran levels fall. This may also explain why plasma amylase levels of dabigatran etexilate–treated *T7K24R* mice with an incomplete response were elevated (see Figure 5E). In this case, a more localized rebound effect may have occurred, resulting in acinar cell damage, as judged by the amylase release.

Chronic feeding of *T7D23A* mice with dabigatran etexilate mixed in with chow resulted in small but measurable increases in their pancreas weight. The pancreas weight gain also occurred with C57BL/6N mice, indicating that this side effect was unrelated to pancreatitis treatment. The growth-stimulating effect of trypsin inhibitor feeding on the rodent pancreas has been extensively documented (44–48), and we believe this was the case here too. Some of the dabigatran etexilate likely was converted to dabigatran in the gut and inhibited luminal trypsins, which, in turn, increased plasma cholecystokinin levels that had a direct trophic effect on the pancreas. This feedback regulation may confound preclinical experiments testing orally administered trypsin inhibitors in rodents, particularly if pancreas size, weight, and function are used as treatment outcome measures. This concern is supported by a study showing that severity of experimental pancreatitis increased after rats and mice were fed camostat for 2 weeks (49). A similar feedback mechanism of functional adaptation seems to exist in humans; however, this may not be clinically relevant (50).

The premise of our studies was that dabigatran inhibits trypsin and thereby ameliorates pancreatitis. Although the results are consistent with this hypothesis, we cannot formally rule out other mechanistic pathways that may inhibit pancreatic inflammation and/or improve pancreas regeneration. In their seminal paper, the Ji laboratory speculated that the anticoagulant activity of dabigatran may be partly responsible for its therapeutic effectiveness in pancreatitis (34). They presented intriguing data showing that the factor Xa inhibitor apixaban (100 mg/kg), which is devoid of trypsin-inhibitory activity, had no therapeutic activity whatsoever. However, when combined with camostat (200 mg/kg), it became highly effective, while camostat alone showed only a partial effect. One possible interpretation of these results is that anticoagulation alone has no therapeutic effect. However, it may improve tissue penetration of the trypsin inhibitor camostat, thereby rendering it more effective. Previous studies demonstrated that heparin improves outcomes of cerulein-induced pancreatitis in rodents, presumably by eliminating fibrin

deposits and improving circulation and oxygenation (51, 52). Furthermore, a recently published retrospective clinical cohort analysis found that systemic anticoagulation is associated with decreased mortality and morbidity in AP, suggesting at least some role for anticoagulation in pancreatitis therapy (53). Finally, thrombin inhibition by dabigatran has been shown to reduce proinflammatory macrophages in atherosclerotic lesions (54) and to improve organ fibrosis in various mouse models (55–57).

The goal of the present study was to offer proof of concept that pancreatic trypsin inhibition can have a therapeutic effect in pancreatitis. We chose to focus on dabigatran etexilate, because this drug is already in clinical use worldwide, is orally bioavailable, and, aside from the adverse effects related to anticoagulation, has an excellent safety profile. Despite the mixed results, we view this study as strongly encouraging because the observations demonstrated that benzamidine derivatives can be highly effective trypsin inhibitors with demonstrable therapeutic efficacy. We note that future clinical trials of trypsin inhibitors in pancreatitis should focus on *PRSS1*-related hereditary pancreatitis and other trypsin-mediated forms of the disease. Furthermore, trial designs should consider that trypsin inhibition is expected to prevent or dampen disease initiation but not severity outcomes, such as organ failure, caused by lipotoxicity (58). Finally, the results warrant revisiting the potential therapeutic utility of other compounds with trypsin-inhibitory activity, such as gabexate, camostat, and nafamostat, in trypsin-dependent pancreatitis.

Methods

Materials. Bovine trypsin (catalog number LS003707) was purchased from Worthington Biochemical Corporation and was active-site titrated with *p*-nitrophenyl *p'*-guanidino-benzoate (catalog number N-8010, MilliporeSigma) (59). Ecotin was produced and purified as reported previously (60). The concentration of ecotin was determined by titration against active-site titrated bovine trypsin. Recombinant human pro-enterokinase (catalog number 1585-SE-010) was purchased from R&D Systems and was activated with human cationic trypsin. The trypsin substrate GPR-pNA (catalog number 4000768.0100) was purchased from Bachem Americas. Benzamidine hydrochloride (code number 401790050) was obtained from Acros Organics (through Thermo Fisher Scientific) and dissolved in distilled water to prepare a 100 mM stock solution, which was further diluted with distilled water to a 10 mM working solution. Dabigatran etexilate mesylate (catalog number D100150) and dabigatran (catalog number D100090) were purchased from Toronto Research Chemicals. Dabigatran used for biochemical studies was dissolved in 0.1N HCl first to prepare an 800 μM stock solution, which was further diluted with distilled water to a 10 μM working solution.

Modeling dabigatran binding to trypsin. The dabigatran chemical structure was downloaded from the PubChem database (https://pubchem.ncbi.nlm.nih.gov/) as canonical SMILES string. The human mesotrypsin structure 1H4W was downloaded from PDB (42). The docking was carried out by the docking server ClusPro LigTBM (https://ligtbm.cluspro.org/) (61). The program performed a similarity search in the PDB database to find all trypsin structures or homologs cocrystallized with ligands similar to dabigatran as templates. An ensemble of 1,000 initial conformations was generated for the ligand. For each template, all conformers were aligned to the template, and only 1 conformer with the lowest root mean square deviation was retained. The resulting protein-ligand structures were subjected to restrained all-atom energy minimization using a CHARMM-based energy function (62) with a GBSA-type solvation term (Analytical Continuum Electrostatics) to remove possible clashes and "relax" the ligand.

Expression, purification, and activation of trypsinogens. Recombinant human and mouse trypsinogens were expressed in *Escherichia coli* BL21(DE3) (Invitrogen), refolded in vitro, and purified by ecotin affinity chromatography (Pharmacia FPLC), according to published protocols (60, 63, 64). Sulfated human trypsinogens were purified from archived samples of human pancreatic juice, as described previously, with minor modifications (65, 66). Briefly, 50 mg freeze-dried pancreatic juice was dissolved in 2 mL 10 mM HCl, clarified by centrifugation (21,000*g*, 5 minutes, 4°C), and loaded onto a MonoQ 5/50 GL column equilibrated with 20 mM Tris-HCl (pH 8.0). Proteins were eluted with a 0–0.5 M NaCl gradient at 1 mL/min flow rate for 30 minutes. The fractions containing the cationic and anionic trypsinogens were further purified with ecotin affinity chromatography. The concentration of trypsinogen preparations was estimated from their UV absorbance at 280 nM using the extinction coefficients reported previously for mouse trypsinogens (64) and 37,525, 38,890, and 41,535/M/cm for human cationic trypsinogen (PRSS1), anionic trypsinogen (PRSS2), and mesotrypsinogen (PRSS3), respectively. To activate trypsinogen to trypsin, approximately 1 μM solution was incubated at 37°C with 28.2 ng/mL human enterokinase (final concentration) in 0.1 M Tris-HCl (pH 8.0), 10 mM $CaCl_2$, and 0.05% Tween 20 for 1 hour. The activation reaction was followed

by measuring trypsin activity: 2 μL trypsin was diluted in 48 μL assay buffer [0.1 M Tris-HCl (pH 8.0), 1 mM $CaCl_2$, and 0.05% Tween 20], and 150 μL of 200 μM GPR-pNA trypsin substrate (in assay buffer) was added. Substrate cleavage resulting in the release of the yellow *p*-nitroaniline was monitored for 1 minute in a Spectramax Plus 384 microplate reader at 405 nm.

Active-site titration of trypsin. The concentration of trypsin solutions was determined by titration with the trypsin inhibitor ecotin. Briefly, a 2-fold serial dilution of ecotin was prepared in 100 μL assay buffer in a microplate, 100 μL of trypsin solution was added, and the mixture was incubated at 24°C for 30 minutes. The final ecotin concentrations in the 200 μL volume were 0, 0.78, 1.56, 3.1, 6.25, 12.5, 25, and 50 nM, and the final nominal trypsin concentration was 10 nM. Trypsin activity was measured after adding 5 μL of 6 mM GPR-pNA substrate to each well, as described above. The trypsin activity was plotted as a function of the ecotin concentration, and the true trypsin concentration was determined from the extrapolated *x* intercept of the linear portion of the inhibition curve.

Enzyme kinetic measurements. Michaelis-Menten kinetic parameters of trypsin isoforms were determined with the chromogenic substrate GPR-pNA at 24°C. The trypsin concentration was 1 nM and the substrate concentration was varied typically between 1.56 and 200 μM in a final volume of 200 μL assay buffer. The substrate concentration range was 3.1–400 μM for mouse trypsin isoform T7 and 0.4–50 μM for mouse trypsin isoform T20. K_m and k_{cat} values were calculated from hyperbolic fits to plots of reaction velocity versus substrate concentration.

Measuring competitive inhibition by benzamidine and dabigatran. Trypsin isoforms were preincubated with increasing concentrations of benzamidine or dabigatran for 15 minutes at 24°C, in 100 μL assay buffer. Michaelis-Menten kinetic parameters were then measured after adding 100 μL trypsin substrate, as described above. The final trypsin concentration in the assay was 1 nM, the final benzamidine concentrations were from 12.5 to 100 μM, and the final dabigatran concentrations were from 25 to 200 nM, as indicated in Tables 1 and 2. To determine the K_i, the K_m values were plotted as a function of the inhibitor concentration, and the K_i was calculated by dividing the *y* axis intercept with the slope of the linear fit. This value corresponds to the negative of the *x* axis intercept. Alternatively, the substrate saturation curves obtained in the absence and presence of the increasing inhibitor concentrations were globally fitted to the competitive inhibition equation $y = v_{max} \times (x/[K_{mObs} + x])$, where y is the reaction velocity, v_{max} is the maximal velocity, x is the substrate concentration, and $K_{mObs} = K_m \times (1 + [I]/K_i)$, where [I] is the inhibitor concentration. Experiments were performed 3 times and each experiment was analyzed separately. The reported K_i values thus represent the mean (± standard deviation) of 3 determinations. Kinetic analysis was performed with the Prism 8 program (GraphPad).

Experimental animals. The generation and properties of the *T7D23A* and *T7K24R* mice carrying trypsinogen mutations were described recently (29, 30). Heterozygous *T7D23A* and homozygous *T7K24R* mice were used. Protocols for genotyping have been reported earlier (29, 30). C57BL/6N mice were purchased from Charles River Laboratories or produced in our breeding facility from the same stock. Both male and female mice were studied. The number of mice used in the experiments is shown in the figures.

Cerulein-induced pancreatitis in T7K24R mice. Pancreatitis was induced in *T7K24R* mice with 8 hourly intraperitoneal injections of the secretagogue peptide cerulein used in a dose of 50 μg/kg. Cerulein (catalog number C9026, MilliporeSigma) was dissolved in sterile normal saline at 10 μg/mL concentration. Mice were sacrificed 1, 24, 48, 72, or 96 hours from the first cerulein injection, as indicated, and the pancreas and blood were harvested. Details of histological analysis and measurement of plasma amylase (4 μL assayed) were reported previously (29–31).

Intrapancreatic protease activity in T7K24R mice. Trypsin and chymotrypsin activities were measured from freshly prepared pancreas extracts of C57BL/6N and *T7K24R* mice using our recently published protocol (67). Activity was expressed as the rate of substrate cleavage in relative fluorescent units per second, normalized to the total protein concentration in milligrams.

Dabigatran etexilate treatment of T7D23A and T7K24R mice. Mice were administered dabigatran etexilate orally either by intragastric gavage of a 20 mg/mL solution to a final dose of 100 or 200 mg/kg using a 24 gauge, 1 inch long feeding needle (catalog number FN7900, Roboz Surgical) or by feeding with solid chow containing the prodrug in 10 mg/g concentration, as indicated in the experimental design. With these treatment protocols, no bleeding, morbidity, or mortality were observed. We note, however, that after administration of dabigatran etexilate, further injections or biopsies were not possible without the risk of significant bleeding. We also inspected hematoxylin-eosin–stained sections of liver, intestine, and kidney

from mice treated with dabigatran etexilate or vehicle but found no signs of organ damage. Control mice were given gavage of the vehicle solution (Captisol; see below) or regular chow.

Preparation of gavage solution and solid chow containing dabigatran etexilate. Dabigatran etexilate solution was always freshly prepared before use by dispersing 20 mg prodrug in 1 mL of 35% Captisol solution in a bath-type sonicator (5510 DTH Ultrasonic Cleaner, Branson) for 5–10 minutes at 24°C. Captisol (β-cyclodextrin sulfobutyl ethers, sodium salts, lot number NC-04A-180185) was obtained from Cydex Pharmaceuticals (through Thermo Fisher Scientific) and was dissolved in sterile normal saline (3.5 g in 10 mL). Dabigatran etexilate–containing chow was prepared using regular chow (5053 PicoLab Rodent Diet 20, LabDiet), which was pulverized with a pestle in a ceramic mortar. Solid dabigatran etexilate mesylate (1 g) was mixed with 100 g of powdered chow (10 mg/g final prodrug concentration), and sterile distilled water was added until the chow became malleable. The mixture was then compressed into pellets using the barrel of a 10 mL plastic syringe and a plunger. The prodrug-containing pellets were allowed to dry at 24°C for 2 days and stored at 4°C until use.

Estimation of absorbed dabigatran etexilate. The oral bioavailability of dabigatran etexilate in humans is around 6.5%, and it is independent of dose and not influenced by food (40). Accordingly, a 100 mg/kg dose of intragastric gavage can provide a 0.13 mg single dose of systemically absorbed dabigatran etexilate in a 20 g mouse. When dabigatran etexilate is given mixed with solid chow (10 mg prodrug/g chow), mice can consume approximately 4 g chow over a 24-hour period. This would yield a 2.6 mg daily dose of absorbed dabigatran etexilate.

Determination of dabigatran plasma concentration. Dabigatran in the blood plasma was quantified using the HEMOCLOT Thrombin Inhibitors (3 × 2.5 mL) kit (catalog number CK002L-RUO, Hyphen BioMed, purchased from Aniara Diagnostica) (68, 69). Reagents were diluted according to the manufacturer's instructions. The BIOPHEN Dabigatran Plasma Calibrator set (catalog number 2222801-RUO, Hyphen BioMed, purchased from Aniara Diagnostica) was used to establish a calibration curve for the clotting time as a function of plasma dabigatran concentration. Mouse blood was collected immediately after CO_2 euthanasia. To achieve rapid anticoagulation, 20 μL of a 3.2% solution of sodium citrate was pipetted into the conus of a needle before attaching it to a 1 mL syringe and collecting approximately 180 μL blood by cardiac puncture. Cellular blood elements were sedimented by centrifugation (2,000*g*, 15 minutes, 4°C); the plasma was saved and further diluted with normal saline before use (20 μL plasma was mixed with 160 μL saline). A clean microscope slide was placed on the surface of a block heater set at 37°C. Aliquots of reagents R1 and R2 (110 μL), and the calibrators or plasma specimen (60 μL), were pipetted onto the glass surface and preheated for 2 minutes. Reagent R1 (100 μL) was then mixed with 50 μL of the calibrator or plasma on the slide and incubated for 1 minute before addition of reagent R2 (100 μL). Time to the appearance of the first fibrin clot was measured. Clotting was detected by manual probing of the incubation mixture for fibrin threads with a small pipette tip.

Statistics. Results are given as mean values ± standard deviation or shown as individual data points with the mean ± standard deviation indicated. Differences between means were analyzed by unpaired 2-tailed *t* test for 2 groups and by 1-way ANOVA for multiple groups, with Tukey-Kramer post hoc analysis for pairwise comparison using Prism 8 (GraphPad). Statistical significance was defined as $P < 0.05$.

Study approval. Animal experiments were performed at the University of California Los Angeles (UCLA) with the approval and oversight of the Animal Research Committee, including protocol review and postapproval monitoring. The animal care program at UCLA is managed in full compliance with the US Animal Welfare Act, the US Department of Agriculture Animal Welfare Regulations, the US Public Health Service Policy on Humane Care and Use of Laboratory Animals, and the *Guide for the Care and Use of Laboratory Animals* (National Academies Press, 2011). UCLA has an approved Animal Welfare Assurance statement (A3196-01) on file with the US Public Health Service, NIH, Office of Laboratory Animal Welfare. UCLA is accredited by the Association for Assessment and Accreditation of Laboratory Animal Care International.

Author contributions

MST conceived and directed the study. MST, ZGP, ZJ, AD, and SV designed the experiments. ZGP, ZJ, AD, BCN, and SV performed the experiments. All authors analyzed the data. MST wrote the manuscript; ZGP, ZJ, AD, and SV prepared the figures. All authors read and approved the manuscript.

Acknowledgments

This work was supported by the NIH grants R01 DK117809, R01 DK082412, and R01 058088 to MST and R35 GM118078 to SV; the Department of Defense grant W81XWH2010134 (PR192583) to ZJ and MST; and a scholarship from the Rosztoczy Foundation to BCN.

Address correspondence to Miklós Sahin-Tóth, 675 Charles E Young Drive South, MacDonald Research Laboratories, Rm 2220, Los Angeles, California 90095, USA. Phone: 310.267.5905; E-mail: msahintoth@mednet.ucla.edu.

1. Yadav D, Lowenfels AB. The epidemiology of pancreatitis and pancreatic cancer. *Gastroenterology*. 2013;144(6):1252–1261.
2. Whitcomb DC, et al. Chronic pancreatitis: an international draft consensus proposal for a new mechanistic definition. *Pancreatology*. 2016;16(2):218–224.
3. Whitcomb DC, et al. Hereditary pancreatitis is caused by a mutation in the cationic trypsinogen gene. *Nat Genet*. 1996;14(2):141–145.
4. Hegyi E, Sahin-Tóth M. Genetic risk in chronic pancreatitis: the trypsin-dependent pathway. *Dig Dis Sci*. 2017;62(7):1692–1701.
5. Mayerle J, et al. Genetics, cell biology, and pathophysiology of pancreatitis. *Gastroenterology*. 2019;156(7):1951–1968.
6. Ascenzi P, et al. The bovine basic pancreatic trypsin inhibitor (Kunitz inhibitor): a milestone protein. *Curr Protein Pept Sci*. 2003;4(3):231–251.
7. Tamura Y, et al. Synthetic inhibitors of trypsin, plasmin, kallikrein, thrombin, C1r-, and C1 esterase. *Biochim Biophys Acta*. 1977;484(2):417–422.
8. Fujii S, Hitomi Y. New synthetic inhibitors of C1r, C1 esterase, thrombin, plasmin, kallikrein and trypsin. *Biochim Biophys Acta*. 1981;661(2):342–345.
9. Takasugi S, et al. Prevention of acute experimental pancreatitis in rats and dogs by intraduodenal infusion of a synthetic trypsin inhibitor. *Digestion*. 1982;24(1):36–41.
10. Lankisch PG, et al. Effect of FOY-305 (camostate) on severe acute pancreatitis in two experimental animal models. *Gastroenterology*. 1989;96(1):193–199.
11. Wisner JR Jr, et al. The effects of nafamostat mesilate (FUT-175) on caerulein-induced acute pancreatitis in the rat. *Int J Pancreatol*. 1989;4(4):383–390.
12. Otsuki M, et al. Beneficial effects of the synthetic trypsin inhibitor camostate in cerulein-induced acute pancreatitis in rats. *Dig Dis Sci*. 1990;35(2):242–250.
13. Manabe T, et al. Protective effect of nafamostat mesilate on cellular and lysosomal fragility of acinar cells in rat cerulein pancreatitis. *Int J Pancreatol*. 1992;12(2):167–172.
14. Kisfalvi K, et al. Beneficial effects of preventive oral administration of camostate on cerulein-induced pancreatitis in rats. *Dig Dis Sci*. 1995;40(3):546–547.
15. Keck T, et al. Regional effects of nafamostat, a novel potent protease and complement inhibitor, on severe necrotizing pancreatitis. *Surgery*. 2001;130(2):175–181.
16. Lee JK, et al. Effects of nafamostat mesilate on the prevention of cerulein-induced acute pancreatitis. *Pancreas*. 2008;36(3):255–260.
17. Motoo Y. Antiproteases in the treatment of chronic pancreatitis. *JOP*. 2007;8(suppl 4):533–537.
18. Smith M, et al. Aprotinin in severe acute pancreatitis. *Int J Clin Pract*. 2010;64(1):84–92.
19. Seta T, et al. Treatment of acute pancreatitis with protease inhibitors administered through intravenous infusion: an updated systematic review and meta-analysis. *BMC Gastroenterol*. 2014;14:102.
20. Yu G, et al. Nafamostat mesilate for prevention of post-ERCP pancreatitis: a meta-analysis of prospective, randomized, controlled trials. *Pancreas*. 2015;44(4):561–569.
21. Hirota M, et al. Continuous regional arterial infusion versus intravenous administration of the protease inhibitor nafamostat mesilate for predicted severe acute pancreatitis: a multicenter, randomized, open-label, phase 2 trial. *J Gastroenterol*. 2020;55(3):342–352.
22. Matsumoto T, et al. Nafamostat mesylate is not effective in preventing post-endoscopic retrograde cholangiopancreatography pancreatitis. *Dig Dis Sci*. 2021;66(12):4475–4484.
23. Mahoney M, et al. A novel class of TMPRSS2 inhibitors potently block SARS-CoV-2 and MERS-CoV viral entry and protect human epithelial lung cells. *Proc Natl Acad Sci U S A*. 2021;118(43):e2108728118.
24. Sun G, et al. Structural basis of covalent inhibitory mechanism of TMPRSS2-related serine proteases by camostat. *J Virol*. 2021;95(19):e0086121.
25. Ito K, et al. Major ongoing clinical trials for COVID-19 treatment and studies currently being conducted or scheduled in Japan. *Glob Health Med*. 2020;2(2):96–101.
26. Gunst JD, et al. Efficacy of the TMPRSS2 inhibitor camostat mesilate in patients hospitalized with Covid-19-a double-blind randomized controlled trial. *EClinicalMedicine*. 2021;35:100849.
27. Sakr Y, et al. Camostat mesylate therapy in critically ill patients with COVID-19 pneumonia. *Intensive Care Med*. 2021;47(6):707–709.
28. Zhuravel SV, et al. Nafamostat in hospitalized patients with moderate to severe COVID-19 pneumonia: a randomised phase II clinical trial. *EClinicalMedicine*. 2021;41:101169.
29. Geisz A, Sahin-Tóth M. A preclinical model of chronic pancreatitis driven by trypsinogen autoactivation. *Nat Commun*. 2018;9(1):5033.
30. Jancsó Z, Sahin-Tóth M. Mutation that promotes activation of trypsinogen increases severity of secretagogue-induced pancreatitis in mice. *Gastroenterology*. 2020;158(4):1083–1094.
31. Jancsó Z, Sahin-Tóth M. Chronic progression of cerulein-induced acute pancreatitis in trypsinogen mutant mice. *Pancreatology*.

2022;22(2):248–257.
32. Demcsák A, Sahin-Tóth M. Rate of autoactivation determines pancreatitis phenotype in trypsinogen mutant mice. *Gastroenterology*. 2022;163(3):761–763.
33. Huang H, et al. Transgenic expression of PRSS1^{R122H} sensitizes mice to pancreatitis. *Gastroenterology*. 2020;158(4):1072–1082.
34. Gui F, et al. Trypsin activity governs increased susceptibility to pancreatitis in mice expressing human PRSS1R122H. *J Clin Invest*. 2020;130(1):189–202.
35. Wan J, et al. Transgenic expression of human PRSS2 exacerbates pancreatitis in mice. *Gut*. 2020;69(11):2051–2052.
36. Wang J, et al. Wild-type human PRSS2 and PRSS1^{R122H} cooperatively initiate spontaneous hereditary pancreatitis in transgenic mice. *Gastroenterology*. 2022;163(1):313–315.
37. Hauel NH, et al. Structure-based design of novel potent nonpeptide thrombin inhibitors. *J Med Chem*. 2002;45(9):1757–1766.
38. Van Ryn J, et al. The discovery of dabigatran etexilate. *Front Pharmacol*. 2013;12(4):12.
39. Ageno W, et al. Dabigatran in clinical practice: contemporary overview of the evidence. *Int J Cardiol*. 2016;220:417–428.
40. Stangier J, Clemens A. Pharmacology, pharmacokinetics, and pharmacodynamics of dabigatran etexilate, an oral direct thrombin inhibitor. *Clin Appl Thromb Hemost*. 2009;15(suppl 1):9S–16S.
41. Wienen W, et al. In-vitro profile and ex-vivo anticoagulant activity of the direct thrombin inhibitor dabigatran and its orally active prodrug, dabigatran etexilate. *Thromb Haemost*. 2007;98(1):155–162.
42. Katona G, et al. Crystal structure reveals basis for the inhibitor resistance of human brain trypsin. *J Mol Biol*. 2002;315(5):1209–1218.
43. Nar Het al. Structural basis for inhibition promiscuity of dual specific thrombin and factor Xa blood coagulation inhibitors. *Structure*. 2001;9(1):29–37.
44. Melmed RN, Bouchier IA. A further physiological role for naturally occurring trypsin inhibitors: the evidence for a trophic stimulant of the pancreatic acinar cell. *Gut*. 1969;10(12):973–979.
45. Göke B, et al. Endogenous CCK release and pancreatic growth in rats after feeding a proteinase inhibitor (camostate). *Pancreas*. 1986;1(6):509–515.
46. Niederau C, et al. Pancreatic growth: interaction of exogenous cholecystokinin, a protease inhibitor, and a cholecystokinin receptor antagonist in mice. *Gut*. 1987;28(suppl):63–69.
47. Smith JC, et al. Hypertrophy and hyperplasia of the rat pancreas produced by short-term dietary administration of soya-derived protein and soybean trypsin inhibitor. *J Appl Toxicol*. 1989;9(3):175–179.
48. Crozier SJ, et al. CCK-induced pancreatic growth is not limited by mitogenic capacity in mice. *Am J Physiol Gastrointest Liver Physiol*. 2008;294(5):G1148–G1157.
49. Leonhardt U, et al. Effect of camostate administration for two weeks on experimental pancreatitis in mice and rats. *Pancreas*. 1993;8(1):98–102.
50. Friess H, et al. Adaptation of the human pancreas to inhibition of luminal proteolytic activity. *Gastroenterology*. 1998;115(2):388–396.
51. Hackert T, et al. Effects of heparin in experimental models of acute pancreatitis and post-ERCP pancreatitis. *Surgery*. 2004;135(2):131–138.
52. Park MJ, et al. HIF1-alpha regulates acinar cell function and response to injury in mouse pancreas. *Gastroenterology*. 2018;154(6):1630–1634.
53. Kröner PT, et al. Systemic anticoagulation is associated with decreased mortality and morbidity in acute pancreatitis. *Pancreatology*. 2021;21(8):1428–1433.
54. Feldmann K, et al. Decreased M1 macrophage polarization in dabigatran-treated Ldlr-deficient mice: implications for atherosclerosis and adipose tissue inflammation. *Atherosclerosis*. 2019;287:81–88.
55. Bogatkevich GS, et al. Antiinflammatory and antifibrotic effects of the oral direct thrombin inhibitor dabigatran etexilate in a murine model of interstitial lung disease. *Arthritis Rheum*. 2011;63(5):1416–1425.
56. Dong A, et al. Direct thrombin inhibition with dabigatran attenuates pressure overload-induced cardiac fibrosis and dysfunction in mice. *Thromb Res*. 2017;159:58–64.
57. Saifi MA, et al. A direct thrombin inhibitor, dabigatran etexilate protects from renal fibrosis by inhibiting protease activated receptor-1. *Eur J Pharmacol*. 2021;893:173838.
58. Navina S, et al. Lipotoxicity causes multisystem organ failure and exacerbates acute pancreatitis in obesity. *Sci Transl Med*. 2011;3(107):107ra110.
59. Chase T Jr, Shaw E. p-Nitrophenyl-p'-guanidinobenzoate HCl: a new active site titrant for trypsin. *Biochem Biophys Res Commun*. 1967;29(4):508–514.
60. Király O, et al. Expression of recombinant proteins with uniform N-termini. *Methods Mol Biol*. 2011;705:175–194.
61. Alekseenko A, et al. ClusPro LigTBM: automated template-based small molecule docking. *J Mol Biol*. 2020;432(11):3404–3410.
62. Brooks BR, et al. CHARMM: a program for macromolecular energy, minimization, and dynamics calculations. *J Comp Chem*. 1983;4(2):187–217.
63. Lengyel Z, et al. Affinity purification of recombinant trypsinogen using immobilized ecotin. *Protein Expr Purif*. 1998;12(2):291–294.
64. Németh BC, et al. Autoactivation of mouse trypsinogens is regulated by chymotrypsin C via cleavage of the autolysis loop. *J Biol Chem*. 2013;288(33):24049–24062.
65. Nemoda Z, Sahin-Tóth M. Chymotrypsin C (caldecrin) stimulates autoactivation of human cationic trypsinogen. *J Biol Chem*. 2006;281(17):11879–11886.
66. Sahin-Tóth M, et al. Human cationic trypsinogen is sulfated on Tyr154. *FEBS J*. 2006;273(22):5044–5050.
67. Mosztbacher D, et al. Measuring digestive protease activation in the mouse pancreas. *Pancreatology*. 2020;20(2):288–292.
68. Samoš M, et al. Monitoring of dabigatran therapy using Hemoclotthrombin inhibitor assay in patients with atrial fibrillation. *J Thromb Thrombolysis*. 2015;39(1):95–100.
69. Cini M, et al. Comparison of five specific assays for determination of dabigatran plasma concentrations in patients enrolled in the START-laboratory register. *Int J Lab Hematol*. 2018;40(2):229–236.